FIRST | SAS | R | 004-1

THE INSTITUTE OF SPACE AND ASTRONAUTICAL SCIENCE
YOSHINODAI, SAGAMIHARA, KANAGAWA 229

ISAS RESEARCH NOTE

ISAS RN 595

Flight Performance of the IRTS

IRTS team

October 1996

Preprints of papers which describe
the flight performance of the IRTS.
They are to be published in
"SPIE Proceedings" and "Cryogenics"

Contact Address:
Infrared Astrophysics Group
The Institute of Space and Astronautical Science
Yoshinodai 3-1-1, Sagamihara, Kanagawa 229, Japan

Flight Performance of the IRTS

IRTS team

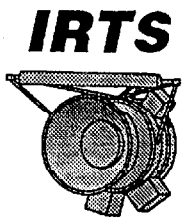

Preface

The *Infrared Telescope in Space* (IRTS) is the first Japanese orbiting telescope dedicated to infrared astronomy. It is a cryogenically-cooled 15 cm telescope onboard the *Space Flyer Unit* (SFU). The SFU was launched on March 18, 1995 by the Japanese H-2 rocket and was retrieved by the NASA's Space Shuttle in January 1996. The IRTS performed an successful survey of 7 % of the sky at wavelengths ranging from 1.4 μm to 700 μm.

This volume is a collection of preprints which describe the flight performance of the IRTS. There are eight papers contained: two are general description of the mission, four are on its focal plane instruments, and two are on cryogenical systems.

October 1996
IRTS team *

* The IRTS team consists of members from California Institute of Technology (USA), Communications Research Laboratory (Japan), Institute of Space and Astronautical Science (Japan), Nagoya University (Japan), NASA Ames Research Center (USA), Tokyo Metropolitan Institute of Technology (Japan), University of California at Berkeley (USA), University of Tokyo (Japan), and University of Tsukuba (Japan).

Table of Contents

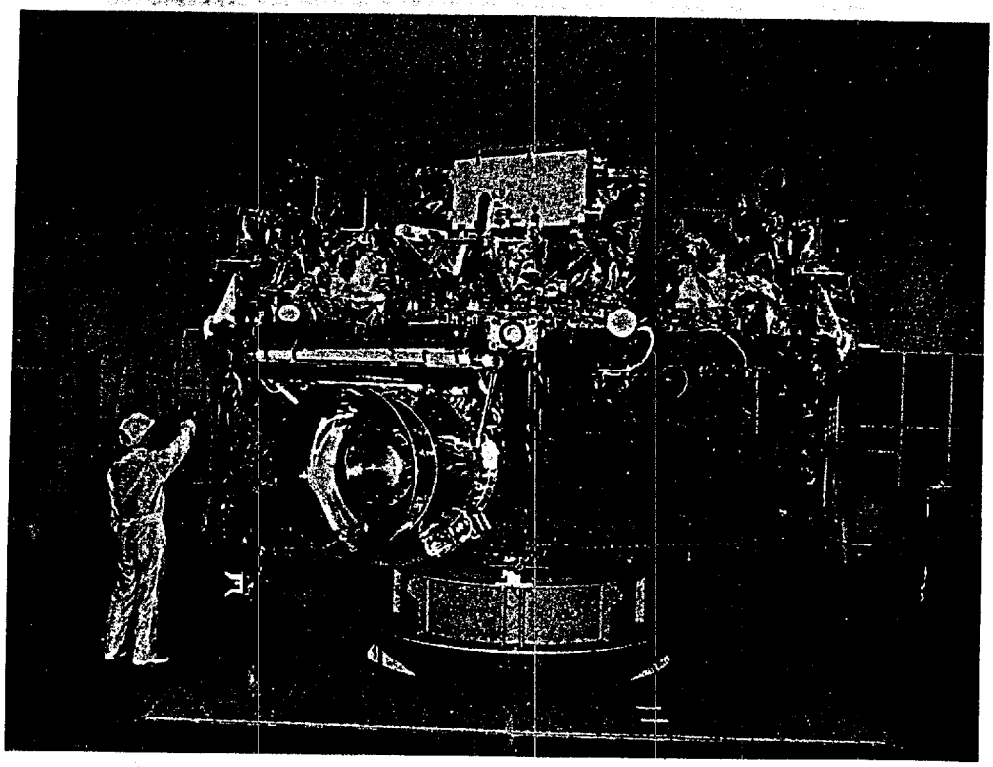

IRTS on SFU

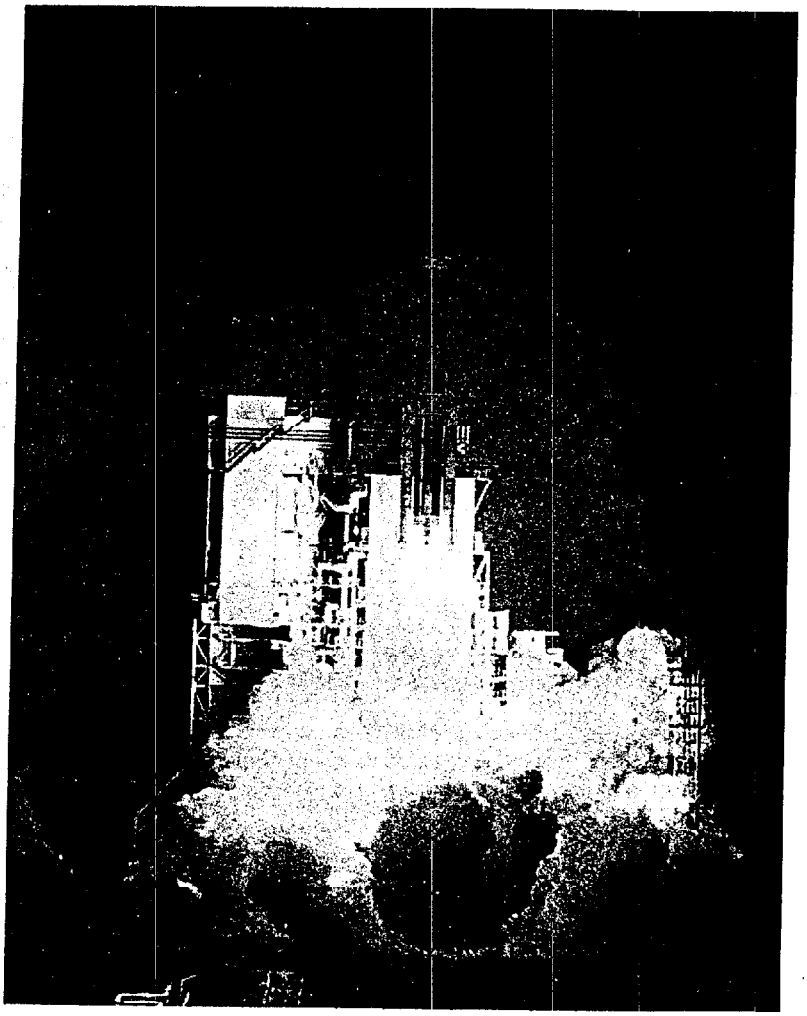

Launched on March 18, 1995

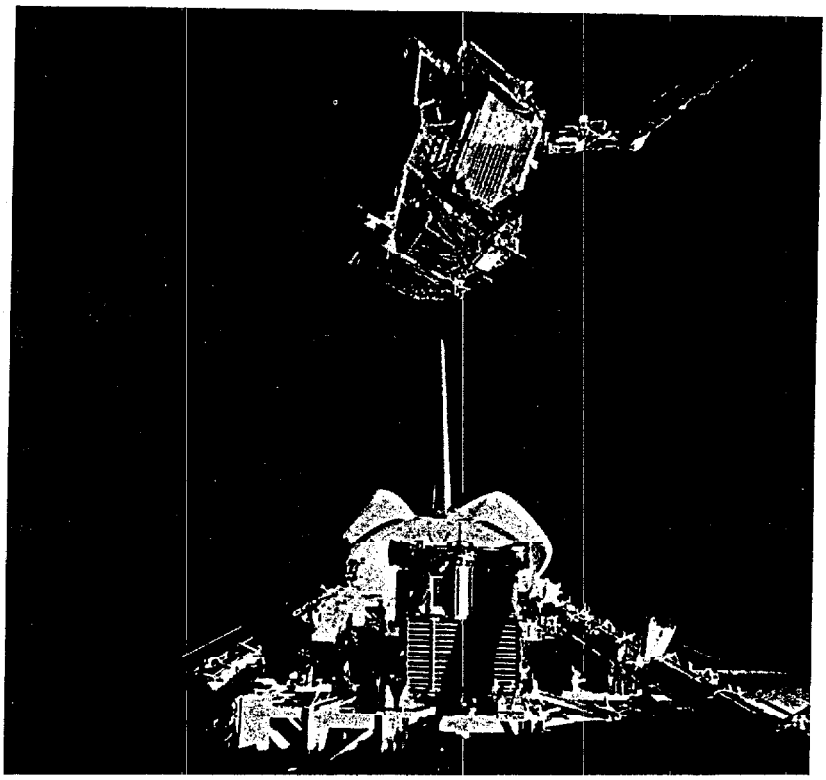

Retrieving SFU on January 13, 1996

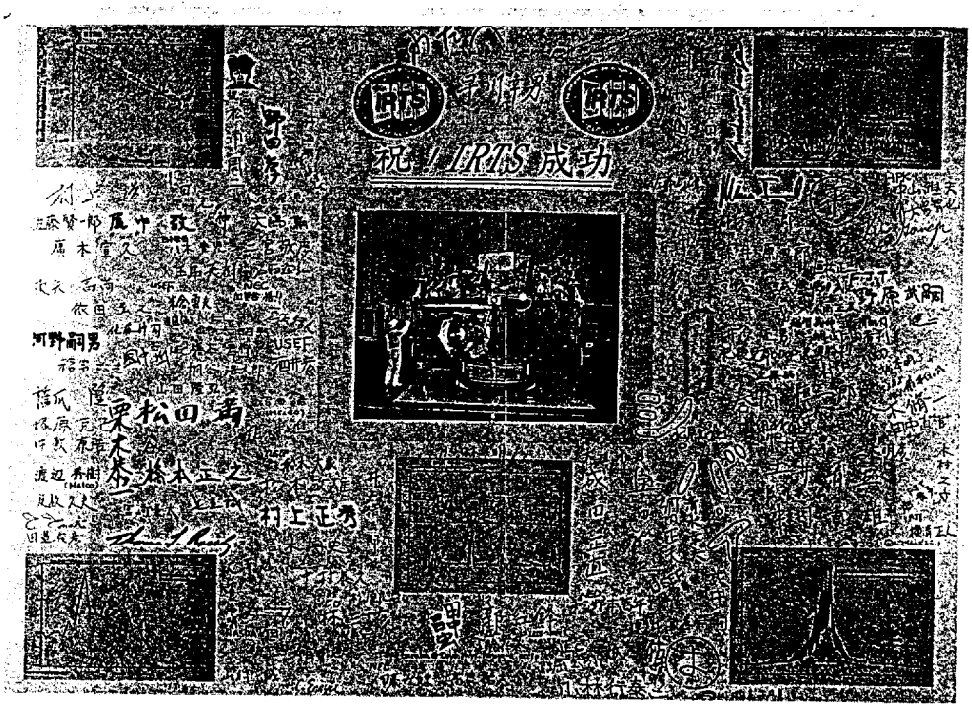

We made it !

accept ed for Proceedings of SPIE 2817, Infrared Spaceborne Remote Sensing IV , ed. M. S. Scholl and B. F. Anderesen

IRTS (Infrared Telescope in Space) Mission

Toshio Matsumoto and Hiroshi Murakami

The Institute of Space and Astronautical Science, 3-1-1 Yoshinodai, Sagamihara, Kanagawa 229, Japan

ABSTRACT

Japanese satellite-borne infrared telescope, the Infrared Telescope in Space (IRTS), was successfully launched on March 18th, 1995 UT. The IRTS consisted of a 15 cm telescope cooled with superfluid liquid helium and installed onboard the Space Flyer Unit (SFU) spacecraft. The IRTS mission started on March 29th UT and terminated on April 26th UT after liquid helium ran out. The cryogenic system operated as designed and held the telescope and the focal-plane instruments at a stable temperature of 1.9 K for 38 days. Four focal-plane instruments which together covered almost the entire infrared wavelength range observed a sky area of about 2700 deg^2 and returned a wealth of new data on variety of objects, including the zodiacal light, interstellar gas and dust, near-infrared background light and point sources.

keywords; IRTS, SFU, Infrared Astronomy, Space Cryogenics

1. INTRODUCTION

A cooled space telescope is a powerful tool to investigate celestial infrared emission, especially the far-infrared emission which is completely obscured by the atmosphere of the earth. Infrared emission of diffuse celestial components are also very hard to be observed from the ground, even within the wavelengths of the atmospheric windows, because of strong background emission from the atmosphere and the telescope itself. In contrast with this, a cooled telescope in space realizes ideal low-background conditions and the absence of any atmospheric absorption. The Infrared Astronomical Satellite (IRAS)[1], the Spacelab 2 Infrared Telescope (IRT)[2], and the Cosmic Background Explorer (COBE)[3] missions have flown previously and have given us new views of the interstellar matter in the Galaxy, external galaxies and the cosmic background emission.

The Infrared Telescope in Space (IRTS), Japan's first orbiting infrared telescope, was successfully launched in March, 1995 and provided the fourth opportunity for astronomical infrared observations from a satellite.

The IRTS was one of the instruments onboard the Space Flyer Unit (SFU)[4] which was a re-usable free flyer spacecraft designed as a multi-purpose common facility for scientific and engineering experiments. The purpose of the IRTS mission was to perform an infrared survey of the diffuse celestial emission with moderate spatial resolution and very high sensitivities in the entire infrared wavelength range. The IRTS data add new information on the zodiacal light, interstellar matter, infrared stars and the infrared cosmic background radiation.

In this paper, we give an outline of the IRTS mission. Since the instrumentation and the flight operation plan of the IRTS have been given by Murakami et al. (hereafter Paper 1)[5], here we overview the instrumentation briefly again and report the actual flight operation as an introduction to the papers describing the flight performance of focal plane instruments aboard the IRTS in this volume.

2. IRTS Instrumentation

The IRTS consisted of a 15 cm telescope cooled with superfluid liquid helium. The major part of the instrument volume was occupied by the cryogenic system, including a ~100 liter liquid-helium tank. Figure 1 shows a cross-sectional view of the IRTS. The helium tank and three vapor-cooled shields were suspended from the outer vacuum shell by support straps made of GFRP (glass fiber reinforced plastic). The telescope and the focal-plane instruments, which were integrated together on a common base plate, directly attached to the helium tank and were cooled to about 2 K inflight. A porous plug made of alumina ceramics was employed to separate the vapor from the super fluid liquid helium in a zero-gravity condition[6].

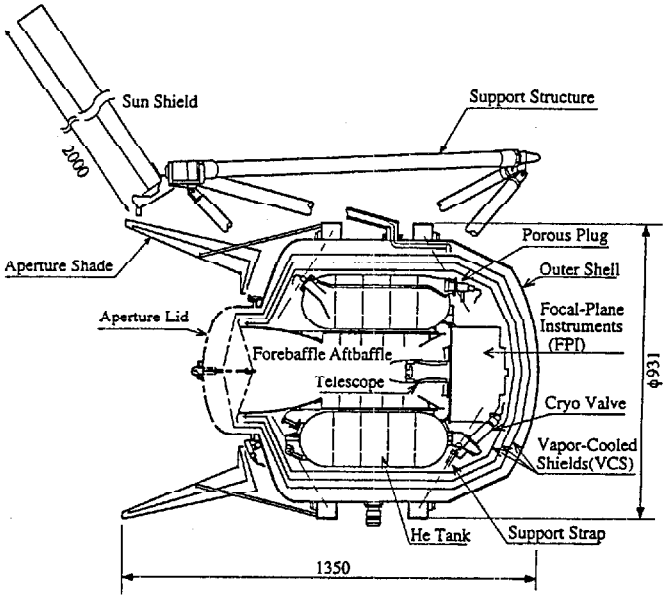

Fig.1 Cross sectional view of the IRTS. The scale is given in mm. The telescope aperture lid, which is ejected in space, is shown by dot-dashed lines.

Since the IRTS intended to make absolute measurements, rejecting the strong emission from the sun and the earth was a critical issue. The IRTS was equipped with four kinds of baffles as is shown in Figure 2. A sun shield consisting of a 2 m long fiber-reinforced plastic sheet blocked the sun light from directly illuminating the telescope aperture. A cone shaped aperture shade reflected the infrared light from the sun shield and the earth back to the sky. A cold reflecting forebaffle[7] also reflected the scattered light and thermal emission from the aperture shade. Finally, a black aftbaffle around the telescope absorbs stray light. For the best condition, the sun and earth avoidance angles were designed to be larger than 70 degree and 58 degree, respectively.

The telescope[8] was a Ritchey-Chretien design with an effective diameter of 15 cm and a focal length of 60 cm. The mirrors were made of aluminum alloy cut by a high-precision numerically-controlled machine. The mirror surfaces were coated with

Ni before final shaping and polishing, and coated with gold and thin SiO_2 layers after polishing.

Four focal-plane instruments (FPI) were developed under the Japan-U.S.A. collaboration and installed in the focal plane of the telescope: the Near-Infrared Spectrometer (NIRS)[9], the Mid-Infrared Spectrometer (MIRS)[10], the Far-Infrared Line Mapper (FILM)[11] and the Far-Infrared Photometer (FIRP)[12]. The NIRS and the MIRS were grating spectrometers with a moderate spectral and spatial resolutions. The two instruments together covered a wavelength range from 1.4 μm to 11.7 μm with a small gap at 4.0 - 4.5 μm. The FILM is a grating spectrometer dedicated to the intensity mapping of the interstellar [C II] and [O I] lines located at wavelengths of 158 μm and 63 μm, respectively. Newly developed concave gratings with varied line-space were employed for the MIRS and FILM to reduce the aberrations. The longest-wavelength instrument, FIRP, was a four-channel photometer whose center wavelengths were 150, 250, 400 and 700 μm. The FIRP employed a closed cycle ^3He refrigerator to cool its bolometric detectors to 0.3 K. The characteristics of these instruments are summarized in Table 1.

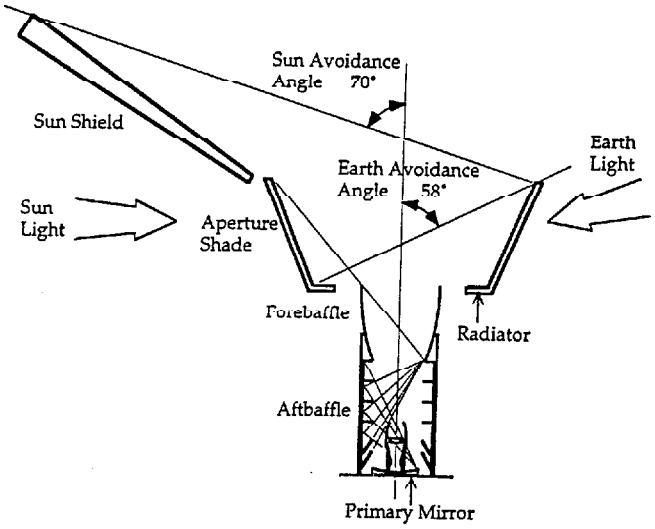

Fig.2 The IRTS baffling system and the definition of the sun and earth avoidance angles are shown

These four instruments shared the telescope beam and operated simultaneously. The FIRP used the on-axis beam and other three occupied positions about one degree off the axis (c.f. Figure 7 of Paper 1). The NIRS and the MIRS beams were aligned along the sky-scan direction and these two instruments observed the same sky with a time difference of about 30 seconds.

Each instrument had a cold shutter which gave the zero signal levels and enabled absolute measurements of the sky brightness. The instruments also had internal light sources which were periodically lighted during the flight to check for sensitivity changes.

A Ge photodiode with a special mask was also installed in the focal plane as a star sensor. This star sensor detected stars passing through its 17' square field-of-view and provided information on the pointing of the telescope.

	NIRS	MIRS	FILM	FIRP
wavelength coverage	1.4-4.0μm	4.5-11.7μm	63μm (OI) 158μm(CII) 155,160μm(cont.)	150,250,400,700μm
wavelength resolution	$\Delta\lambda$= 0.13μm	$\Delta\lambda$= 0.23-0.36μm	$\lambda/\Delta\lambda$=400(OI,CII) 130(cont.)	$\lambda/\Delta\lambda$=3
beam size	8'x8'	8'x8'	8' x 13'	30' circle
detectors	InSb 24ch. array CIA, hybrid	Si:Bi 32ch. array CIA discrete	Ge:Ga x 1 Ge:Ga stressed x 3	0.3K bolometer x 4 AC biased bridge

Table 1. Characteristics of focal plane instruments

3. FLIGHT PERFORMANCE

3.1 Flight operation

The SFU was launched at 8:01 UT on March 18th, 1995 aboard an H-2 rocket of the National Space Development Agency (NASDA) from the Tanegashima Space Center. One day prior to the launch, the cryogen tank of the IRTS was filled with superfluid helium. Pumping of the helium tank to keep the superfluid state lasted until 12 hours before launch and then the tank was sealed. At the launch, there was about 85 liters of superfluid helium on board and the temperature was lower than 1.7 K. About 30 minutes after the launch, the IRTS electrical power was turned on and the helium tank was opened to the outer space through the porous plug by an automatic valve operation.

The first 11 days after launch were spent to check the SFU bus system and the payload instruments. The SFU changed its orbit in this period from a low-altitude orbit, into which the SFU was initially placed, to a circular orbit with an altitude of 486km and an inclination angle of 28.5 degree.

The focal plane instruments of the IRTS were turned on at 18:00 on March 29th UT and the sun shield was deployed shortly after that. The attitude control mode of the SFU was changed to the IRTS attitude mode mentioned below at 23:49 on March 29th. The IRTS survey then started by ejecting the telescope aperture lid. The major events during the IRTS observation are given in Table 2.

On April 24th, the liquid helium ran out and the temperatures of the telescope and the FPI began to rise immediately. The MIRS and the FILM were turned off at this time, while the NIRS continued observation for one day more. As the electronics for the star sensor were included in the FIRP electronics, the FIRP was also kept on till the end of mission for the star sensor operations. The electrical power of the IRTS was turned off at 16:06 on April 26, after jettison of the sun shield.

During the survey, the IRTS data were normally collected at a rate of 6 kbps. Those data were sent to the ground stations of ISAS, NASDA and NASA/DSN and transferred to ISAS through networks. The data rate was occasionally changed to 3kbps by reducing the sampling frequency when an overflow of the onboard data recorder was expected.

About 5% of the entire possible survey data was unfortunately lost due to occasional failures of the ground receiving stations and some other minor troubles. The telescope looked at the moon in several orbital revolutions on April 9th and April 21-22th. This resulted in saturations of all the infrared detectors. Since some electric interference was observed between the FILM and the FIRP, the FIRP and the star sensor were turned off for three days during the middle of the mission for a high-quality survey at high galactic latitudes by the FILM. The ^{3}He refrigerator of the FIRP needed about 18 hours for each recycling. This also caused additional losses of the FIRP data while this operation took place.

Date/Time (UT)	Events
95/03/18 08:01	SFU launch
08:29	IRTS power on
95/03/29 18:00	FPI power on
18:15	Sun Shield deployed
23:49	North Scan started
23:59	Aperture Lid open
	(Survey started)
95/03/30 10:25 - 95/03/31 00:45	^{3}He refrigerator cooling operation
95/04/05 20:36	Scan mode change to South Scan
95/04/06 22:09 - 95/04/09 20:10	FIRP and Star Sensor off
95/04/10 06:40 - 95/04/10 21:00	^{3}He refrigerator cooling operation
95/04/18 20:15 - 95/04/19 18:00	^{3}He refrigerator cooling operation
95/04/24 09:27	Liquid helium ran out
12:08	FILM off
13:48	MIRS off
95/04/25 11:34	NIRS off
95/04/26 07:58	Sun Shield jettisoned
12:38	IRTS Attitude Mode end
16:06	IRTS power off

Table 2. Major events in the IRTS mission

3.2 Attitude control

The IRTS sky survey was performed by rotating the SFU around its sun-pointed axis, which was perpendicular to the IRTS optical axis, at a constant rate of one spin per orbital revolution (see Paper 1). The period of the orbital revolution was approximately 94 min and the sky-scan speed of the IRTS was therefore about 3.8 arcmin/s.

The spin axis of the SFU was actually fixed slightly off of the sun center line to minimize radiation from the earth limb.

The magnitude and direction of the spin-axis offset were selected to maximize the avoidance angles, depending on the orbit orientation relative to the sun (see figure 3).

Since the SFU orbit passed the northern side of the subsolar point at the beginning of the survey period, the IRTS survey started in the north-scan mode, and the spin axis offset was south from the solar center line. The orbit orientation gradually changed due to precession and the orbit crossed the subsolar point on April 5th. The magnitude of the spin axis offset was changed in a step wise fashion from -19 degree to -24 degree during this phase (the negative sign means a southward offset) and it jumped to 24 degree when the scan mode was changed to the south-scan mode at 20:36 on April 5th. The orbit crossed the southern side of the subsolar point after that. The south-scan mode lasted until the end of mission with offset angles of the spin axis in the range from 24 degree to 18 degree.

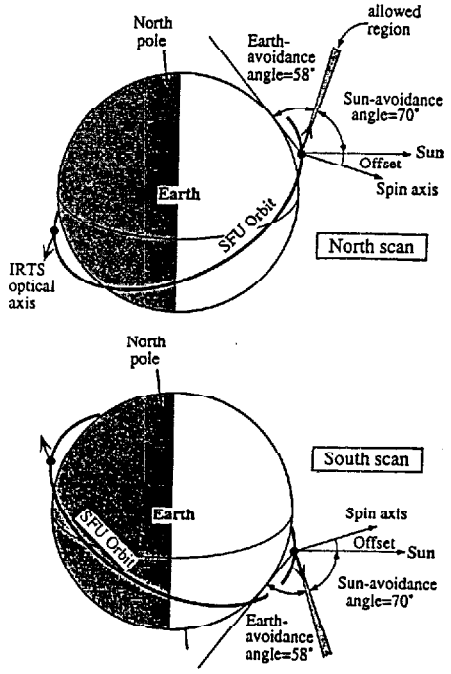

Fig.3 IRTS attitude control modes. In the north-scan mode, the offset direction of the spin axis was southward from the sun and the telescope observed the northern sky in the day side. Both the offset and the spin direction were opposite in the south-scan mode. The avoidance angles were determined by the baffling system to guarantee a good observing condition against the sun and the earth (see figure 6 of Paper 1).

The IRTS sky-scan paths are plotted in galactic coordinates in figure 4. The two strips in the figure show the scan paths in the north-scan mode and the south-scan mode. The sky area observed in the north-scan mode included a part of the galactic center region, certain star-forming regions such as NGC6334 and NGC6357, and the reflection nebula NGC7023. In the south-scan mode, the scan paths crossed the galactic plane near the star-forming region W51 (l~49 degree) and reached high

galactic latitudes ($|b|$~50 degree). Since the attitude control of the SFU was stable within 1', the scan paths were aligned almost regularly with an interval of about 4' on the ecliptic plane. At high ecliptic latitudes, the scan paths had a higher density, but there were some gaps corresponding to the times of the spin axis changes. Two scan modes together covered about 2700 deg^2 of the sky.

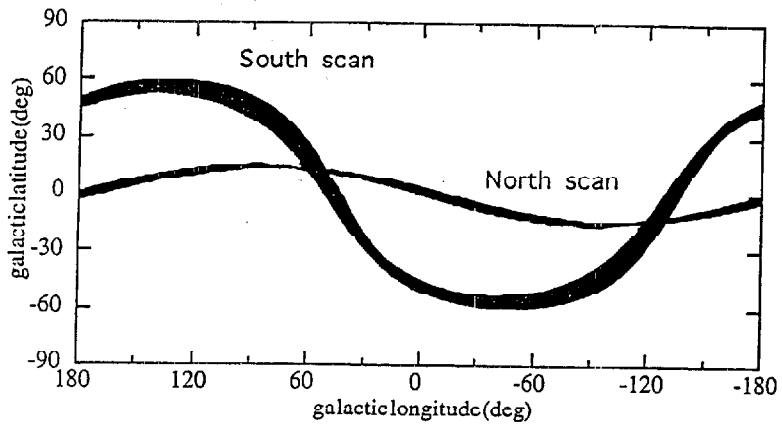

Fig.4 Sky region observed by the IRTS. The scan paths are plotted in the galactic coordinates. Two strips are the observed area in the north-scan mode and the south-scan mode.

3.3. Cryogenics and focal plane instruments

The operation of the cryogenic system throughout the mission was as predicted[13]. Figure 5 shows temperatures of the helium tank (Tank), porous plug (PP) and forebaffle (FG) during the IRTS mission. The helium tank temperature gradually rose and settled to an equilibrium temperature of about 1.9 K within 70 hours after the valve was opened. At the periods of the ^{3}He condensation of the FIRP, thermal pulses were observed. Later condensation caused higher temperature pulses since the liquid helium mainly carried the heat capacity and its content was decreasing. The holding time of the liquid helium was about 38 days, which was consistent with the predictions based on the ground testing.

We should note that the avoidance requirements set by the baffling system (see figure 2) were violated for several days around the north-to-south flip maneuver. During this time, the scattered sun light and the thermal emission from the earth limb directly illuminated the forebaffle. This caused a temperature rise of the forebaffle up to a maximum of 13 K. Figure 6 indicates the temperature variation of the forebaffle for one orbital phase at the worst condition. The forebaffle temperature amounted to 12K at the sub-solar point where both of the earth and the solar avoidance angles were minimum. This implies that the scattered sun light is a dominant heat source, and the reflectance for the infrared radiation is high enough. Even at this case, no excess emission due to this temperature rise was detected. Figure 7 shows dependence of the 700 μm sky brightness observed by the FIRP on the forebaffle temperatures near the sub-solar point. No clear correlation is found, which means that thermal radiation of the forebaffle was negligible.

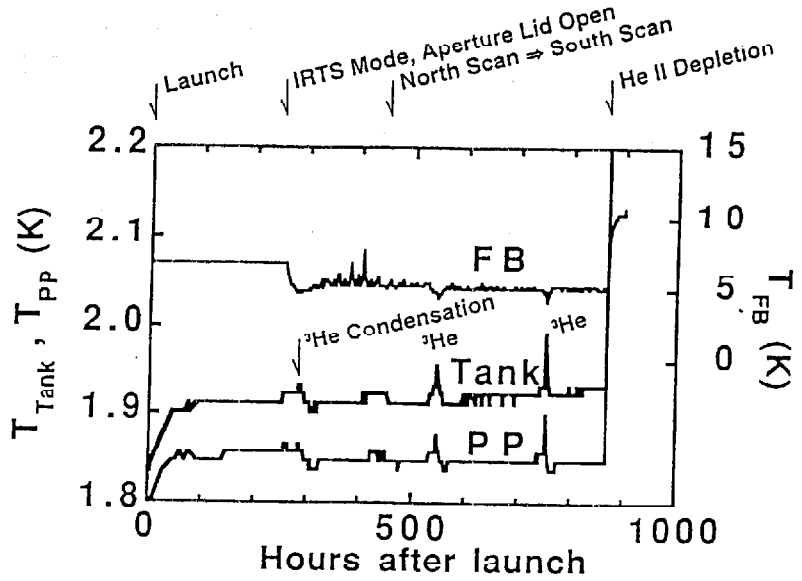

Fig.5 Overall thermal performance of the Helium tank (Tank), porous plug (PP) and forebaffle (FB) are shown. Major thermal events are also indicated.

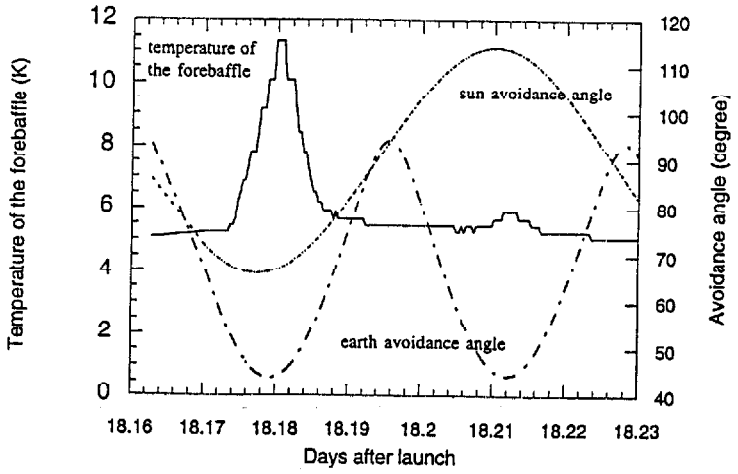

Fig.6 Variation of the forebaffle temperature for one orbital phase at the worst thermal condition. Sun and earth avoidance angles are also shown.

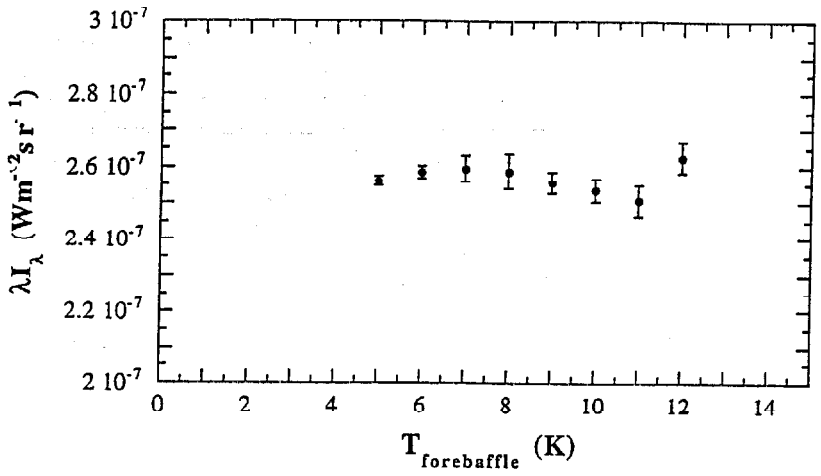

Fig.7 Dependence of the sky brightness at 700 μm on the forebaffle temperature at the sub-solar point.

The infrared sensors functioned almost as expected. When the SFU passed through the South Atlantic Anomaly (SAA; an area of anomalous geomagnetic field near Brazil), charged particles generated continual spikes on the signals of all the infrared detectors. The SAA passages also caused increases in the dark current in the InSb photodiodes of the NIRS and in the Si:Bi photoconductors of the MIRS. The responsivities of photoconductors, Si:Bi detectors of the MIRS and Ge:Ga detectors of the FILM, also increased in the SAA. Bias boosting, a curing method for radiation effects of the FILM[11] was found to be very effective.

The NIRS observed the emission which was thought to originate from the gas released from the spacecraft surfaces. The emission was seen at wavelengths around 2.8 μm and at a fixed phase of the orbital revolution in the day side. It was bright at the beginning of the mission ($\lambda I_\lambda = 10^{-6}$ W m^{-2}sr^{-1}) and exponentially decayed with a time constant of about 5 days. The NIRS was otherwise quite normal and the sensitivities were determined by the star confusion at short wavelengths. The MIRS and the FILM almost achieved their designed sensitivities. The MIRS sensitivity was limited by zodiacal background emission over most of its wavelength range. The final data accuracies of the MIRS and the FILM depend on how accurately the responsivity changes due to the radiation effects can be modeled. Excess noises observed in 150, 400 and 700 μm channels of the FIRP somewhat degraded the data quality. The origin of this excess noise is still unknown. The details of the flight performance of the FPIs are described in this volume.

The SFU was retrieved in January, 1996 by NASA's Space Shuttle Endeavor. Post-flight re-calibration being planned for some FPIs will further improve the data quality from these instruments.

4. DATA REDUCTION

The entire IRTS data set amounted to almost 2 Gbytes. Those portions of the data separately downlinked to the ground were sorted into time order and concatenated. A rough estimate of the telescope pointing was made using the data from the

gyroscopes and the orbital elements, and added to the above data set. The accuracy of this preliminary pointing reconstruction was about one degree.

The accurate pointing reconstruction are now being performed by the NASA/Infrared Data Processing and Analysis Center (IPAC). In this analysis, the data from the star sensor have been included. The star sensor data had a high enough signal-to-noise ratio for the stars brighter than 6th magnitude at J band for position reconstruction, although source confusion reduced the available number of stars near the galactic plane. To date, the pointing reconstruction for the observation period from April 10th to April 24th has been completed. Preliminary analysis of the point sources detected by the MIRS show that the telescope pointing thus determined is accurate to within about 2'. Basic analysis of the infrared data including flux calibrations have been completed for the data in the period where the more accurate pointing is known.

5. ACKNOWLEDGEMENTS

The authors would like to thank the SFU project team for their support in all aspects, including the integration of the instruments, the flight operation, and the preparation of data on the orbit and attitude of the spacecraft. The authors are grateful to other IRTS members for their collaborative works. The authors also thank IPAC for their help in the pointing reconstruction of the IRTS.

6. REFERENCES

1. G. Neugebauer et al., "The Infrared Astronomical Satellite (IRAS) Mission", Astrophys J., Vol. 278, L1-L6, 1984.

2. G. J. Melnick et al., "Preliminary Results of the Space Lab-2 Infrared Telescope Survey of the Galactic Plane at 2.4μm", in AIP Conf. Proc. 155, The Galactic Center, ed. D.C.Backer (New York: AIP), pp. 157-161, 1987.

3. N. W. Boggess et al., "The COBE Mission: Its design and Performance Two Years After Launch", Astrophys.J., Vol. 397, pp. 420-429, 1992.

4. M. Natori, and K. Kuriki, "SFU Mission One Experiments", Space Technology Vol. 11, pp. 159-165, 1991.

5. H. Murakami et al., "The Infrared Telescope in Space (IRTS)", Astrophys.J., Vol. 428, 354 -362, 1994 (Paper I).

6. G. Fujii et al., "Thermal and Mechanical Performance of Superfluid Helium Dewar for IRTS" 1990, in Advanced Cryogenics Engineering, Vol. 37, ed. R.W. Fast (New York: Plenum Press), pp. 1359-1366, 1992.

7. J. J. Bock et al., "Performance of a Cooled Baffle System for Space-born Infrared Telescope", Appl. Optics, Vol. 34, 2268-2277, 1995.

8. T. Onaka et al., "Optical System of the Infrared Telescope in Space", Appl. Opt. Vol. 33, pp. 1880-1888, 1994.

9. M. Noda et al., "Near Infrared Spectrometer on the Infrared Telescope in Space", Astrophys.J. Vol. 428, pp. 363-369, 1994.

10. T. L. Roellig et al., "The Mid-Infrared Spectrometer on the Infrared Telescope in Space" Astrophys.J., Vol. 428, 370-376, 1994.

11. H. Shibai et al., "Far-Infrared Line Mapper (FILM) on the Infrared Telescope in Space", Astrophys.J., Vol. 428, pp. 377-392, 1994.

12. A. E. Lange et al., "The Far-Infrared Photometer on the Infrared Telescope in Space", Astrophys.J., Vol. 428, 384-392, 1994.

13. G. Fujii et al., "On-Orbit Thermal Behavior of the IRTS Cryogenic System", Cryogenics, in press.

accept ed for Proceedings of SPIE 2744, Infrared Technology and Applications XXII, ed. B. F. Anderesen and M. S. Scholl

Flight performance of the Infrared Telescope in Space (IRTS)

Hiroshi Murakami, Hiroshi Shibai

The Institute of Space and Astronautical Science, Research Division for Space Astrophysics
3-1-1 Yoshinodai, Sagamihara, Kanagawa 229, Japan

Takashi Onaka

The University of Tokyo, Department of Science
2-11-16 Yayoi, Bunkyo-ku, Tokyo 113, Japan

Takanori Hirao

Nagoya University, Department of Science
Furo-cho, Chikusa-ku, Nagoya 464-01, Japan

ABSTRACT

The Infrared Telescope in Space (IRTS) is a cryogenically-cooled 15cm telescope onboard the Space Flyer Unit (SFU), a small space platform. The SFU was launched in March 1995 by Japanese H-2 rocket and retrieved by NASA's Space Shuttle in January 1996 after successful execution of the mission. The IRTS has performed an infrared sky survey successfully in the wavelength range from 1.4μm to 700μm. About 7% of the entire sky has been surveyed.

The cryogenic system of the IRTS held the telescope and the focal plane instruments at a stable temperature of 1.9K for more than one month. The infrared sensors worked well, although remarkable radiation effects were observed especially at the South Atlantic Anomaly. We need further analysis to clean these radiation effects, but the obtained data will give important scientific information on the interstellar matter, extragalactic background light.

keywords; IRTS, SFU, space, infrared astronomy, space cryogenics

1. INTRODUCTION

The Infrared Telescope in Space (IRTS)[1] is a Japanese satellite-borne infrared telescope. The IRTS was designed as one of the user payloads onboard the Space Flyer Unit (SFU)[2], which is a multi-purpose satellite providing a platform for space experiments in various fields such as biology and material science. The IRTS contained a 15cm telescope cooled with super-fluid liquid helium. Its mission was an infrared survey of diffuse celestial components with a wider wavelength coverage than the IRAS[3] and a higher spacial resolutions than the COBE[4] mission. The major astronomical objectives were the interstellar gas and dust, the circumstellar dust, the interplanetary dust and the near-infrared extra-galactic background light.

The SFU which had the IRTS onboard was successfully launched on March 18th, 1995 by a Japanese launch vehicle H-2. More than ten experiments had been completed almost on schedule, and the SFU was recovered by NASA's Space Shuttle on January 13th, 1996. The IR survey with the IRTS was performed at the beginning of mission period, prior to other experiments. The IRTS operated normally throughout the observation period of about a month. About 7% of the whole sky was surveyed and the data amounted to 2 GBytes.

In the following sections, we describe an outline of the IRTS instrumentation (§2), the flight operations (§3) and the flight performance (§4).

2. IRTS INSTRUMENTATION

Details of the IRTS hardware are described by Murakami et al. (1994)[1]. We summarize the important features here.

The IRTS telescope[5] is a Rechey-Chretien type cooled telescope. The effective diameter of the primary mirror is 150mm and the synthesized focal length is 600mm. The primary mirror, the secondary mirror and the supporting system were all made of an aluminum alloy in order to minimize the effect of thermal deformation.

The IRTS containes four focal-plane instruments for infrared observation. They are the Near Infrared Spectrometer (NIRS)[6], the Mid Infrared Spectrometer (MIRS)[7], the Far Infrared Line Mapper (FILM)[8] and the Far Infrared Photometer (FIRP)[9]. The NIRS and the MIRS are grating spectrometers and together cover the wavelength range from 1.4μm to 11.7μm almost continuously with low spectral resolution. The FILM is also a grating spectrometer dedicated to the observation of the far-infrared lines emitted by interstellar carbon ions at 158μm and neutral oxygen atoms at 63μm. The FIRP is a four channel photometer which covers the sub-millimeter region with wavelengths of 150, 250, 400 and 700μm. The FIRP has a compact closed-cycle ^{3}He refrigerator to cool the bolometers to 0.3K. The refrigerator consists of two parts, a liquid ^{3}He container (an evaporator) and a charcoal-filled sorption pump. The ^{3}He gas is absorbed at low temperatures inside the charcoal and is released by heating the pump. The ^{3}He gas then condensed in the evaporator. The sorption pump is then cooled and pumps back the ^{3}He gas, which lowers the temperature of the evaporator.

Each instrument has a cold shutter and an internal calibration source. These were operated periodically during the observations and provided zero signal levels and references for the responsivities. The optical paths and major features of the instruments are given in Fig. 2 to Fig. 5. In addition to the these instruments, a Ge photodiode is put on the focal plane as a star sensor.

The baffling system of the IRTS consists of a deployable sun shield, an aperture shade, a reflecting forebaffle and a black aftbaffle (see Fig.1). A unique feature of this baffling system is the forebaffle. It reflects back the infrared light emitted by the aperture shade and reduces the heat load on the liquid helium.

The telescope and the focal-plane instruments are installed in a liquid helium cryostat[10] and cooled to 1.9K. The cryostat has a helium tank with a capacity of 100 liters and three nested vapor-cooled shields. The helium gas evaporats through a porous plug phase separator, which first cools the forebaffle and then cools the vapor-cooled shields.

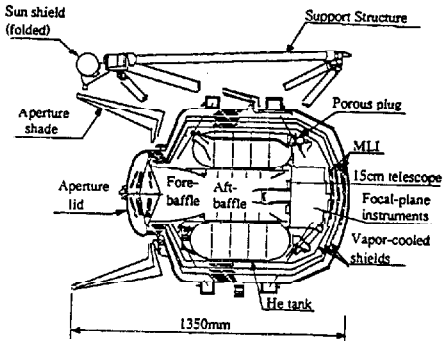

Fig. 1. Cross sectional view of the IRTS.
The sun shield becomes 2-meter long when it is deployed.

3. FLIGHT OPERATION

The SFU was launched at March 18 8:01 UT. The liquid helium tank of the IRTS was filled with super-fluid liquid helium 26 hours prior to the launch. A vapor evacuation was continued until 12 hours before launch to keep the super-fluid state and then the tank was closed up. The helium temperature was below 1.7K and the quantity of the helium was 84 liters at the moment of valve off. About 29 minutes after launch, 15 minutes after the SFU was launched into the orbit, the IRTS electric power was turned on and the pumping of the He gas through the porous plug into the outer space started.

The first 11 days were spent on the checkout of the SFU core system and the science payloads, including the IRTS. The SFU went up from a low-altitude orbit to a circular experiment orbit with an altitude of 486km and an inclination angle of 28 degrees.

At 18:00 on Mar. 29 UT all focal-plane instruments were turned on and the sun shield was deployed. The attitude control mode of the SFU was changed from the sun-pointing mode to a special mode for the IRTS survey at 23:49. The IRTS started the survey observations by ejecting the aperture lid just after the attitude change.

The cooling operation of the FIRP ^{3}He refrigerator started at 10:25 on Mar. 30 and lasted for about 14 hours. The FIRP

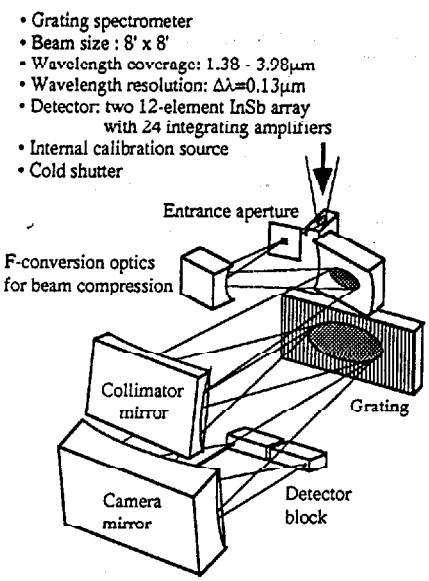

Fig. 2. The Near Infrared Spectrometer (NIRS)

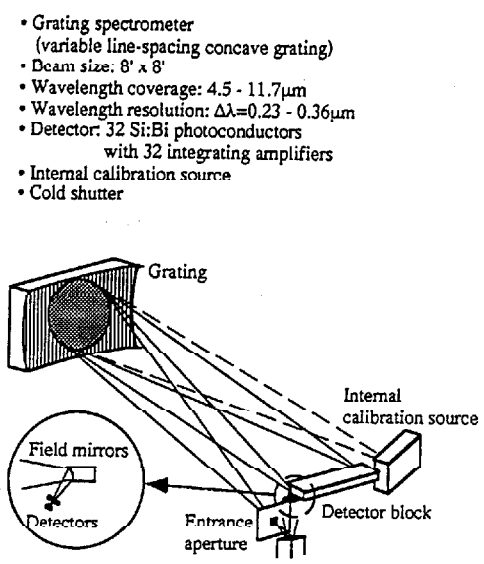

Fig. 3. The Mid Infrared Spectrometer (MIRS)

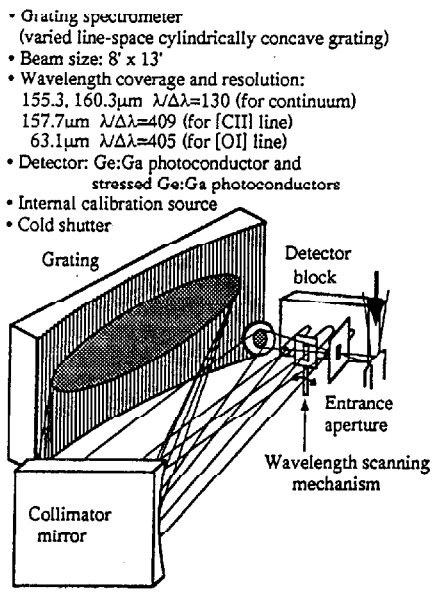

Fig. 4. The Far Infrared Line Mapper (FILM)

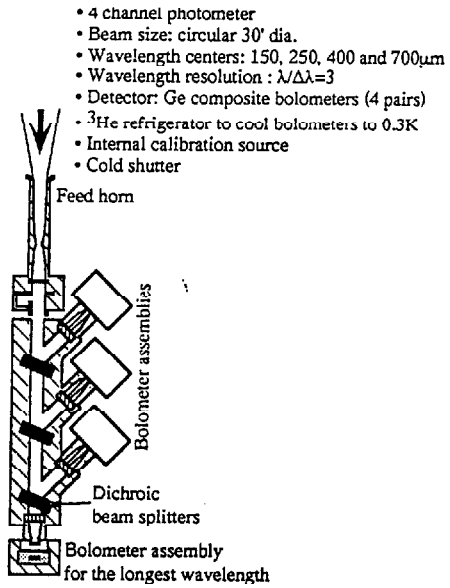

Fig. 5. The Far Infrared Photometer (FIRP)

joined the sky survey at that time. The refrigerator was cycled two more times during the observation with an interval of 7 days.

In the IRTS survey mode, the telescope scanned the sky as the SFU rotated once an orbital revolution. The rotation axis was perpendicular to the optical axis of the telescope and it was pointed nearly to the sun. The telescope was directed in the opposite direction from the earth center at the day-night border and to either the north or south at the centers of the day side and the night side. At first the IRTS was directed to the north in the day side and southward in the night side because the orbit passed northern side of the sub-solar point and therefore the avoidance conditions were better for the northern sky in the day side. The avoidance conditions varied as the ascending node shifted due to the precession. On April 5th, the IRTS met with the worst condition where the sun passed the zenith for the satellite, and then the observations of southern sky in the day side became advantageous. The attitude mode was changed at 20:36 on April 5th UT to cope with this situation. The IRTS observed the southern sky in the day side and the northern sky in night after that.

During the survey an automatic sequence for calibration of the infrared detectors was executed once every 1049sec (1024 x 1.024sec) except for the FIRP, which had an calibration sequence every 262 seconds. Although the detailed calibration procedures of the focal-plane instruments were different from each other, the essential parts were common, i.e. closing the cold shutters and lightening the internal calibration sources. In addition to the above sequence, the calibration source of the FILM and the cold shutter of the FIRP were used for frequent calibration and backround subtraction.

A bias boosting was executed after each passage of the South Atlantic Anomaly in order to cure the radiation effect on the Ge:Ga photoconductors of the FILM. The resetting of the charge accumulated in the charge-integrating amplifiers of the NIRS was made every 1 minute. The time interval was shortened to 1sec when the Galactic plane was observed to keep the signals within the dynamic range of the final-stage amplifiers.

All the liquid helium was exhausted at 09:27 on Apr. 24 UT. The electric power of the focal-plane instruments except for the NIRS was turned off within several hours from the helium exhaustion. The NIRS worked almost one more day, although a large signal drift due to the rise in temperature was seen.

The sun shield was jettisoned and the helium tank was directly opened to outer space without the porous plug for the sake of safety in the retrieval operation by the Space Shuttle. Finally all the electric power for the IRTS was turned off at 16:06 on April 26 UT.

4. FLIGHT PERFORMANCE

4.1. Cryogenic System

The IRTS cryogenic system generally operated as expected from the pre-flight testing[11].

The helium tank temperature settled to an equilibrium temperature of 1.91K within 70 hours after the evacuation of the helium tank started in the orbit. After that the temperature was very stable and no anomalous thermal behavior was observed until 9:27 on April 24 UT when all the helium was exhausted. The cold life was found to be fairly close to the prediction based on the ground test data.

The temperature of the forebaffle, which was cooled by evaporated helium gas, was usually 5K, low enough even for the sub-millimeter observations. However, a temperature rise up to 13K was observed in the bad avoidance conditions on Apr. 5, where the day-side earth limb directly illuminated the forebaffle. The infrared signals were not affected even in this case, indicating that the design of the baffling system was adequate.

4.2. Focal plane instruments

4.2.1. NIRS

The actual flight performance of the NIRS demonstrated that the InSb photodiodes had excellent characteristics. The variation of the responsivities of the photodiodes throughout the observation period was less than 5%, within the uncertainty of the internal calibration source itself. The radiation effects in the South Atlantic Anomaly (SAA) caused continual spikes in the signal and a large increase of the dark current. But the dark current recovered to the normal level with a time constant of 20min after the SAA passage and no responsivity change was observed.

The absolute values of the responsivities agreed with the pre-flight measurements within 10% for the shorter-wavelength array and 20% for the longer-wavelength array. Since many bright stars are available as calibration sources in the near-infrared region, we expect a final photometric accuracy of 2 to 5%.

The noise characteristic of the detection system was evaluated using the data obtained before the ejection of the aperture lid.

The resulting readout noises were about 300 electrons for all the channels, which was a factor of 2 to 3 larger than those measured in the pre-flight testing of the NIRS alone. The power spectra had a steeper gradients than 1/f in the frequency range below 0.1Hz. These low-frequency noises determined the NIRS detection limits. The detection limits of the NIRS for the diffuse celestial components are shown in figure 6. These limits are still deep enough to search for faint extra-galactic background lights. In this figure, we also show the observed fluctuations of the sky brightness in the dark sky areas with high galactic and ecliptic latitudes. These fluctuations are a few times larger than the dark noise at wavelengths shorter than 2.5μm and are thought to be caused by unresolved stars. The NIRS sensitivities are actually limited by these star confusion in the shorter wavelength channels.

Although the major scientific targets of the NIRS were continuum or broad band emissions from diffuse sources, more than 10,000 point sources were detected. The detection limits for these point sources are shown in figure 7.

4.2.2. MIRS

It is well known that extrinsic type photoconductors are very much affected by high energy radiation. The effects of the SAA passage were noticeable also for the Si:Bi detectors employed in the MIRS. The flight data showed that the responsivities changed proportionally to the total radiation dose during the SAA passage, and the responsivities recovered exponentially with a typical time constant of about 1000sec.

The dark currents measured in space were about twice those measured on the ground. It is not clear if this excess dark current is due to the radiation effect or not, because the dark current did not change noticeably with a single SAA passage.

The detection limits of the MIRS for the diffuse sources depend on how far we can remove these anormalous effects. As the detailed modeling of the detector behavior is still under way, the detection limits shown in figure 6 are very conservative estimates. They will be improved by further analysis.

The situation for the point source observations is better, because both the responsivities and the dark currents do not change for a short duration, 2sec, of a point source crossing through the field of view. Although the radiation effects influence the photometric accuracies, the detection limits are determined by the statistical errors due to the zodiacal light at longer wavelengths. The 3σ detection limits are shown in figure 7.

4.2.3. FILM

Large radiation effects were observed also for the Ge:Ga detectors of the FILM. However, the FILM had a bias boost capability, which was very effective. Bias voltages twenty times higher than normal were applied for one minute after every SAA passage. The responsivities increased about twice during the SAA passages, and cured immediately to levels within 20% of the base levels by bias boosting.

The base levels of the Ge:Ga responsivities were found to be about three times larger than those measured on the ground. This may also be due to the radiation effects, but the base levels of the responsivities were fairly stable and not affected by the bias boosting.

The responsivity change when a bright source was observed, which is also well known for the photoconductors, was small compared with the effects of cosmic rays. The flight data of the FILM showed that it had good enough sensitivities to observe the faint [CII] line emission from the general cirrus clouds at high galactic latitude. Figure 6, 7 and 8 show the detection limits determined only by statistical errors for the continuum emission from diffuse and point sources, and the [CII] line emission, respectively. The sensitivity of the [OI] channel has not yet been evaluated.

4.2.4. FIRP

The ^{3}He refrigerator of the FIRP worked as expected. The time dependence of the temperatures of the evaporator and the charcoal pump exactly reproduced those observed in the pre-flight tests. The evaporator achieved a temperature of 300mK. The design lifetime of the cold phase was more than ten days. Although the lifetime was not confirmed in orbit, because it was recycled every 7 days, no sign of exhaustion of the liquid ^{3}He was observed within 7 days.

The signal of the 250μm channel was quite normal and showed a high sensitivity. The sensitivity of that channel was almost the same as that achieved during a one-year mission by DIRBE on the COBE satellite. However, we observed excess noise in other three channels. The excess noise may be due to electromagnetic interference, but the origin of the noise is not certain. The preliminary sensitivities of the FIRP are shown in figure 7. Those sensitivities are still high enough for the investigation of the temperature distribution of the interstellar dust particles across the galactic plane.

4.2.5. Star sensor and pointing reconstruction

The performance of the star sensor was consistent with the prediction from the ground based testing. The 1σ detection limit was about 8th magnitude at J-band. We can use stars brighter than 6th magnitude for the pointing reconstruction. The reconstruction is now being performed by NASA's Infrared Processing Analysis Center (IPAC) using the data from this star sensor and the gyros.

The official specification for the attitude control stability of the SFU was 1 degree, but the actual stability was found to be much better, as well as 1 arcmin in quiescent conditions. Thanks to this control stability and the good performance of the star sensor, an accuracy of pointing determination of ±1 arcmin is expected.

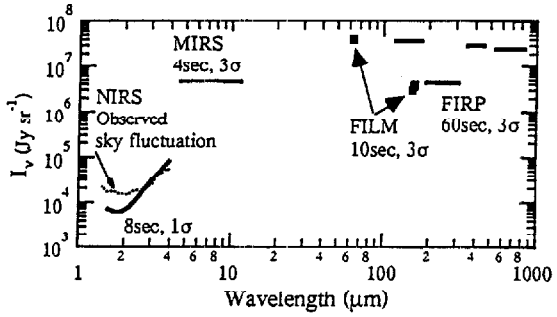

Fig. 6. IRTS detection limits for diffuse sources.

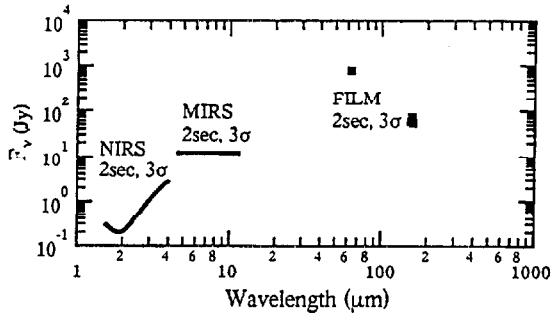

Fig. 7. IRTS detection limits for point sources.

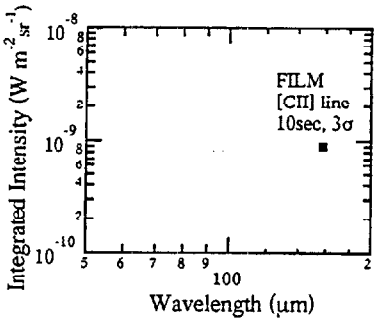

Fig. 8. IRTS detection limit for [CII] line.

5. CONCLUSION

The IRTS mission successfully performed in March and April, 1995. The main results of this mission are;

- The SFU and the IRTS systems operated normally in space. Especially, the attitude control of the SFU was very stable. The mechanical actions of the IRTS such as the aperture lid ejection, sun shield deployment and jettison, as well as the operations of the cold valve were all successful.
- The cooling life of the liquid helium cryostat was 38 days, as predicted. No anomalous thermal behavior was seen in the cryogenic system.
- The focal plane instruments generally worked well. The InSb photodiodes showed excellent performance characteristics. The radiation effects on the photoconductive detectors were remarkably strong, but those effects on the astronomical data will be sufficiently cleaned using the cold shutter and the internal calibrators.

The SFU was recovered on January 13th 1996. A re-calibration is planned for some focal-plane instruments. In addition, we can investigate all phenomena on the IRTS resulting from the stay in space for 10 months. This unique post-flight hardware analysis will increase the reliability of the IRTS data, and will be helpful for the future projects.

6. REFERENCES

1. H. Murakami et al., "The Infrared Telescope in Space (IRTS)", Astrophys. J., Vol. 428, pp. 354-362, 1994.
2. M. Natori and K. Kuriki, "SFU Mission-1 Experiments", Space Technology, Vol. 11, No. 4, pp. 159-165, 1991.
3. G. Neugebauer et al., "The Infrared Astronomical Satellite (IRAS) Mission", Astrophys. J., Vol. 278, pp. L1-L6, 1984.
4. J. C. Mather, "The Cosmic Background Explorer (COBE)", Opt. Engineering, Vol. 21, No.4, pp. 769-774, 1982.
5. T. Onaka et al., "Optical System of the Infrared Telescope in Space", Applied Optics, Vol. 33, pp. 1880-1888, 1993.
6. M. Noda et al., "Near-Infrared Spectrometer on the Infrared Telescope in Space", Astrophys. J., Vol. 428, pp. 369, 1994.
7. T. Roellig, T. Onaka, T. McMahon and T. Tanabe, "The Mid-Infrared Spectrometer on the Infrared Telescope in Space (IRTS) Mission", Astrophys. J., Vol. 428, pp. 370-376, 1994.
8. H. Shibai et al., "Far-Infrared Line Mapper (FILM) on the Infrared Telescope in Space", Astrophys. J., Vol. 428, pp. 377-383, 1994.
9. A. E. Lange et al., "The Far-Infrared Photometer on the Infrared Telescope in Space", Astrophys. J., Vol. 428, pp. 384-392, 1994.
10. M. Murakami, H. Okuda, T. Matsumoto, G. Fujii and M. Kyoya, "Design of Cryogenic System for IRTS", Cryogenics, Vol. 29, No. 5, pp. 553-558, 1989.
11. G. Fujii et al., "On-Orbit Thermal Behavior of the IRTS Cryogenic System", Cryogenics, in press.

accept ed for Proceedings of SPIE 2817, Infrared Spaceborne Remote Sensing IV , ed. M. S. Scholl and B. F. Anderesen

Flight performance of the Near-Infrared Spectrometer

Manabu Noda

Nagoya Municipal Industrial Research Institute, 3-4-41 Rokuban, Atsuta-ku, Nagoya 456, Japan

Toshio Matsumoto, Hiroshi Murakami, Mitunobu Kawada

The Institute of Space and Astronautical Science, Sagamihara, Kanagawa 229, Japan

Masahiro Tanaka

Department of Astrophysics, Faculty of Science, Nagoya University
Chikusa-ku, Nagoya 464-01, Japan

Shuji Matsuura

Communications Research Laboratory, 588-2 Iwaoka, Nishi-ku Kobe 651-24, Japan

Hongfeng Guo

Beijing Astronomical Observatory, Chinese Academy of Science, Beijing 10080, China

ABSTRACT

The Near-Infrared Spectrometer (NIRS) is one of the focal plane instruments of the Infrared Telescope in Space (IRTS). The NIRS is a simple grating spectrometer with two 12 element InSb linear arrays, and was designed to measure the absolute sky brightness at the wavelengths from 1.4 to 4.0 μm with a spectral resolution of 0.13 μm and a beam size of 8' × 8'. The IRTS was launched on 1995 March 18. The NIRS worked well throughout the observation period from March 29 to April 25, and scanned about 7% of the entire sky. Multiple passage of bright stars through the NIRS field of view enabled us to reconstruct the beam pattern and to calibrate the sensitivity. Those flight data confirmed good performance of the NIRS on the orbit as was expected from the preflight measurements.

Keywords : IRTS, NIRS, instrumentation, infrared astronomy

1. INTRODUCTION

The origin of the light of the night sky has been one of the interesting subjects of astrophysics. The diffuse near-infrared celestial emission mainly consists of the zodiacal light, thermal emission from the interplanetary dust particles, the starlight in our Galaxy and the extragalactic background light. The Diffuse Infrared Background Experiments (DIRBE)[1,2] on the COBE satellite obtained absolute brightness maps of the full sky. However, the DIRBE observations were limited in four photometric bands in the near-infrared range. The Near-Infrared Spectrometer (NIRS) on the Infrared Telescope in Space (IRTS)[3] was designed to measure the near-infrared spectrum of the diffuse emission[4]. The NIRS surveyed about 2,700 square degrees in the observation period of about a month. Although the surveyed sky area was not wide as the DIRBE/COBE, the spectrum in the wavelength range from 1.4 to 4 μm obtained by the NIRS gave us new information such as the unidentified infrared (UIR) band emissions[5]. In this paper, we describe the performance of the NIRS based on the in-flight data.

2. INSTRUMENTATION

The NIRS is one of the four focal plane instruments of the IRTS. It is a grating spectrometer with two 12-elements InSb linear arrays. The NIRS as well as the telescope and other focal plane instruments were cooled with superfluid liquid

helium. The schematic view of the optical system is shown in figure 1. The 1.4 mm × 1.4 mm entrance slit is located at the IRTS telescope focus. The light entered through the slit is compressed in Z-direction by F-conversion optics (CM1 and CM2) to reduce the height of the spectrometer. The beam is made parallel by the parabolic mirror (PM), diffracted by the grating and focused again on the detector by the spherical mirror (SM). The two 12 element InSb lineal arrays are aligned in the focal sphere, and each of them has an order-sorting band pass filter. The wavelength range of the shorter wavelength array is from 1.43 to 2.54 μm and that of longer wavelength array is from 2.88 to 3.98 μm. The characteristics of the NIRS are summarized in Table 1.

In order to check D.C. drifts of the electronics and to measure the zero signal level, a cold shutter is located behind the entrance slit and was closed for 8.192 seconds every 65.54 seconds automatically. A small wolfram lamp is installed near the shutter for an internal calibrator, which turned on for 8.192 seconds every 17.5 minutes to monitor the stability of the instrumental response.

Charge integrating amplifiers were employed to read out the photocurrents from the InSb photodiodes. The element size of the InSb is 1 mm by 0.5 mm and the total capacitance, including stray capacitance, is about 50 pF. The typical dark current at 2K is several times 10^{-17} A. The integrated charges are periodically discharged every 65.54 seconds through a reset FET. The full well capacity is typically 3×10^7 electrons. The actual dynamic range of this detection system was limited to 10% of the full well by a following electronics to keep the linearity.

Table 1 Characteristics of NIRS

Characteristic	Value of Specification
Size (mm^3)	135 × 154 × 102 overall
Weight (kg)	1.18
Entrance Aperture (mm^2)	1.4 × 1.4
Field of View ($arcmin.^2$)	8 × 8
Temperature (K)	~1.8
Detection System:[a]	
Detector	InSb
Element size (mm^2)	1 × 0.5 (per element)
Number of elements	24 (2×12 elements)
Wavelength coverage (μm)	1.43 – 2.54, 2.88 – 3.98[b]
Resolution (μm)	0.12 (0.10 at channel 1)
Dark current (A)	several times 10^{-17}
Total capacitance (pF)	~50
Readout method	Charge-integrating amplifier
Temperature of J-FETs (K)	~70

[a] Two 12 channel linear arrays with low-resolution grating spectrometer.
[b] 0.1 μm interval.

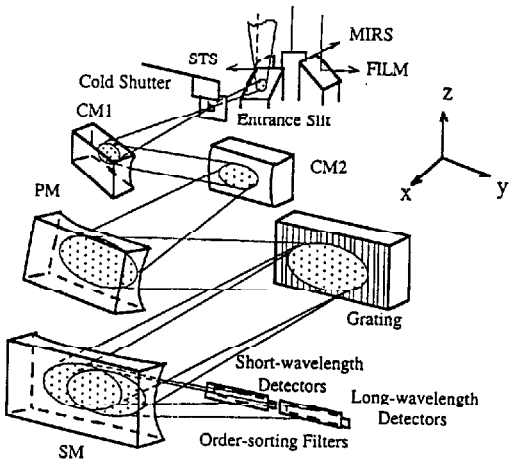

Fig. 1. The schematic view of the optical system of the NIRS.

3. OBSERVATIONS

The IRTS onboard the first Space Flyer Unit mission (SFU-1) [6] was launched from Tanegashima Space Center at 08:01 UT on March 18, 1995. The IRTS orbited the earth with the telescope sweeping across the sky at a rate of 3.'82 /sec along great circles, and approximately 7% (2,700 square degrees) of the sky was observed from March 29 to April 25 [7].

Typical charge integration curves of the NIRS and their differentials are shown in figure 2. The charge reset

timings are shown by arrows in this figure. In the middle of the charge integration period, the cold shutter was closed for 8.192 seconds, which caused flat integration curves. Several point sources can be seen in this figure. More than 10,000 point sources were detected through the whole observation period. Near the galactic plane, when the sky was expected to be so bright as to saturate the signal in the 65.54 seconds charge integration period, reset interval was changed to the 1 second.

The IRTS data were normally collected at a rate of 6 kbps and the sampling frequency for each detector of the NIRS was 3.9 Hz. When an overflow of the onboard data recorder was expected, the data rate was changed to 3 kbps and the data of the even channels were skipped and abandoned to reduce the sampling frequency.

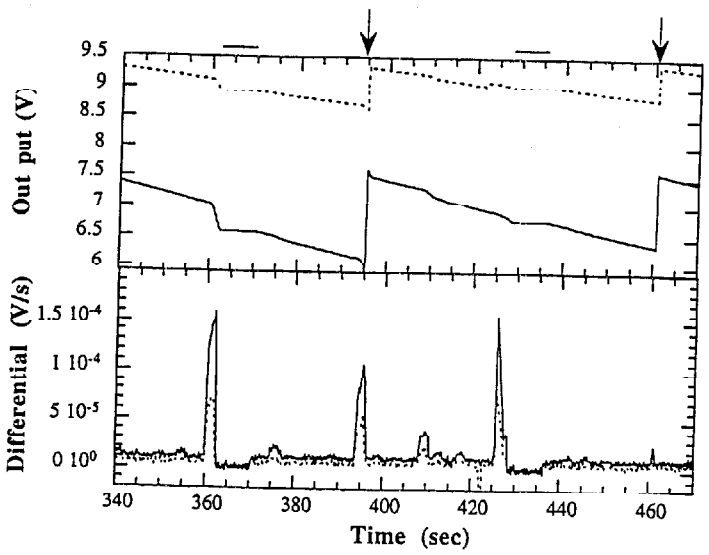

Fig. 2. Integrating output voltages (top) and the differentials (bottom) of 1.64 μm channel (solid line) and 2.23 μm channel (dashed line). The charge reset timings are shown by arrows. In the middle of the charge integration period shown by holizontal bars, the cold shutter was closed for 8.192 seconds, which caused flat integration curves. Spike-like signals in the differentials are point sources.

3.1. The influence of the SAA

When the IRTS passed through the South Atlantic Anomaly (SAA: an area of anomalous geomagnetic field near Brazil), high-energy charged particles generated continual spikes on the signals of the detectors. The high energy radiation also caused a change of the dark signal levels which is determined by the dark current and the drift of the electronics. Figure 3 shows the time variation of the differential of the output voltage of one of the 24 channels when the cold shutter was closed. This figure shows that the zero levels increased after the spacecraft passed the SAA. The zero levels slowly decreased to the previous levels in about 30 min.

The output levels for the calibration lamp are plotted for one day in figure 4. Typical 1σ error is shown by the vertical bar. The responsivity of the NIRS did not change even in the SAA. Photoconductive detectors such as Ge:Ga are

known to be changed the response by the high energy particles, but photovoltaic InSb detectors did not show serious damages. The responsivity also have not changed through the observation period with in the error.

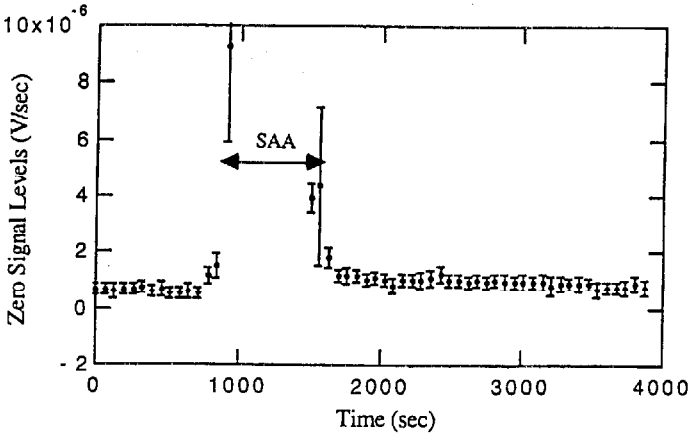

Fig. 3. The time variation of the differential of the output voltage of the 2.14 μm channel when the cold shutter was closed. The zero levels increased after the spacecraft passed the SAA. The zero levels slowly decreased to the previous levels in about 30 min.

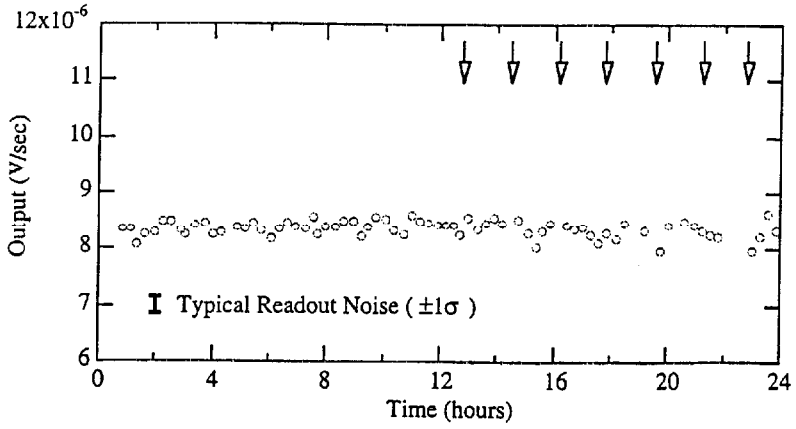

Fig. 4. The differential of theoutput voltage of the 2.14 μm channel for the calibration lamp for one day. The timing when the satellite came into the SAA are shown by arrows. The responsivity of the detector did not change even in the SAA.

3.2. Light leak from the shutter

The outputs of some shortest wavelength channels correlated the sky brightness even when the cold shutter was closed, which showed that there were some light leaks. Small fraction of the light focused on the shutter might penetrated into the spectrometer through the gap between the entrance slit and the shutter. The leakages are shown in table 2. Those are significant in the six shortest wavelength channels and negligible small in longer wavelength channels.

3.3. Non-linearity after the charge reset

After the reset, an anomalous behavior could be seen as shown in figure 5. Open circles show mean out put level of the 3.68 μm channel and the reset switch turned on at t=0. Infrared laboratories, inc. reported[8] that the reset anomaly arises when the reset switch is left closed for extended periods of time and is eliminated by the closing the switch for only a few milliseconds. According to the report, we kept the reset switch close for a short time, but the phenomenon has not completely disappeared. Since the shapes of the reset anomaly were almost same, we corrected it by exponential fitting with a time constant common for all channels:

$$y = \alpha+\beta\cdot t+ \gamma\cdot\exp(-t /t_0)$$

where y (V) is the output voltage, t (s) is time after reset, t_0 (s) is the time constant and α, β, γ are fitting parameters. Parameter β represents the photocurrent. The exponential and the linear part of the fitted function are separately shown in figure 5, by a solid curve and a dashed line, respectively.

Table 2. Light leak from the shutter

wavelength (μm)	light leak (%)
1.43	3.9
1.53	3.5
1.63	2.6
1.73	2.1
1.83	1.5
1.93	1.4
2. 03~3.98	< 1.0

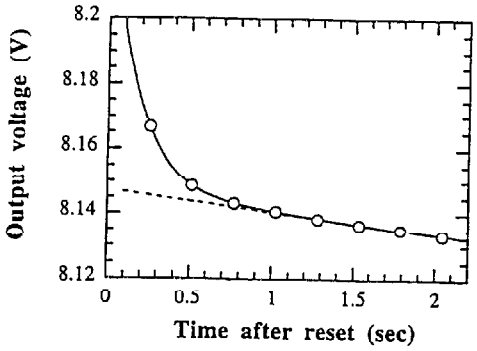

Fig. 5. Anomalous behavior of the 3.68 μm channel after the reset (open circles). The exponential and the linear part of the fitted function are shown by a solid curve and a dashed line, respectively.

3.4. Environmental emission

The NIRS observed the emission which was thought to originate from the gas released from the spacecraft surfaces. The emission was seen at wavelengths around 2.8 μm as shown in figure 6. This emission was observed at a fixed phase of the orbital revolution in the latter half of the day side. In figure 7, open and filled circles represent the sky brightness at 2.54 μm and excess brightness at 2.88 μm , respectively. The amount of the excess was estimated by subtracting the brightness extrapolated from the shorter wavelength data assuming the same spectrum as that taken at

different orbital phase where no environmental emission was seen. The full scale of the horizontal axis corresponds to one orbital revolution. The day side of the spacecraft begins at about t=0 and eclipse begins at about t=2700 in this figure. The environmental emission was bright at the beginning of the mission ($\lambda I_\lambda \sim 10^{-6} Wm^{-2}sr^{-1}$) and exponentially decayed with a time constant of about 5 days. The origin of the emission is expected to be the vibrational band of NO or OH (cf. Ahmadjian et al.[9]).

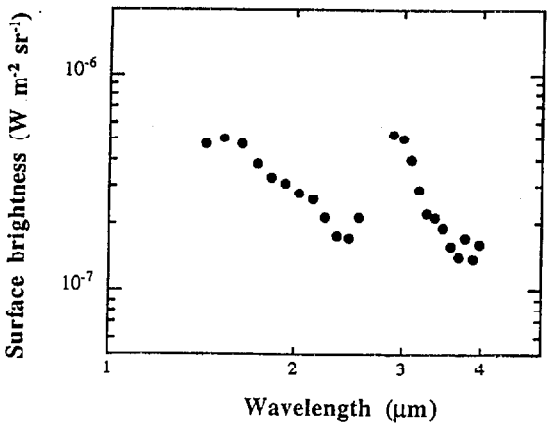

Fig. 6. The spectrum of the sky contaminated by the environmental emission. The excess brightness was seen at wavelengths around 2.8 μm.

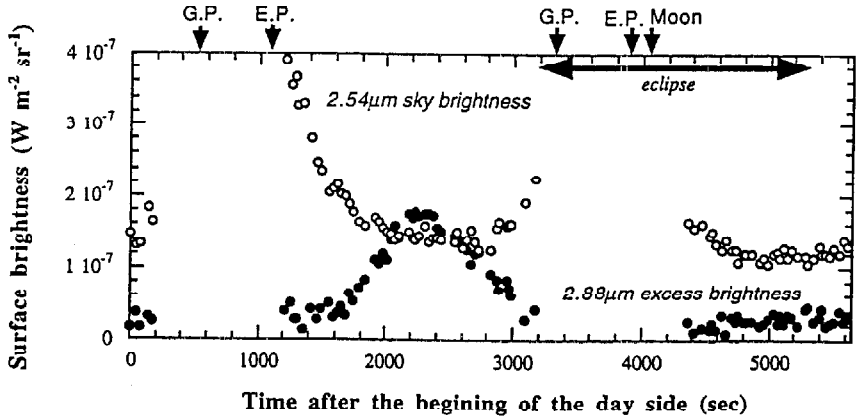

Fig. 7. The sky brightness of the 2.54 μm channel (open circles) and excess brightness of the 2.88 μm channel (filled circles) of one orbital revolution at April 10. Eclipse on the spacecraft begins at about t=2700. G.P. and E.P. on the upper side represent galactic plane and ecliptic plane, respectively.

4. IN FLIGHT CALIBRATION

4.1. Measurement of the beam pattern

Multiple passage of a bright star through the NIRS field of view made a reconstruction of the beam pattern possible. The K-type star, IRC+60231 was observed in the 9 scan paths from 23h40m on April 20 to 21h38m on April 21. Several examples of the obtained beam patterns are shown in figure 8. The contours are drawn every one tenth of the peak level of each channel. The derived beam widths are consistent with the designed values (8' x 8'). The beam shapes, however, are a little different from channel to channel. This is probably due to differences of the aberration patterns.

4.2. Sensitivity calibration

The templates of the infrared spectral energy distribution (SED) about 180 stars have been produced by M. Cohen[10] as calibration sources. Thy are continuous spectra from 1.2 μm to 35 μm constructed from the stellar model and actual observed spectral fragrance[11]. Some of these calibrated stars were observed by the NIRS. Using 4 stars among Cohen's reference stars (θ-Her, θ-Cnc, κ Gru, IRC+50276) and the beam pattern which was obtained from IRC+60231, the sensitivities (S_λ), conversion factor from the output voltage (V/s) to the surface brightness ($W \cdot m^{-2} \cdot sr^{-1}$), were calculated as below:

$$S_\lambda = \frac{I_{ref} \cdot \Omega}{\lambda \cdot F_\lambda} \quad \left(\frac{V \cdot s^{-1}}{W \cdot m^{-2} \cdot sr^{-1}} \right).$$

where, I_{ref} (V/s) and F_λ ($W \cdot m^{-2} \cdot \mu m^{-1}$) are output and the flux of the reference star, respectively, Ω (sr) is the field of view obtained from IRC+60231, λ (μm) is the observed wavelength.

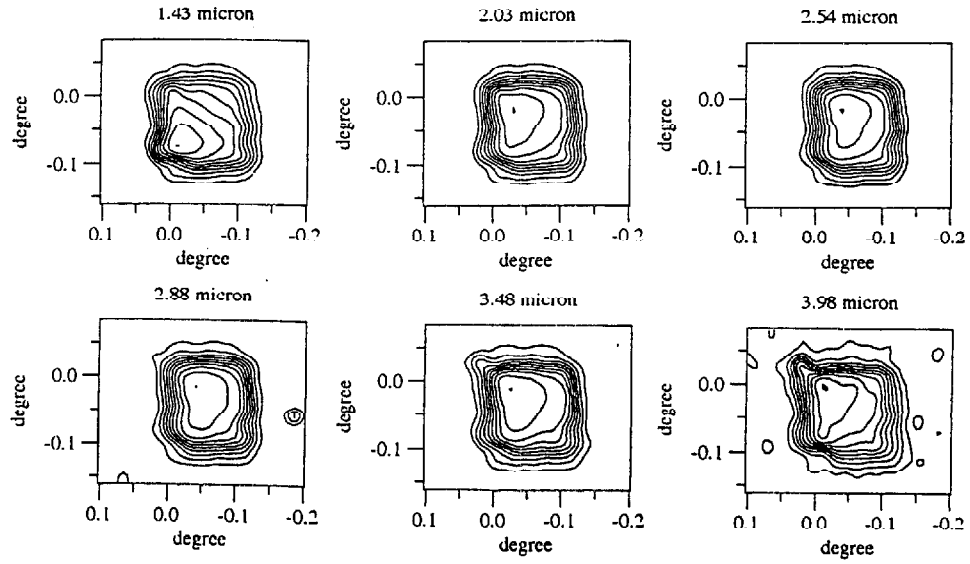

Fig. 8. The beam patterns of the several channels. The contours are drawn every one tenth of the peak level of each channel.

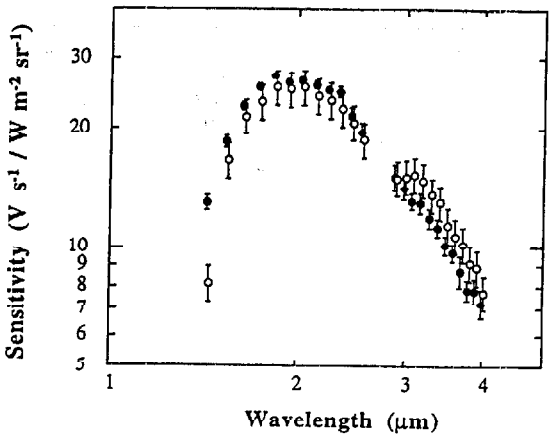

Fig. 9. In flight sensitivity calibration of the NIRS (filled circles). The open circles represents the sensitivity measured in the laboratory.

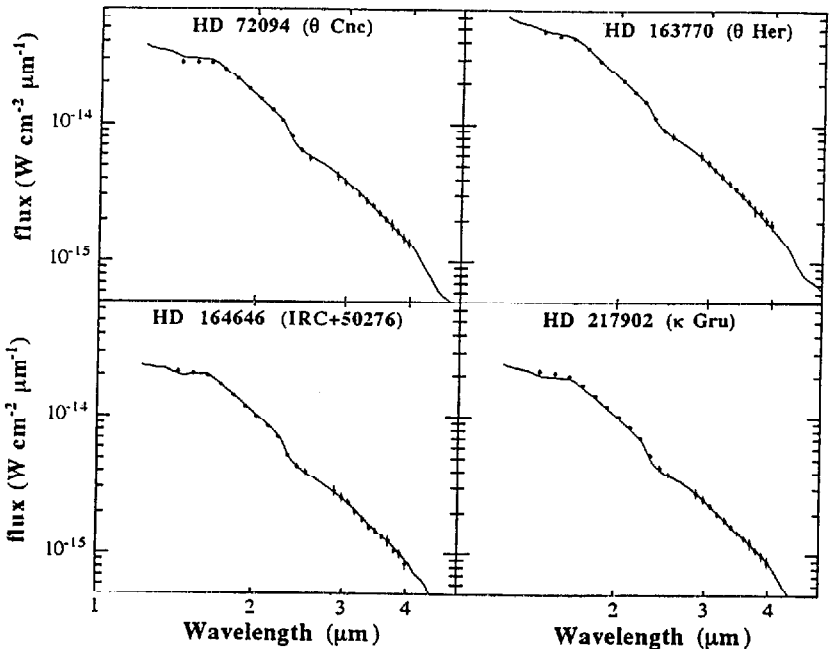

Fig. 10. The SEDs calculated using the mean sensitivity (filled circles). The solid corves represent the SED templates by M. Cohen.

The filled circles in figure 9 shows mean value of S_λs with standard error calculated from the 4 reference stars. The error bar includes the subtraction error of the background from star brightness. The open circles represents the S_λ measured in the laboratory before the flight[4]. Because of the strong background emission of the room temperature and absorption by the atmosphere, the measurements in the laboratory were so difficult that the accuracy of the laboratory measurements was as large as 10%. These two measurements are consistent within the error bars. The SEDs calculated using the mean S_λ shown in figure 9 are represented in figures 10 by filled circles. The solid curves represent the SED templates by M. Cohen. Deviations of the NIRS data points from Cohen's template are a little larger at three shortest wavelength channels than other channels. This is because the beam patterns of these channels has almost no flat part (see figure 8) and photometric results are sensitive at the position in the beam where stars passed through.

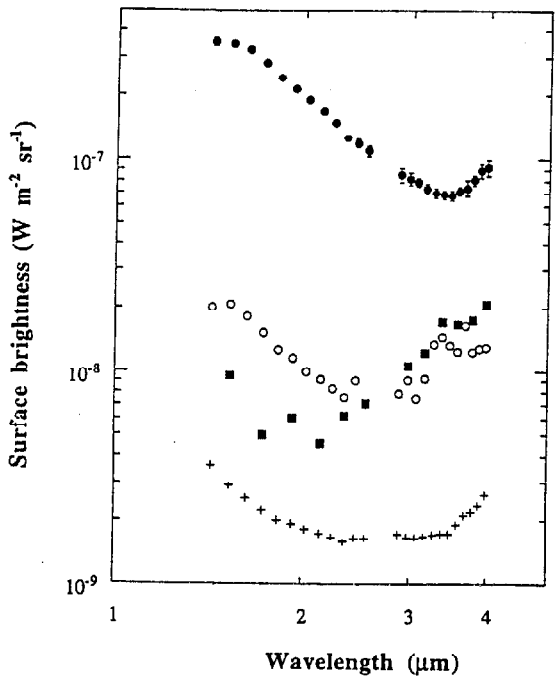

Fig. 11. The mean spectrum of the dark sky for the 5 seconds integration (filled circles), its photon noise (diamonds), standard deviation of the observed dark sky spectrum (open circles) and the read out noise for the 5 seconds integration before lid open on the orbit

4.3 Detection limit

Using the calibration factors obtained with the flight data, we estimated the detection limit of the NIRS. In figure 11, filled circles and crosses represent the mean spectrum of the dark sky derived from the 5 second integration data and its photon noise, respectively. Open circles are standard deviations of the sky brightness observed at many positions in the dark sky. Squares show the read out noise for the 5 second integration when the aperture lid was closed before observation on

the orbit. Since the telemetry rate was 3 kbps before lid open, we did not get the data of the even channels. In the short wavelength side, the standard deviation is bigger than the read out noise, while they are almost same in the long wavelength side. This means that sky fluctuation caused by the star distribution can be seen in the short wavelength side.

Detection limit improves as increase the integration time about until 5 seconds. The linearly improvement with integration time is the feature of the charge integrating method. Longer than 5 seconds, however, the improvement rate decreases because of a strong 1/f noise.

4. ACKNOWLEDGMENTS

We would like to thank M. Cohen for providing us with the calibrated spectra of standard stars and the Infrared Processing and Analysis Center (IPAC) for their help in the pointing reconstruction of the IRTS. We are much indebted to all the SFU project members for their efforts which brought the success of the IRTS observation. We are grateful to all the members of the IRTS team for their kind support and pleasant discussions through the projects.

5. REFERENCES

1.N. Boggess et al., "The COBE Mission: Its Design and Performance Two Years After Launch," Astrophys. J.,Vol.397, p.420, 1992.

2.M. Hauser, "Searching for the Cosmic Infrared Background" in *unveiling the cosmic infrared background*, ed. E. Dwek, AIP Conf. Proc. 348, pp.11-21, 1996

3. H. Murakami et al., " The Infrared Telescope in Space (IRTS)," Astrophys. J.,Vol.428, pp.354-362, 1994.

4. M. Noda et al., "Near-Infrared Spectrometer on the Infrared Telescope in Space," Astrophys. J.,Vol.428, pp.363-369, 1994.

5. M. Tanaka et al., "IRTS Observation of the Unidentified 3.3 Micron Band in the Diffuse Galactic Emission," PASJ, 1996 submitted.

6. M. Natori and K. Kuriki, "SFU Mission-1 Experiments," Space Technology, Vol.11, No.4, pp.159-165, 1991.

7. H. Murakami et al., "The IRTS Mission," PASJ, 1996 submitted.

8. "Advanced Components for Spaceborne Infrared Astronomy: Reset switch development, " Infrared Laboratories, Inc. final report, Jul. 1987

9. Ahmadjian et al., "Infrared Spectral Measurement of Space Shuttle Glow," Geophys. Res. Lett.,Vol.19, pp.989-992, 1992.

10. M. Cohen. private communication

11. M. Cohen, F.C. Witteborn, R.G. Walker, J.D. Bregman, and D.H. Wooden, "Spectral Irradiance Calibration in the Infrared. IV.," Astronomical J., Vol.110,pp.275-289, 1995.

accept ed for Proceedings of SPIE 2817, Infrared Spaceborne Remote Sensing IV , ed. M. S. Scholl and B. F. Andersen

Flight performance of the Mid-Infrared Spectrometer on the Infrared Telescope in Space mission

Thomas L. Roellig

MS 245-6, NASA Ames Research Center
Moffett Field, CA 94035

Kenji Mochizuki, Takashi Onaka

Department of Astronomy, University of Tokyo
Bunkyo-ku, Tokyo 113, JAPAN

Toshihiko Tanabe, Issei Yamamura

Institute of Astronomy, University of Tokyo
Mitaka, Tokyo 181, JAPAN

Lunming Yuen

Astronomy Program, University of Massachusetts
Lederle Graduate Research Tower B538, Amherst, MA 01003

ABSTRACT

The Mid Infrared Spectrometer (MIRS) was one of four focal-plane science instruments that flew aboard the orbiting Infrared Telescope in Space (IRTS). This telescope was a joint NASA/Japanese Scientific Space Agency (ISAS) project that was launched on March 18, 1995 aboard a Japanese HII expendable launch vehicle and was subsequently retrieved by the space shuttle. The telescope itself was liquid helium-cooled with a 15 cm aperture and surveyed approximately 7% of the sky over the course of its 26 day mission life before its cryogen expired and it began to warm up. The MIRS was developed jointly by NASA, the University of Tokyo, and ISAS and operated over a wavelength range of 4.5 to 11.7 microns with a spectral resolution of 0.23 to 0.36 microns. The MIRS has a conventional entrance aperture, so that spectral studies could be made of extended as well as point-sources. A cold shutter and an internal calibrator allowed accurate absolute flux determinations. The realized in-flight performance of the MIRS followed the pre-launch calibration performance as measured on the ground, with the exception of some degradation in the spectrometer throughput, some unanticipated detector behavior due to the passages through the South Atlantic Anomaly, and two unavoidable observations of the moon.

Keywords: Astronomy, Infrared, Space Missions, Infrared Telescope in Space, Infrared Spectrometer

1. INTRODUCTION - A SHORT DESCRIPTION OF THE MID-INFRARED SPECTROMETER

The Infrared Telescope in Space (IRTS) was one of seven experiments on the first Space Flyer Unit (SFU-1) that was launched from Tanegashima Space Center in Japan on March 18, 1995 (all times in UT). After orbital adjustments, the IRTS operated in a 28° inclination, approximately 500 km altitude, circular orbit. Four scientific instruments and a near-infrared star sensor used for telescope pointing reconstruction shared a common focal plane in the telescope. Science data-taking started on March 29, 1995 and continued until the liquid helium exhausted on April 24, 1995. Detailed descriptions of all four science instruments can be found elsewhere [1,2,3,4]. This paper summarizes the on-orbit performance of the Mid-Infrared Spectrometer (MIRS) instrument. Descriptions of the on-orbit performance of the other instruments and a description of the IRTS mission can be found elsewhere in these proceedings [5,6,7,8].

The IRTS telescope scanned the sky along nearly great-circle tracks at a rate of $0.064° \text{ sec}^{-1}$. The separation between these tracks was determined by orbital precession and periodic adjustments of the spacecraft spin axis, but in general, the successive scans were offset by approximately 4 arc-minutes at 90° away from the scan pattern nodes, or one half of the MIRS aperture size [9]. On April 5, 1996, the spacecraft orbital path crossed the sub-solar point and the spacecraft was re-oriented the next day to improve the earth and sun avoidance angles. Before this re-orientation, the telescope scan paths

stayed within 13° of the galactic plane. After the repositioning, the scan paths went as far as 60° out of the galactic plane so that measurements could be made of the diffuse emission located far from the plane.

The modest scale of the IRTS mission presented all of the focal plane instruments with severe size, weight, power dissipation, and data rate constraints. As the IRTS facility did not provide infrared calibration sources, each instrument had to incorporate its own. To meet the MIRS science goals, a low resolution spectrometer operating from at least 5 to 11 μm was indicated. In order to meet the power and weight constraints, it was decided that the MIRS would have a fixed grating with a cold instrument entrance aperture shutter as the only moving part. Closing this shutter provides an absolute zero infrared background condition for measuring detector dark currents and also blocks the emission of stray infrared light from the MIRS when the internal calibration source is on. Since all of the IRTS focal plane instruments were operated simultaneously, it was important that all sources of optical, electrical, thermal, and mechanical interference between the instruments be eliminated. The MIRS optical design that was developed to meet the above constraints is shown in Figure 1. The overall specifications are given in Table 1.

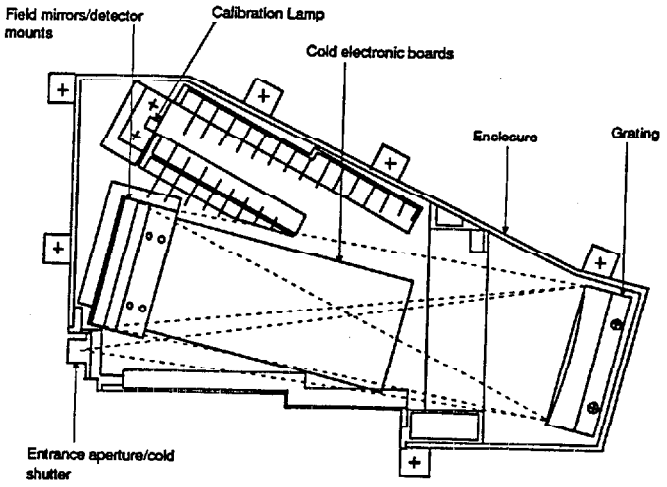

Figure 1. Schematic diagram of the optical layout of the Mid-Infrared Spectrometer.

The photo-current output from the 32 Si:Bi detectors was collected in 32 integrating amplifiers operating within the MIRS housing at cryogenic temperatures. The outputs of these amplifiers were multiplexed, filtered, further amplified, and then digitized with 16-bit resolution. The IRTS operated in two data rate modes, with the higher data rate being the nominal rate and the lower rate used only when the configuration of ground receiving stations was such that the spacecraft's onboard data recorder would otherwise overflow. When the MIRS was operated in the high data rate mode, the integrating amplifier outputs were each sampled approximately two times a second. This sampling rate was halved when the IRTS was in the low data rate mode. The integrated output level from two specified detectors was monitored in the MIRS warm electronics. When the integrated charge passed a threshold level, all of the integrating amplifiers were reset. The frequency of these resets depended on the infrared background level, but normally occured once every few minutes.

Table 1

MIRS SPECIFICATIONS

Wavelength range:	4.495 to 11.703 μm
Spectral resolution:	0.23 to 0.36 μm
Size:	Irregular shape - 210 mm x 137 mm x 75 mm overall
Weight:	805 g
Electrical power dissipation:	Cold electronics - 4 mW Warm electronics - 2.9 W
Operating temperature:	1.8 K
Detectors:	32 discrete Si:Bi photoconductors, each 1 mm x 1 mm x 0.5 mm in size, Aerojet ElectroSystems
Entrance Aperture:	1.4 mm x 1.4 mm (0.134° x 0.134° on the sky)
Integrating Amplifiers:	Model JF-4, IR Labs
Detector bias voltage:	2.0 V
Warm electronics package:	Hamamatsu Photonics K. K.
MIRS data rate:	1,188 bits/sec (standard operating mode) 594 bits/sec (reduced data-rate mode)
Detector sampling rate:	2 Hz (standard operating mode) 1 Hz (reduced data rate mode)
Detector samples/object aperture crossing:	4 (standard operating mode) 2 (reduced data rate mode)

2. ON-ORBIT PERFORMANCE OF THE MIRS

Characterization of the in-flight MIRS instrument performance is still underway, but some preliminary results are now available. These are summarized below.

2.1 Wavelength response

The MIRS wavelength response was measured on-orbit by observations of various astronomical objects with known absorption or emission features. These features were found to lie exactly at the positions along the detector array predicted from pre-flight calibration.

2.2 Beam size

Many of the major science objectives of the MIRS included measurements of diffuse extended sources. On-orbit calibration of the MIRS response to diffuse sources was difficult, since there were no standard sources of this nature observed in the IRTS scans. In order to translate point-source calibrations into extended source calibrations, an accurate measurement of the beam size is needed. The MIRS aperture size and telescope focus were measured on-orbit by observations of point sources as they were scanned across the entrance aperture on different orbits. Figure 2 shows one such contour plot of the aperture as measured by observations of the star IRC-10529. This star was situated such that it passed over the MIRS entrance aperture in 31 different orbital scan paths, thus allowing good mapping of the MIRS aperture. The MIRS aperture

equivalent area was found to be close to the designed value, although there was some variation with wavelength in the in-scan dimension. The entrance aperture area as measured at the shortest MIRS wavelength was 62.1 square arc-minutes, while the aperture area as measured at the longest MIRS wavelength was 50.5 square arc-minutes. This is in contrast to the designed geometrical area of 64.3 square arc-minutes at all wavelengths. The discrepancy was probably due to a combination of diffraction effects and perhaps some internal mis-alignment of the MIRS optics. Now that the MIRS has been retrieved by the space shuttle, further laboratory testing of the instrument should determine the cause.

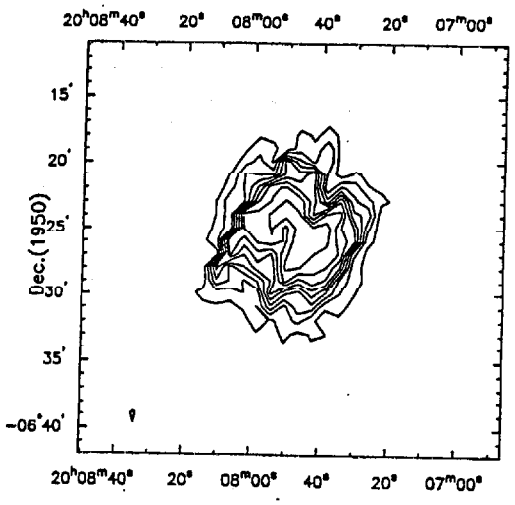

Figure 2. The MIRS entrance aperture mapped at 7.1 μm by scans of the star IRC-10529. The scan direction ran at an approximately 45° angle from the upper right to the lower left. The contour levels run from 10% to 90% of the peak signal. The physically square shape of the MIRS entrance aperture is clearly seen, aligned along the scan path. The small-scale structure shown is an artifact of the discrete sampling used to acquire the data.

2.3 Shutter

On-orbit, the MIRS shutter was found to be only partially functional; due to some mechanical interference the shutter only closed to block 55% of the incoming radiation instead of the designed 100%. Although this partial closure increased the difficulties in measuring the detector dark currents, the degree of shutter closure was stable throughout the life of the mission. Operation of the MIRS internal calibration source did not lead to any optical pick-up in any of the other IRTS instruments.

2.4 Calibration lamp and thermometry

Aside from the shutter problem described above, the MIRS internal calibration source and thermometers operated exactly as they were designed and tested in the pre-flight tests. Calibration sequences were conducted every 1,048 seconds throughout the mission, apart from a few periods in the first two days of operations when a software glitch disabled the calibration sequences every time the IRTS data rate changed. Each of the calibration sequences lasted 64 seconds and consisted of a period of shutter closure with the calibration lamp off, to measure the dark current, and a period of shutter closure with the calibration lamp on, to measure detector responsivity changes.

2.5 Detector performance - radiation effects

The 32 Si:Bi infrared photoconductor detectors used in the MIRS all basically functioned as expected based on their pre-flight tests. However, their performance was strongly affected by ionizing radiation hits, especially during and subsequent to passages of the IRTS through the South Atlantic Anomaly (SAA), a region off the coast of Brazil where a disturbance in the earth's magnetic dipole field allows the Van Allen charged particle belts to come closer to the earth's surface. The IRTS

encountered the SAA in approximately one-third of its orbits each day. An intensity map of the SAA at the IRTS orbital altitude, as measured by the number of particle hits recorded in the MIRS detectors, is shown in Figure 3.

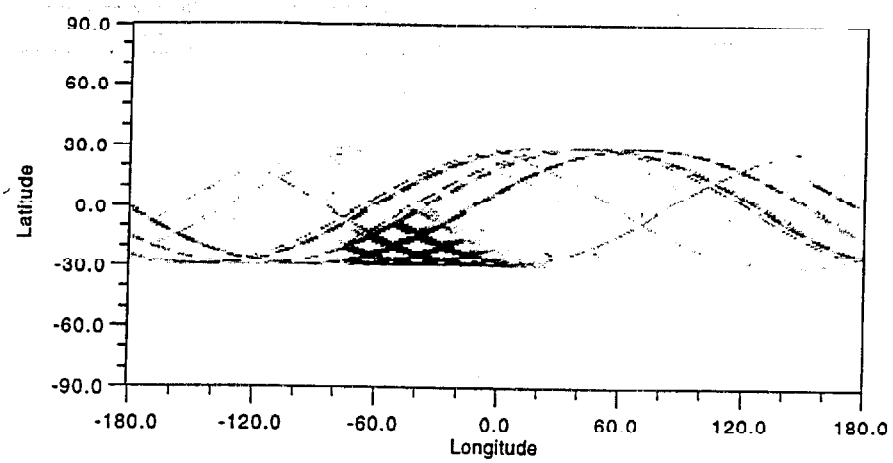

Figure 3. A grey-scale intensity map of the energetic particle hits in the MIRS detectors over the course of the entire IRTS mission. The intensity ranges from <0.1 (white) to >100 (black) cosmic ray hits/second. Note that the IRTS orbit was almost perfectly quantized over the course of the mission. In other words, the orbital period and the precession of the orbit were such that nearly the same orbital paths were followed over the earth each day.

During the passage through the SAA the MIRS detectors suffered such a high hit rate that the instrument data was unusable. Furthermore, lingering effects of the SAA passage affected the detectors for periods up to 45 minutes or more after exiting the SAA. These effects were manifested by a decrease in the detector responsivity and could be observed by monitoring the signal from the calibration lamp. A typical example of this is shown in Figure 4. The responsivity changes could be well-fit by an exponential form:

$$R = R_0 [1 - C_{saa} \exp(-t/\tau)] \qquad (1)$$

where R_0 is the detector responsivity without the effects of the SAA, C_{saa} is a constant describing the magnitude of the responsivity change just after exiting the SAA, τ is a time-constant, and t is the time after exiting the SAA.

Analysis of the data showed that R_0 varied from detector to detector, but did not significantly change over the course of the mission for each detector. These values were also nearly identical to the values measured using the internal calibration source in the pre-flight testing. Therefore, there were no long-term responsivity changes in the base responsivity in any of the detectors due to accumulated radiation damage over the course of the mission. The constant C_{saa} also varied from detector to detector. Within each detector, the magnitude of C_{saa} was a linear function of the total radiation dose received in a SAA passage. Typical values of C_{saa} therefore ranged from negligible after a passage through the outskirts of the SAA, up to 30% after a passage through the core of the SAA. The time constant τ also varied from detector to detector, but had only a weak dependence on the total radiation dose received in a SAA passage. Instead, τ did show a dependence on the integrated IR signal received after the SAA passage. This indicates that the incident IR flux served to heal the radiation damage responsible for the responsivity decrease. This recovery was particularly noticeable after observations of strong IR sources, such as the internal calibration lamp or the galactic plane. Typical values of τ were 1,500 seconds.

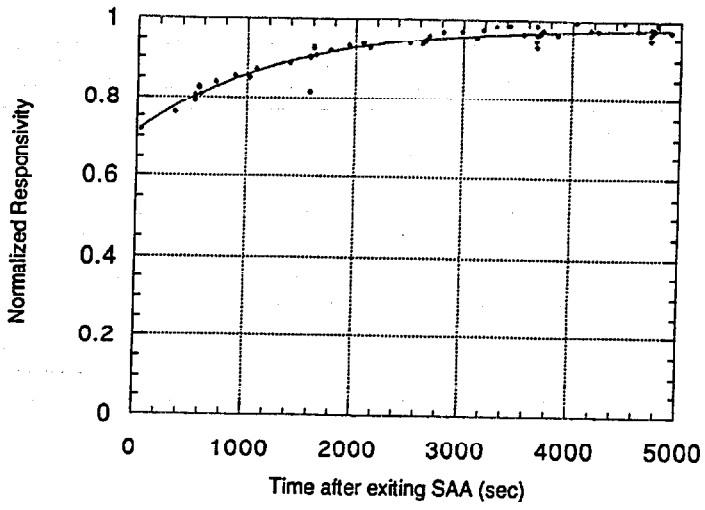

Figure 4. Detector responsivity of the 7.1 μm detector channel after exiting the core of the SAA, normalized to the measured responsivity long after the last SAA passage of the day. The line is a fit to equation (1) in the text.

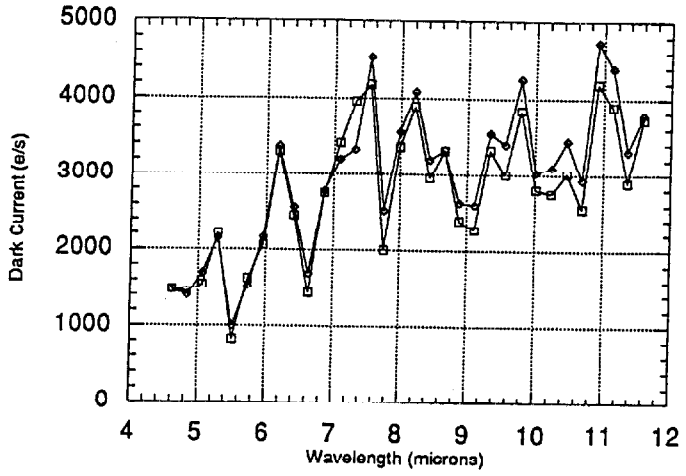

Figure 5. A plot of the dark current in the MIRS detectors from the on-orbit measurements and the pre-flight tests. The pre-flight data is indicated by the open diamond symbols and is multiplied by a factor of 1.8 (see text). The on-orbit data is indicated by the open squares.

The on-orbit dark current in the MIRS detectors is shown in Figure 5. For comparison, the dark current as measured in the pre-flight tests is also shown, multiplied by a constant factor of 1.8. At present, the reason that the dark current increased in each detector by nearly a factor of two is not known. If this increase was due to radiation damage, it must have

occured in the eleven day's period between the launch of the IRTS and the start of operations. Gain changes in the output electronics chain are not likely to account for this factor, since the on-orbit detector signals generated by the calibration lamp are identical to the pre-flight ground test signals. The dark current stayed constant in all the detectors throughout the duration of the mission, thus indicating that no additional changes occured after the IRTS operations began. This increase in the dark current was unfortunate, since the shot-noise in the dark current electrons then became greater than the photon shot-noise in the Zodiacal background over most of the MIRS wavelength range.

2.6 Sensitivity

Outside of the SAA passages, the noise level of the MIRS was essentially identical to that measured in the pre-flight testing. Cosmic ray hits occured throughout the mission, but were fairly easy to correct for outside of the SAA in post-mission data processing. The MIRS instrumental signal response was measured by observing a variety of standard point-sources. The primary point-source calibration objects were a subset of the standard IR calibration sources compiled by Cohen, et al. [10, 11] for use in space IR observations. The observed on-orbit signal response was lower than that estimated from pre-flight testing. Since the detectors gave nearly identical on-orbit responses to the internal calibrator as were measured on the ground, there probably was not any degradation in the intrinsic detector responsivity or the amplifier chain. Thus the signal responsivity change may have been due to some degradation in the optical train performance, perhaps caused by the strong launch vibrations. This will be investigated in more detail now that the MIRS has been retrieved.

Plots of the MIRS single-scan point-source and diffuse-source sensitivities with a spatial resolution of one MIRS aperture size are given in Figures 6 and 7. It can be seen that the shot noise in the dark current is the primary origin of the MIRS sensitivity limits. The sensitivities plotted in Figures 6 and 7 can be improved in two ways. Over most of the observed sky area, each point was observed in multiple orbital scans. These can be co-added to increase the sensitivity. Also, since the MIRS had integrating amplifiers, the sensitivity limits due to read noise in the detectors can be lowered, even for point-sources, at the expense of spatial resolution in the in-scan direction. This is because the photo-electrons collected in an object's passage across the MIRS aperture will stay in the amplifier until the next reset, thus allowing them to be read many times. This has the effect of reducing the read noise to negligible levels, so that the total noise level is set by the combination of shot-noise in the detector dark current and photon-noise in the Zodiacal background.

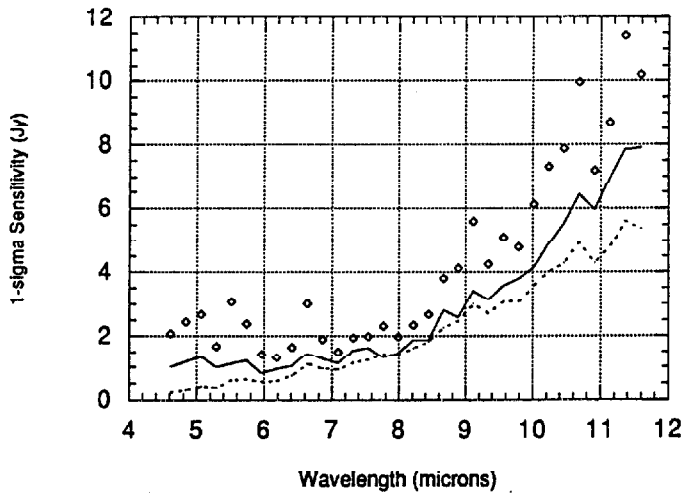

Figure 6. The measured MIRS one-sigma point-source sensitivity in Janskys is indicated by the open diamonds. This is the sensitivity that would be reached in one orbital passage as a point sources passes over the MIRS aperture. For comparison, the average zodiacal photon background-limited sensitivity is indicated by a thin dotted line. The sensitivity limit set by the shot-noise in the dark current is indicated by the thin solid line.

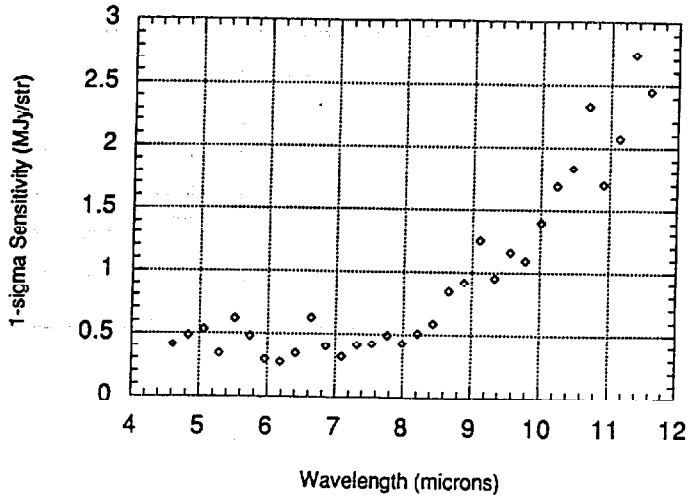

Figure 7. The MIRS one-sigma diffuse-source sensitivity in Mega-Janskys/steradian. This sensitivity includes the effects of the variation in the effective aperture size with wavelength mentioned in the text.

2.7 Environmental effects

The MIRS proved to be remarkably free from external environmental effects on-orbit. There was no sign of any effects from outgassing from the space craft, although other instruments on the IRTS did see some such effects [9]. The MIRS did see firings of the spacecraft hydrazine thrusters. Fortunately, these generally only occured once per orbit, when the spacecraft emerged from the earth's shadow and attitude control passed from the gyros to the sun sensor. In any case, the thruster firings had a very distinctive spectral signature, so that they could not be confused with astronomical objects in the data set. The only other external effects noticed by the MIRS were brief periods of unusual noise that were observed every time the Far-Infrared Line Mapper instrument activated its bias boost circuitry after exiting the SAA.

3.0 CONCLUSION

The Mid-Infrared Spectrometer on the Infrared Telescope in Space mission collected excellent data in a survey of 7% of the sky. Although there was some minor performance degradation in a few areas, these did not compromise the overall quality of the data set. In particular, the MIRS was able to perform a survey of diffuse extended regions in the galaxy with unprecedented sensitivity. The MIRS is fulfilling its science objectives and the first scientific results are just now being reported [12, 13]. Now that the IRTS has been retrieved by the space shuttle, it will be possible to perform further laboratory tests to determine the cause of the observed performance anomalies.

4.0 ACKNOWLEDGMENTS

T. Roellig and L. Yuen would like to acknowledge the support of the NASA Astrophysics Grants program. T. Onaka and T. Tanabe would like to acknowledge the support of ISAS and the Ministry of Education, Science, Sports, and Culture in Japan. I. Yamamura and K. Mochizuki are supported by JSPS Research Fellowships for Young Scientists. All of the authors would like to thank the entire IRTS team for their efforts in ensuring the success of the IRTS mission.

5.0 REFERENCES

1. M. Noda, T. Matsumoto, S. Matsuura, K. Noguchi, M. Tanaka, M. A. Lim, and H. Murakami, "Near Infrared Spectrometer on the Infrared Telescope in Space," *Ap.J.*, 428, pp. 363-369, 1994.

2. T. L. Roellig, T. Onaka, T. J. McMahon, and T. Tanabe, "The Mid-Infrared Spectrometer on the Infrared Telescope in Space (IRTS) mission," *Ap.J.*, 428, pp. 370-376, 1994.

3. H. Shibai, M. Yui, H. Matsuhara, N. Hiromoto, T. Nakagawa, and H. Okuda, "Far-Infrared Line Mapper on the Infrared Telescope in Space," *ApJ.*, **428**, pp. 377-383, 1994.

4. A. E. Lange, M. MN. Freund, S. Sato, T. Hirao, T. Matsumoto, and T. Watabe, "The Far-Infrared Photometer on the Infrared Telescope in Space," *ApJ.*, **428**, pp. 384-392, 1994.

5. T. Matsumoto, "IRTS mission," *Proc. SPIE*, **2817**, these proceedings, 1996.

6. M. Noda, T. Matsumoto, M. Tanaka, H. Murakami, and M. Kawada, "Flight performance of the Near-Infrared Spectrometer (NIRS)," *Proc. SPIE*, **2817**, these proceedings, 1996.

7. H. Shibai, T. Nakagawa, H. Okuda, S. Makiuti, H. Matsuhara, K. Okumura, N. Hiromoto, Y. Doi, and T. Tohya, "Flight performance of the Far Infrared Line Mapper (FILM)," *Proc. SPIE*, **2817**, these proceedings, 1996.

8. T. Hirao, T. Matsumoto, S. Sato, and A. E. Lange, "Flight performance of the Far-Infrared Photometer," *Proc. SPIE*, **2817**, these proceedings, 1996.

9. H. Murakami. et al.. "The IRTS (Infrared Telescope in Space) mission," *Pub. Astron. Soc. Japan*, submitted, 1996.

10. M. Cohen, F. C. Witteborn, R. G. Walker, J. D. Bregman, D. H. Wooden, "Spectral Irradiance Calibration in the Infrared.IV. 1.2-35 μm Spectra of Six Standard Stars," *Astron. J.*, **110**, pp 275-289, 1995.

11. M. Cohen, *private communication*, 1996.

12. T. Onaka, I. Yamamura, T. Tanabe, T. L. Roellig, and L. Yuen, "Detection of the Unidentified Bands in the Diffuse Galactic Emission by the IRTS," *Publ. Astron. Soc. Japan*, submitted, 1996.

13. I. Yamamura, T. Onaka, T. Tanabe, T. L. Roellig, and L. Yuen, "Mid-Infrared Spectral Observations of Point Sources by the IRTS," *Publ. Astron. Soc. Japan*, submitted, 1996.

accept ed for Proceedings of SPIE 2817, Infrared Spaceborne Remote Sensing IV , ed. M. S. Scholl and B. F. Anderesen

Flight Performance of the Far-Infrared Line Mapper (FILM)

Hiroshi Shibai[1], Takao Nakagawa[1], Sin'itirou Makiuti[2], Hideo Matsuhara[3], Norihisa Hiromoto[4], Ken'ichi Okumura[4], Yasuo Doi[4], Takahisa Toya[2], and Haruyuki Okuda[1]

1 The Institute of Space and Astronautical Science (ISAS), Yoshino-dai 3-1-1, Sagamihara, Kanagawa 229, Japan
2 The Faculty of Science, The University of Tokyo, Yayoi 2-11-16, Bunkyo-ku, Tokyo 113, Japan
3 The Faculty of Science, Nagoya University, Hurocho, Chikusa ku, Nagoya 464, Japan
4 Communications Research Laboratory (CRL), Nukui-kitamachi 4-2-1, Koganei, Tokyo 184, Japan

ABSTRACT

The Far-Infrared Line Mapper (FILM) is a far-infrared spectrometer as one of four focal plane instruments of the Infrared Telescope in Space (IRTS) and it was designed for the purpose of wide area intensity mapping of far-infrared emission from the interstellar gas and dust in the Galaxy. The targets are the [CII] 158 μm line of the ionized carbon, the [OI] 63 μm line of the oxygen atom, and the continuum emission at 155 and 160 μm from the interstellar dust grain. A cylindrically concave varied line-space grating and a linear array of stressed Ge:Ga had successfully developed and allowed us to make a compact spectrometer compatible to severe limitations of the small cryogenic telescope. The IRTS, onboard the Space Flyer Unit (SFU), was launched by the HII rocket on March 18th, 1995 and was recovered by a STS on January 13th 1996. The FILM had been working very well within the period of four weeks allocated for the IRTS observation and produced a lot of valuable data of line intensities of the [CII] and [OI] as well as of continuum intensities at 155 and 160 μm. The sensitivity and/or the spatial resolution for the [CII] line are an order of magnitude better than the previous work.

key words: infrared satellite, astronomy, grating, spectrometer, the Galaxy, interstellar matter, far-infrared radiation

1. INTRODUCTION

The far-infrared wavelength region is heavily obscured by the earth's atmosphere. In order to measure astronomical far-infrared radiation, we must lift up the instruments to the stratosphere at least. The Infrared Astronomical Satellite (IRAS)[1] has mapped the far-infrared continuum radiation with high sensitivity and high spatial resolution over the entire sky. On the other hand, spectroscopic measurements in the far-infrared region using balloons and aircraft have not been extended over wider area of the sky such as the Galactic plane. Recently, two balloon projects, the Balloon-Borne Infrared Telescope (BIRT)[2] and the Balloon-Borne Infrared Carbon Explorer (BICE)[3], have succeeded in making line intensity maps of [CII] 158 μm of the Galactic plane with good spatial resolution and wide sky coverage. It has been demonstrated by their observational results that measurements of the [CII] line emission are important and powerful tools for investigating the interstellar gas. On the other hand, the Cosmic Background Explorer (COBE)[4] has provided all sky intensity maps of [CII] 158 μm and [NII] 205 μm. The maps reveal an entire view of the Galactic interstellar gas. However, because of its large beam size of 7 degree, the maps do not have enough spatial resolution to resolve the Galactic plane.

This paper describes the Far-Infrared Line Mapper (FILM), which has been developed to be the first satellite-borne instrument optimized to map far-infrared line intensities; the hardware and the laboratory calibration have already been presented by Shibai et al. (1994)[5]. The FILM was one of the four focal plane

instruments of the Infrared Telescope in Space (IRTS)[6,7,8], which is one of the eleven experiments of the Japanese Space Flyer Unit (SFU) which was launched on March 18, 1995.

2. FILM Behaviors in Flight

2.1 Brief summary of the FILM hardware

The FILM has a noble design in its optical system. It uses a "varied line-space cylindrically concave grating" which has been developed for the first time for the FILM. This grating allows us to achieve high throughput, reliability, moderately high resolution in the strict limits of small volume and light weight. All optical components as well as the grating itself are made of aluminum alloy by machining and are evaporated with gold.

Figure 1 shows the optical system of the FILM. At the focal plane of the IRTS, a small diagonal mirror is mounted for the FILM. The incident light from the telescope is reflected by 90 degrees and makes a focus on the input slit of the FILM. The slit is a rectangle of 1.4 × 3.5 mm whose elongated direction is perpendicular to the scanning direction of the IRTS. The light passes through the input slit with a F/4 divergence, is reflected by a plane mirror again, and is collimated by a cylindrical mirror in the Z-axis. The light diverging in the other direction reaches the cylindrically concave grating which has a ruling along the Z-axis. After reflection and dispersion by the grating, the light goes back nearly along the path of the incident light and makes a focus at the front of the detector aperture. The location of the focus is shifted by 20 mm above that of the input slit in the Z-axis. The direction of the spectral dispersion at the focus is along the Y-axis. The slit width of the detector aperture is the same as that of the input slit.

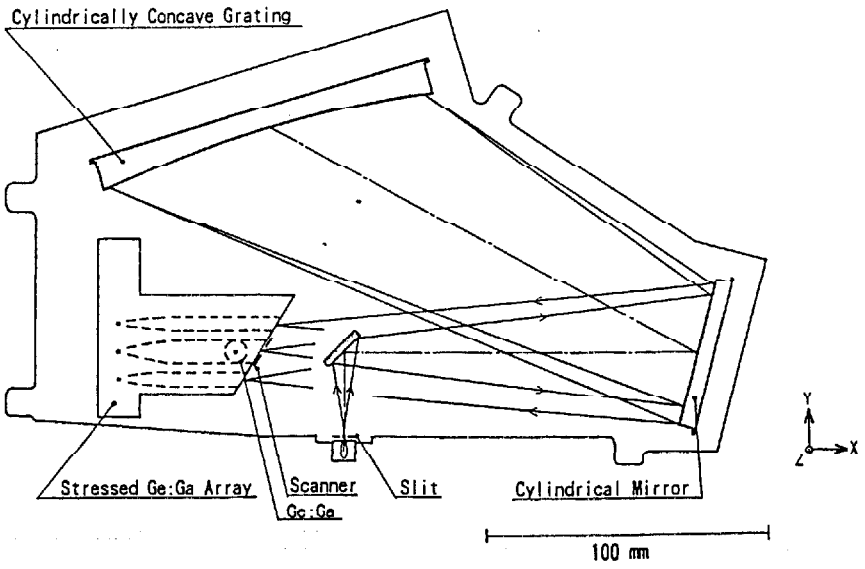

Fig. 1. Schematic diagram of the FILM, viewed from behind the focal plane at the optical axis of the telescope.

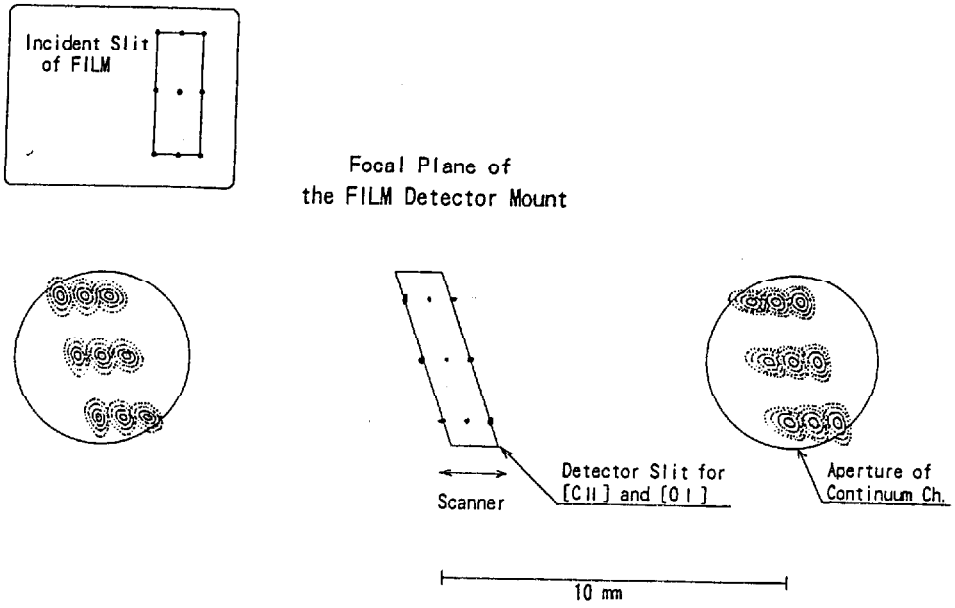

Fig. 2. A result of the ray trace of the FILM optical system. The shape of the incident rectangular slit is projected as a rhomboid at the focus in front of the detector mount. The residual aberration of the [CII] channel is very small as shown in the figure. The aberration of the continuum channels on both sides is larger but small enough compared to the FILM slit size and the diffraction limited image size.

Conventional concave gratings which have envelopes of a part of a sphere do not need any collimator optics. However, in order to minimize the size in the perpendicular direction of the paper in Figure 1, we adopted a unique idea which uses a cylindrical mirror and a cylindrically concave grating. A result of a geometrical ray trace is shown in Figure 2. The aberration for the [CII] and the [OI] channels is much smaller than the slit size, which is nearly equal to the diffraction-limited image size for 158 μm. It is noted that the image of the rectangular shape of the input slit is deformed into a rhomboid. The pitch of the grating was controlled so that the [CII] 157.7408 μm line is exactly equal to the second order light of the spectrometer. Then the [OI] 63.1837 μm line is almost the 5th order light. The separation of the two lines at the focus is only 0.7 mm. The pitch surface of the grating is exactly a part of the cylinder but the ruling pitch is varied within ± 0.9 % in order to decrease the aberration. This grating has been made by Nikon for the FILM.

Figure 3 shows a schematic diagram of the filtering system of the FILM. A SrF_2 filter coated with diamond powder is used to block radiation at wavelength shorter than 50 μm. After the dispersion by the grating, lights of all orders near the blaze wavelengths are selected for the two line channels. Then, a KCl beam splitter reflects only fourth to sixth order light to the [OI] channel, and an interference filter passes only fifth order light. On the other hand, the light passing through the KCl beam splitter contains first to fourth and sixth orders of the light reflected by the grating. A Yoshinaga filter passes only first and second orders and completely blocks higher order light. Because a stressed Ge:Ga detector cannot detect the first order light (315 μm), only the second order light (158 μm) is selected. The two continuum channels have a nearly identical filtering system with the [CII] channel except that they do not have a KCl beam splitter.

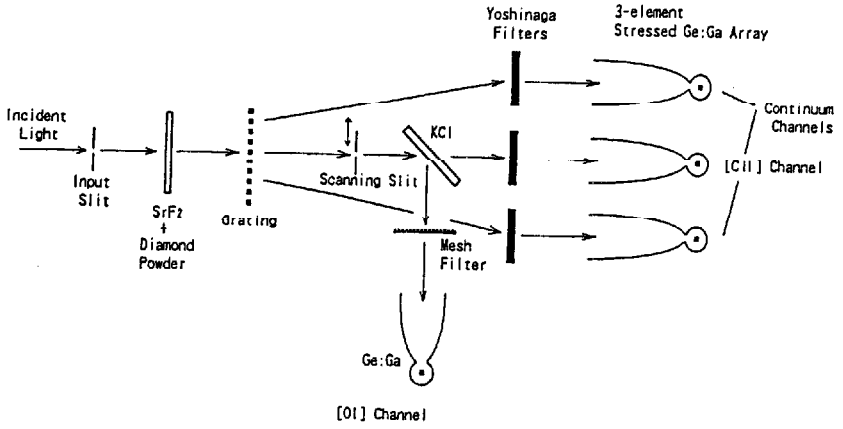

Fig. 3. Schematic diagram of the filtering system.

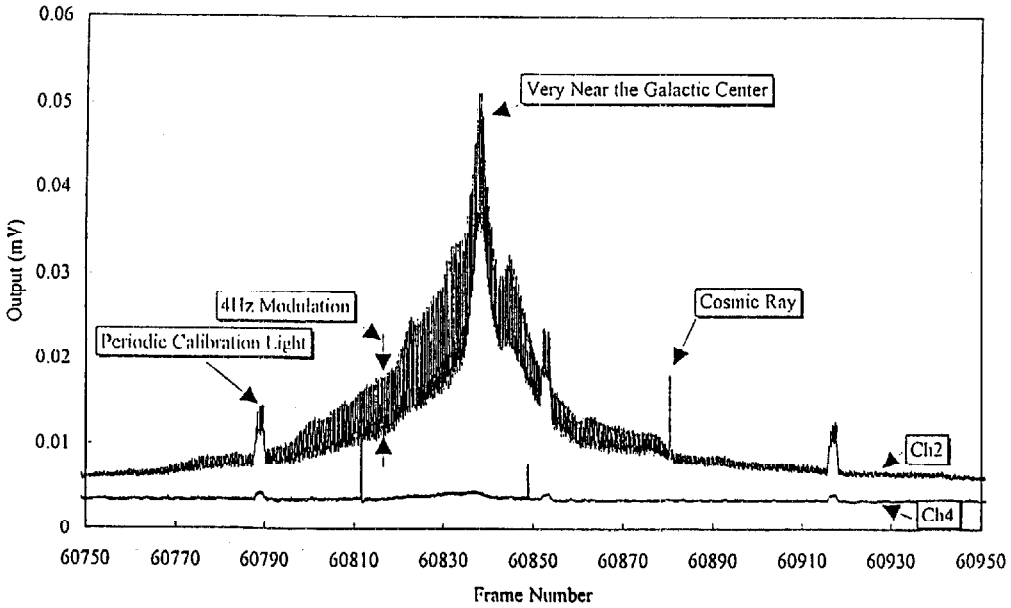

Fig. 4. An example of the output signals of Channel 2 for the [CII] 158 μm line and Channel 4 for the [OI] 63 μm line. The scanning path goes through within 1 degree of the center of the Galaxy. The 4 Hz modulation produced by the [CII] line emission is seen as the thick width of Channel 2.

2.2 Cold Shutter

A cold mechanical shutter was mounted just after the incident aperture slit. This shutter was closed during 32 seconds every 1024 seconds as an operation of the IRTS standard calibration sequence in order to determine the zero flux level of the incident light. It had been known that there was an internal light source we did not intend. It may be a leakage photons emitting from the JFET modules in which JFET ships were kept at higher than 50 K. The contribution of this internal light to the detector output signals were removed with the output when the shutter was closed. It was also found that the shutter had a small leakage in the closing position. However, as this leakage was less than 10 percent of the incident light. it was precisely corrected for.

2.3 Scanner

In order to accurately extract the line intensities from the incident light. the slit at the detector aperture of the [CII] and [OI] channel was mechanically scanned in the dispersion direction at 2 Hz. As the result, the output signals produced by the line emissions were modulated at 4 Hz as shown in Figure 4. This method allows us to detect weak line emissions against the 1/f noise of the detectors/preamplifiers and against instability of the detector responsivities. The scanner had been moving during the whole observation time and the total number of cycles was about 4.5 million times. In the first period of the observation. the movement was quite stable, but it became slightly unstable in the later period for unknown reason. However, it did not affect to the modulation efficiency.

2.4 Calibration Lights

The FILM had two internal light sources to monitor detector responsivities. The source itself was a very thin stainless steel wire that was applied with a small electrical current. The light source was turned on during 2 seconds every 64 seconds and was lit in 4 seconds every 1024 seconds. The latter operation was done during the shutter was closed. Thus light source was inevitably useful for monitoring the detector responsivities. By this light, we found the changes in the detector responsivities both of short-term and long-term by high energy particle hitting and other effects. In Figure 4, there is seen response profiles of the detectors for the calibration light.

2.5 Bias Lights

Since it was known that photoconductive detectors. such as Ge:Ga, have a large dependency of its responsivity on the incident photon flux, we installed the light sources of a certain constant luminosity in order to keep the incident flux nearly constant and to stabilize the detector responsivities. However, as described above, there was an unintentional light source inside the FILM which seemed to be constant. Therefore. we adopted this as the constant light source instead of the bias lights.

2.6 Detectors

Detectors used in the FILM[9,10] have been developed by a collaboration between ISAS and CRL. A linear three element array of Ge:Ga photoconductor with a stress assembly is used for the [CII] 158 μm and the two continuum channels. On the other hand, a single element unstressed Ge:Ga photoconductor is used for the [OI] 63 μm channel. The two line channels have a common slit which is scanned in the direction of the spectral dispersion at 2 Hz by a spectral scanner.

It has been known that performance of detectors is also affected by cosmic high energy particles in space. During the IRAS mission[1], cosmic rays hit on each detector at the rate of about one per twenty seconds. Because the volume of the detector element (0.125 mm^3) is less than one-tenth of that of the IRAS (2 mm^3) and because the orbital altitude is 482 km while the IRAS into 900 km, the rate of cosmic rays hits was expected to be much smaller than that of the IRAS. Except for passage through the South Atlantic Anomaly (SAA), the hit rate is estimated to be about one event in ten minutes. For annealing the radiation effect after passing through the SAA, the detector bias voltage can be increased above the breakdown voltage ("bias boosting"). The behavior of the detectors that were triggered and affected by the high energy particles will be described in a separate paper[11].

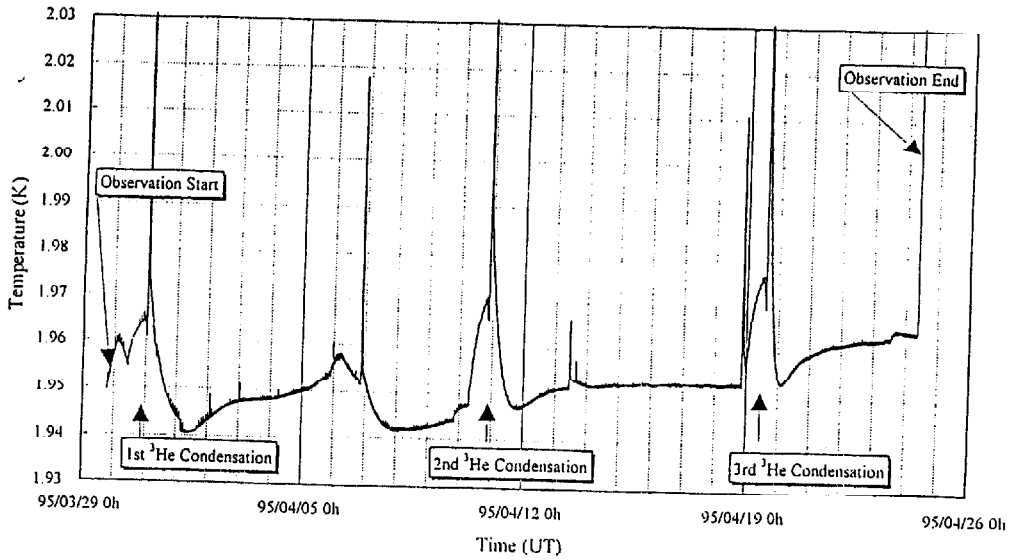

Fig. 5. The temperature profile of the stressed Ge:Ga array module. The temperature was stable within ± 10 mK except for three recycling process of 3He cooler and for two spontaneous increases on April 6 and 13.

3. System Performances

3.1 Temperature Stability

Figure 5 shows a temperature profile of the stressed Ge:Ga array module in the whole period. It was known the dark current of the stressed Ge:Ga used increases as the temperature at more than 2.1 K. We thermally connected the detector assembly to the cryogen tank wall with a specially annealed pure copper strap. During the recycling periods of the 3He refrigerator of the Far-Infrared Photometer (FIRP)[12], the temperature changed seriously. However, except for those periods, the temperature of the detector assembly was usually stable within ± 0.01K of 1.95K. The temperature difference between the tank and the assembly was less than 0.05K as was designed before launch.

3.2 Calibration

Absolute calibration of the detector responsivities were achieved by using the laboratory measurement on the ground before launch and by using the signal output for periodic calibration light source. The results were compared with the previous work. Concerning to the continuum emission, the flux densities observed by the FILM are, in average, 10 % larger than those the COBE/DIRBE. Since both measurements have more than 10 % uncertainty in their absolute calibration, this value of 10 % means they are well consistent with each other. On the other hand, the absolute calibration for the [CII] line intensity does not seem to be accurate at present. The average line intensities determined from the FILM observation approximately 70 % of those from the series of our balloon-borne observations. Since, both of them have ± 30 % uncertainty, they are consistent with each other. However, those observed intensities of the FILM and of the balloon-borne telescopes are systematically smaller

Table 1. FILM Summary

Size	:	250 × 150 × 130(H) mm			
Weight	:	1950 g			
Grating	:	a varied line-space cylindrically concave grating			
Beam size (FWHM)	:	8 arcmin (dispersion direction) × 13 arcmin			
Channel	:	Ch.1	Ch.2	Ch.3	Ch.4
Band Center (cm^{-1})	:	64.4	63.4[a]	62.4	158.4[b]
Resolving Power	:	130	109	130	405
Detectors	:	(linear 3-el. stressed Ge:Ga array)			Ge:Ga
Optical through-put[c]	:	0.34	0.30	0.34	0.15
S(detector) (A/W)[d] on the ground	:	12.9	9.72	11.7	0.4
in flight	:	37	33	26	1.6
System NEP (10^{-17} W $Hz^{-1/2}$)	:	7.67	2.52	10.1	36
NE Flux Density (MJy sr-1 Hz-1/2)	:	5.16	5.42	7.01	30.5
NE Line Intensity (ergs cm-2 s-1 sr-1 Hz-1/2)	:	-	7e-07	-	(to be estimated)

a scanning range is 63.2-63.6 cm^{-1}
b scanning range is 157.9-158.9 cm^{-1}
c calculated efficiency of the FILM optics including filters
d including all unknown losses

then those of the COBE/FIRAS. The reason of this inconsistency might come from the large difference of the beam size; the FIRAS beam was 7 degree and the FILM and the balloons telescopes had about 0.2 degree beams. Detail processes of these comparison were described in Makiuti et al. (1996)[13] and Okumura et al. (1996)[14]. As the IRTS on the SFU was successfully recovered by the STS in January 1996, a post-flight measurement of the responsivities will make the absolute calibration much more reliable.

3.3 Sensitivity

On the basis of the flight performance described above, we have calculated the sensitivity and the detection limits for the [CII] spectral line as well as for the continuum emission in space. The results are listed in Table 1. The result of a comparison with other instruments for the [CII] line is shown in Figure 6.

The 3 σ detection limit of the [CII] line intensity per beam is approximately 5×10^{-7} ergs cm^{-2} s^{-1} sr^{-1} if the noise is dominated by the electrical random noise not by long term variations. This value is one to two orders of magnitude better than those of the air-borne and balloon-borne telescopes and the COBE/FIRAS, and is comparable with a rocket-borne measurement by Bock et al. (1994)[15]. The FIRAS on the COBE has measured the extended [CII] emission (Bennett et al. 1994)[4], but the beam size of 7 degrees is too large to distinguish the individual Galactic components from the general Galactic plane component in the [CII] intensity map of the whole sky. By contrast, the FILM has achieved to resolve those components with its smaller beam size of 8 × 13 arcminutes. The FILM also demonstrated an advantage over the LWS on the ISO[16] in observing the [CII] emission from sources which extend over more than tens of arcminutes. As for the detection limit of the [OI] channel, we are still under analysis.

4. SUMMARY

The Far-Infrared Line Mapper (FILM) on the Infrared Telescope in Space (IRTS) has successfully been operated in space, and measured the [CII] 158 μm line intensities and the far-infrared continuum emission at 155 and 160 μm with high sensitivity for extended sources and spatial resolution of 8 arcmin × 13 arcmin, and provide intensity maps over 7 % of the sky. The first series of the scientific results are seen in separate papers[13,14,17]. The SFU was successfully recovered by STS January, 1996 and we are preparing a post flight test of the FILM, which will give us much more accurate evaluation about the behavior of the FILM in flight.

Many people of ISAS have contributed to the development and the operation of the FILM. Mrs. Y. Yamashita Yui fabricated an excellent low-pass filter for the FILM. We have been supported technically by Prof. H. Ishimoto at University of Tokyo for making a high thermal conductive copper, by Mitaka Kohki for machining the complex FILM structure, and by Nikon for developing a unique grating. We specially thank T. Matsumoto, H. Murakami, T. Onaka, M. Narita, and other members of IRTS project.

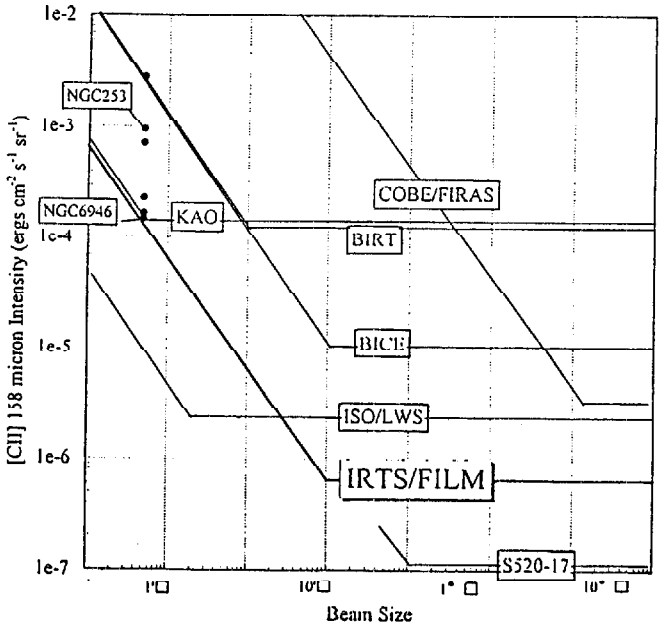

Fig. 6. The sensitivity of the [CII] channel of the FILM (3s, 1 FOV), compared with those of BICE (3s, 1 FOV) (Nakagawa et al. 1993), BIRT (3s, 1 FOV) (Shibai et al. 1991), the COBE/FIRAS, and LWS on ISO (3s, integration time is 1 second) (Scientific Capabilities of the ISO Payload 1991). The detection limit of the FIRAS is an approximate estimate using the all-sky [CII] 158 μm map of Bennett et al. (1994). The limit of the ISO/LWS is inversely proportional to the square root of the integration time.

5. REFERENCES

1. *IRAS Catalogs and Atlases: Explanatory Supplement.* 1988, ed. C. A. Beichman, G. Neugebauer, H. J. Habing, P. E. Clegg, & T. J. Chester (Washington, DC:GPO)
2. Shibai, H., Okuda, H., Nakagawa, T., Matsuhara, H., Maihara, T., Mizutani, K., Kobayashi, Y., Hiromoto, N., et al. 1991, Ap. J., **374**, 522
3. Nakagawa, T., Doi, Y., Mochizuki, K., Yui, Y.Y., Okuda, H., Yui, M., Shibai, H., Nishimura, T., & Low, F.J. et al. 1995, in Proc. of The Physics and Chemistry of Interstellar Molecular Clouds, ed. G. Winnewisser & G. C. Pelz (Berlin; Springer), p22.
4. Bennett, C.L., Fixsen D.J., Hinshaw, G., Mather, J.C., Moseley, S.H., Wright, E.L., Eplee, Jr., R.E., Gales., J., et al. 1994, Ap. J., **434**, 587
5. Shibai, H., Yui M., Matsuhara H., Hiromoto N., Nakagawa T., & Okuda H. 1994, Ap. J., **428**, 377
6. Murakami, H., Bock J., Freund, M.M., Guo, H., Hirao, T., Lange, A.E., Matsuhara, H., Matsumoto, T., et al. 1994, Ap. J., **428**, 354
7. Murakami, H., Freund, M.M., Ganga, K.M., Guo, H., Hirao, T., Hiromoto, N., Kawada, M., Lange, A.E., et al. 1996, submitted to Publ. Astron. Soc. Jpn.
8. Matsumoto T. & Murakami H. 1996, in this volume of Proc. SPIE.
9. Hiromoto, N., Itabe, T., Shibai, H., Matsuhara, H., Nakagawa, T., & Okuda, H. 1992, Appl. Opt. **31**, No.4, 460
10. Hiromoto, N., Fujiwara, M., Shibai, H., & Okuda, H. 1996, Jpn. J. Appl. Phys. **35**, 1676
11. Nakagawa, T., et al. 1996, in preparation.
12. Hirao, T., Matsumoto, T., Sato, S., Ganga, K., Lange, A. E., Smith B. J., & Freund, M. M. 1996, in this volume of Proc. SPIE.
13. Makiuti, S., Shibai, H., Okuda, H., Nakagawa, T., Matsuhara, H., Hiromoto, N., & Okumura, K. 1996, submitted to Publ. Astron. Soc. Jpn.
14. Okumura, K., Shibai, H., Okuda, H., Nakagawa, T., Makiuti, S., Matsuhara, H., & Hiromoto, N. 1996, submitted to Publ. Astron. Soc. Jpn.
15. Bock, J.J., Hristov, V.V., Kawada, M., Matsuhara, H., Matsumoto, T., Matsuura, S., Mauskopf, P.D., Richards, P.L., Tanaka, M., & Lange A. 1993, Ap. J.(Letters), **410**, L115
16. *ISO Scientific Capabilities of the ISO Payload.* 1991, ISO-SSD-8805, Issue 1.0, ESA
17. Shibai, H., Okuda, H., Nakagawa, T., Makiuti, S., Matsuhara, H., Hiromoto, N., & Okumura, K. 1996, submitted to Publ. Astron. Soc. Jpn.

accept. ed for Proceedings of SPIE 2817, Infrared Spaceborne Remote Sensing IV , ed. M. S. Scholl and B. F. Anderesen

Flight performance of the Far-InfraRed Photometer (FIRP)

Takanori Hirao

Communications Research Laboratory, Koganei, Tokyo, 184, JAPAN

Toshio Matsumoto

Institute of Space and Astronautical Science, Sagamihara, Kanagawa, 229, JAPAN

Shinji Sato

Department of Physics, Nagoya University, Nagoya, Aichi, 464-01, JAPAN

Ken Ganga, Andrew E. Lange and Beverly J. Smith

California Institute of Technology, Pasadena, CA, 91125, USA

Minoru M. Freund

NASA, Ames Research Center, CA, 94035-1000, USA

ABSTRACT

We present the flight performance of the Far Infrared Photometer (FIRP) onboard the Infrared Telescope in Space (IRTS). The FIRP was designed to measure the absolute sky brightness in four submillimeter wavelength bands centered on 150, 250, 400, and 700 μm with a spectral resolution of $\lambda/\Delta\lambda = 3$, and with spatial resolution of 0.5°. The bolometers were cooled to 300 mK by a ^{3}He refrigerator, and an AC bridge readout circuit was used to achieve high sensitivity. The ^{3}He refrigerator achieved a temperature of ~300 mK during each of three ^{3}He condensations carried out in orbit. The hold time was confirmed to be at least 7 days per cycle. We observed ~7% of the sky during a mission time of 3 weeks. Some excess noise was observed in most of the channels. Adequate sensitivity was achieved in all channels for observations at low galactic latitudes, where emission from intersteller dust is relatively bright. The preliminary sensitivities (60sec integration, 1σ) are estimated to be $7.7 \times 10^{-7}, 3.1 \times 10^{-8}, 7.7 \times 10^{-8}$, and 3.7×10^{-8} Wm^{-2}sr^{-1} for the 150, 250, 400, and 700 μm channels, respectively.

Keywords: IRTS, submillimeter, 300 mK bolometer, 3He refrigerator

1. INTRODUCTION

The Infrared Telescope in Space (IRTS) was one of the mission experiments aboard the Japanese small space platform, Space Flyer Unit (SFU), and was designed to make absolute measurements of the sky brightness from 1 μm to 1 mm.[1] To reduce the thermal emission of the telescope, the whole telescope system was cooled down to ~2K with liquid ^{4}He. The Far Infrared Photometer (FIRP) is one of the four focal plane instruments on the

IRTS. The FIRP is an absolute photometer using bolometers, with four passbands centered at 150, 250, 400, and 700 μm. The spectral resolution, $\lambda/\Delta\lambda$, was $\sim$3 for all channels, and the spatial resolution was 0.5° (FWHM). To achieve high sensitivity, the bolometers were cooled to 300 mK by a ^{3}He refrigerator, and AC biased bridge readouts were used.

The sky has previously been surveyed at submillimeter wavelengths by the Diffuse Infrared Background Experiment (DIRBE) and the Far Infrared Absolute Spectrophotometer (FIRAS) on the Cosmic Background Explorer (COBE) satellite.[2] The spatial resolution of the DIRBE was 0.7° which was comparable to that of the FIRP, however it did not have photometric bands at wavelengths longer than 240 μm. The spatial resolution of the FIRAS was 7°. The FIRAS was equipped with a Fourier spectrometer that provided spectral coverage from 100 μm to 1 cm and spectral resolution much higher than that of the FIRP.

2. INSTRUMENTATION

The detailed instrumentation of the FIRP is described in Lange et al.[3] We used low-background, long time-constant bolometers in the readout circuit electronics shown in figure 1. A pair of thermally and electrically matched bolometers was placed in each channel of a bridge circuit, and one of the two bolometers was illuminated. The four bridge circuits were biased with a square-wave AC voltage in the frequency range of 100–200 Hz depending on the channel. The output of the bridge was fed into a cold J-FET source follower and amplified by a differential amplifier. To eliminate the 1/f noise originating from cold J-FETs, a lock-in amplifier was used. The electrical noise equivalent power (NEP) of each detector itself measured in the laboratory was $\sim 2 \times 10^{-17}$ WHz$^{-1/2}$.

The bolometers were cooled by the ^{3}He refrigerator which was designed to be operated in zero gravity.[4] Figure 2 is a schematic diagram of the refrigerator. The refrigerator was filled with 16.8 liter-STP of ^{3}He, and had an expected hold time of $\sim$10 days. At 2 K, the ^{3}He gas is absorbed in the charcoal pump filled with activated charcoal. On the start of the condensation, the pump is heated by a 31 mW heater and the ^{3}He gas is desorbed. The evaporator is filled with a silicose sponge (Space shuttle tile), and is thermally linked to the ^{4}He tank by a heat switch, which keeps the temperature of the evaporator at $\sim$2 K, allowing the liquid ^{3}He to condense. After all of the ^{3}He gas is desorbed, the evaporator is thermally isolated and the heat switch on the pump is turned on. The ^{3}He gas is absorbed by the pump and the vapor pressure in the evaporator is reduced. As a result, the evaporator is cooled to $\sim$300 mK. The photometer containing the bolometers is connected to the evaporator by a high purity Cu heat strap.

The incident beam first passes through a low-pass filter with cutoff frequency of 100 cm^{-1}.[5] A 2K cold shutter located immediately behind the low-pass filter modulates the signal at 1/8 Hz to provide a zero-reference. An internal calibrator made of doped Ge is placed just behind the shutter and is activated every 256 seconds to measure gain stability. After passing the cold shutter, the beam enters the 300 mK photometer, and is incident on a series of three dichroic beamsplitters that act as low-pass filters with half-power points at 200, 350, and 600 μm. A thick grill filter in front of each illuminated bolometer provides low frequency blocking. Each passband is formed by the combination of these filters.

There existed many noise sources on the SFU, including on-board computers and switching power regulators. For this reason, we added compact low-pass electrical filters working at cryogenic temperatures in order to suppress RF voltage noise fed to the bolometers.[6] These filters were two pole LC filters with a cutoff at $\sim$100 kHz, and an attenuation of -24 dB/octave. Surface mounted devices were used to meet the limits of mass and volume. One standard thin film resistors (25.5 Ω), two NPO capacitors (10 nF), and two unshielded inductors (18 μH) were used in each filter. The filters were placed in two RF tight housings and installed just before the input connectors of the FIRP. Several electromagnetic compatibility (EMC) tests were performed before flight. Before installing the electrical filters, the output signal was severely degraded by RF interference. In the worst case, the excess noise was about 200 times larger than the ideal noise. After installation of the filters however, no apparent RF

interference was found.

3. FLIGHT PERFORMANCES

Observations started on March 30, 1995 and terminated on April 24, 1995 when the liquid ^{4}He in the IRTS cryostat ran out. The ^{3}He refrigerator was successfully cycled three times during the observation period, and achieved a temperature of ~300mK each time.[7] All three in-flight condensations reproduced the successful pre-flight condensations done with the flight cryostat (See figure 3(a)). It was impossible to measure the hold time because the first and the second cycles were terminated by telemetry commands due to the limited flexibility of the operation of the SFU. The third cycle was terminated by running out of liquid ^{4}He. The longest hold time achieved in orbit was ~7 days. A detailed description of the flight performance is given by Freund et al.[7]

From the analysis of the signal of the calibration lamp, we found that the responsivities of the bolometers were stable overall (See figure 4), consistent with the stability of the temperature of the 300 mK heat sink. The temperature on the still rose by ~5 mK at 4–5 days after the condensation, producing ~2 % decrease in the responsivity of the bolometer. Such a temperature rise was reproduced in every cycle on orbit. It was never observed in the ground tests, which never lasted more than 36 hours.

The DC analog output of the FIRP signal was sampled at 8 Hz by a 16 bit A/D converter. Typical digitally sampled output of the detector channels is shown in figure 5. Due to the long time constants of the bolometers, ~1.5 seconds was needed to stablize the signal. Thus we normally mask 12 samples immediately following the shutter transient. We also mask 4 samples just before the shutter transient to avoid an anomaly, caused by the moving shutter. The rest of the 16 samples are regarded as the 'signal' for each shutter state and averaged. When these averaged signal are expressed as $S_{\mathrm{open},n}$ etc. as shown in figure 5, the sky signal, S_n, for each shutter cycle, n, is estimated to be

$$\langle S_n \rangle = \langle S_{\mathrm{open},n} \rangle - \frac{1}{2}\left(\langle S_{\mathrm{closed},n-1} \rangle + \langle S_{\mathrm{closed},n} \rangle\right). \quad (1)$$

This scheme was chosen in order to reduce the effects of possible drifts in the dark level. We then calculated the standard deviation about the mean of each shutter open period and each shutter closed period. Any cycles with open or closed periods with standard deviations that exceeded 3σ were defined as 'noisy data', and excluded from the analysis.

Degradation of some data was caused by passage through the South Atlantic Anomaly (SAA). The signal of 250 μm channel while passing through the SAA is shown in figure 6. Many spikes were detected in the SAA, however no after effect was observed.

Stray light was detected after each ^{3}He condensation. The 700 μm signal at the third condensation is plotted in figure 3(b). Only $|b| > 50°$ data were selected for this plot. The intensity of the stray light decreased as a function of time. The spectrum of the stray light three hours after the 3rd condensation is fit by a two component blackbody function, one at ~5 K blackbody with an emissivity of >50 %, and the other one being a several tens of kelvin blackbody with an emissivity of <1 %. Since the stray light was well correlated with the ^{3}He condensations, and its intensity and spectrum was apparently different from that of the natural sources, the origin is assumed to be internal. The stray light had vanished after one day after the end of each condensation. Additional stray light was observed after some Moon passes as shown in figure 7. The nature of that stray light was similar with that of observed after the ^{3}He condensations. The source of the stray light may be thermal emission from an internal part heated by the Moon. The stray light caused by the Moon passes disappeared after several hours. Either kind of stray light was not observed in the laboratory tests.

The preliminary sensitivities are calculated in the following way. The difference between the signals of two adjacent closed shutter periods is $S_{\mathrm{closed},n-1} - S_{\mathrm{closed},n}$ in figure 5. The standard deviation for the differences over a certain time period (60 seconds for this estimation) is derived and the average of the standard deviations is

regarded as the noise level of the 60 seconds integrated data. As a result, the sensitivities (60sec integration, 1σ) are estimated as $7.7 \times 10^{-7}, 3.1 \times 10^{-8}, 7.7 \times 10^{-8}$, and 3.7×10^{-8} $Wm^{-2}sr^{-1}$ for the 150, 250, 400, and 700 μm channels, respectively (figure 8).

4. CONCLUSIONS

- We successfully measured the brightness of ~7 % of the sky at submillimeter wavelengths.
- The ^{3}He refrigerator was successfully cycled three times in orbit and it achieved a temperature of ~300mK.
- We detected some stray light which was not observed in preflight tests. However it was easily rejected, and did not affect the scientific results.
- Some excess noise was seen in most of the channels during the whole observation period. The excess noise severely degraded the sensitivity in some channels. Adequate sensitivity was achieved in all channels for observations at low galactic latitudes, where the emission from intersteller dust is relatively bright.

5. ACKNOWLEDGEMENT

Many people at the University of California at Berkeley and Nagoya University contributed to the development of the FIRP. We acknowledge Clare Tector at California Institute of Technology for the excellent noise analysis. T.H. was supported by the Research Fellowships of the Japan Society for the Promotion of Science for Young Scientists. K.G. acknowledges support from NASA grants NAGW-4623 and 4870. The authors especially thank all the members of the IRTS team for their kind support.

6. REFERENCES

1. H. Murakami et al., "The Infrared Telescope in Space (IRTS)", Astrophys.J., Vol.428, pp.354-362,1994.
2. J. C. Mather, "The Cosmic Background Explorer (COBE)", Opt. Engineering, Vol.21, No.4, pp.769-774, 1982.
3. A. E. Lange et al., "The Far-Infrared Photometer on the Infrared Telescope in Space", Astrophys.J., Vol.428, pp.384-392, 1994.
4. L. Duband et al., "", Cryogenics, Vol.30, pp.263-, 1990.
5. J. J. Bock and A. E. Lange, "Performance of a low-pass filter for far-infrared wavelengths", Applied Optics, Vol.34, No.31, pp.7254-7257, Nov. 1995.
6. M. M. Freund et al., "Compact low-pass electrical filters for cryogenic detectors", Rev.Sci.Instrum., Vol.66, No.3, pp.2038-2040, March 1995.
7. M. M. Freund et al., "Design and Flight Performance of a Space Borne ^{3}He Refrigerator for the Infrared Telescope in Space", Cryogenics, in press.

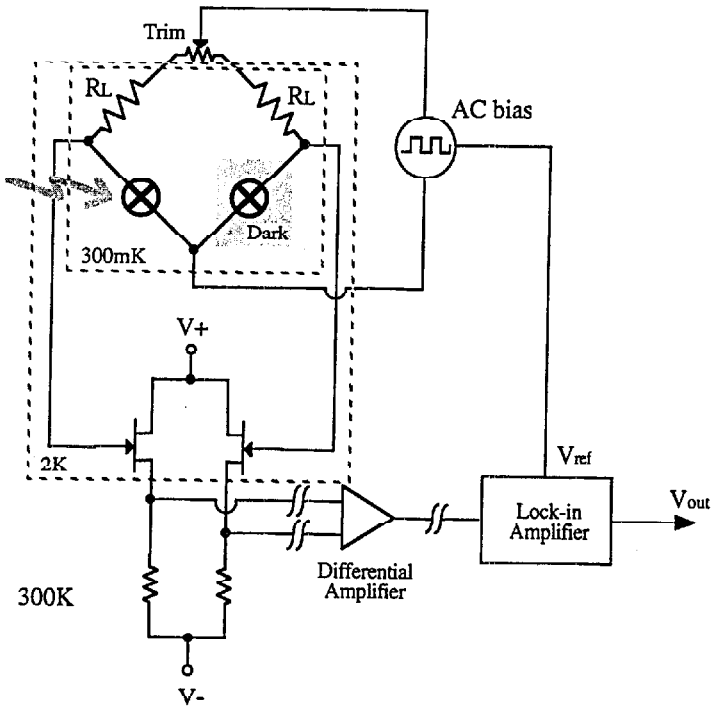

Figure 1: (a) Schematic of the AC bridge readout used for the bolometers. A circle with a cross represents a bolometer. Each load register, R_L, is 10 MΩ.

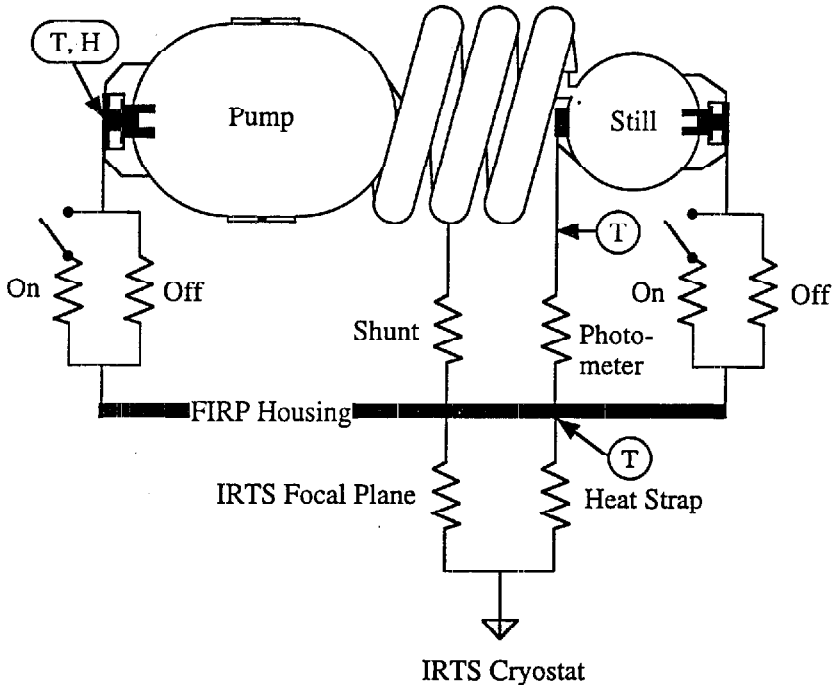

Figure 2: Schematic view of the ^{3}He refrigerator. A helical pump tube connects a still to a sorption pump filled with activated charcoal. A silicone sponge which is inside the still (the evaporator) holds the ^{3}He liquid by surface tension during operation. Thermal connection from the ^{4}He tank to the pump and the still are made via gas-gap heatswitches. 'T' and 'H' represent thermometers and a heater on the pump, respectively.

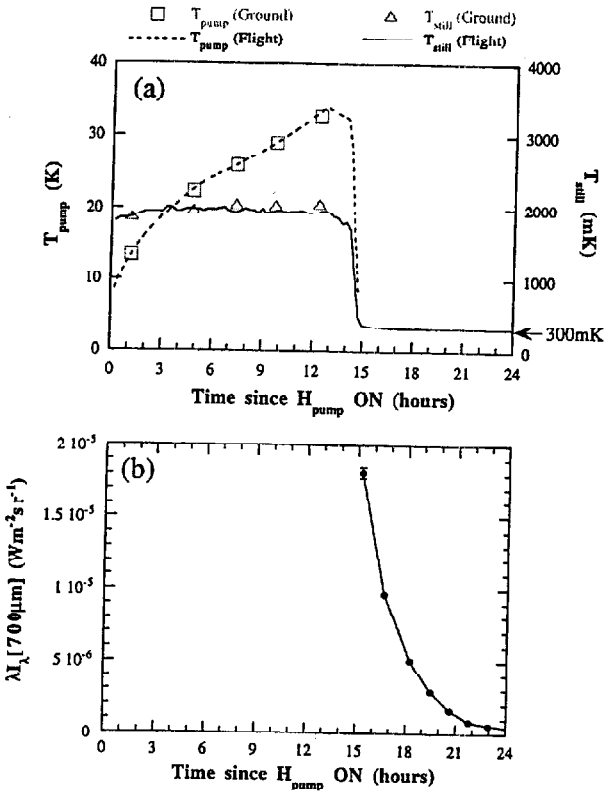

Figure 3: (a) The variation of the pump temperature and the still temperature during condensation versus time since the heater on the pump was turned on. The dashed line and the solid line represent the pump temperature and the still temperature measured during a flight condensation, respectively. The results of a condensation cycle done in a pre-flight test are shown as open rectangles (the pump temperature) and open triangles (the still temperature) for comparison. (b) The signal of the 700 μm channel versus the time since the heater on the pump was turned on. Each closed circle corresponds to the averaged signal for the region where $|b| > 50°$ (b represents the galactic latitude).

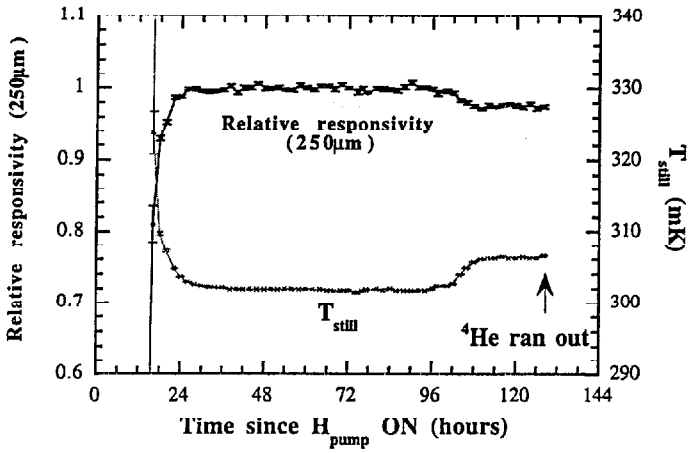

Figure 4: The relative responsivity of the 250 μm channel (solid black line) versus time since the heater on the pump was turned on. The still temperature, gray line, is shown for comparison. The relative responsivity is well correlated with the still temperature. This run was terminated when the liquid ^{4}He ran out.

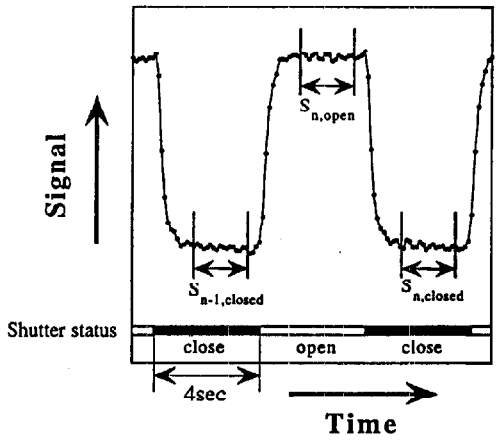

Figure 5: Digitally sampled signal output. Small dots represent the sampled data points. There are 32 samples for each shutter state. The meanings of $S_{open,n}$ etc. are described in the text.

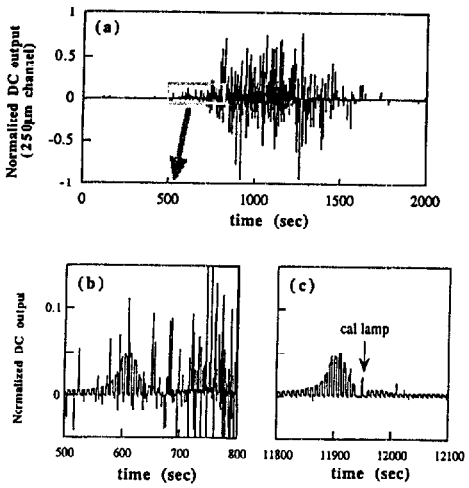

Figure 6: (a) The DC output of the 250 μm channel while passing through the south Atlantic anomaly (SAA). No after effect was observed. (b) A magnified figure of the data inside the rectangle shown in (a). We detected many spikes in addition to the signal of the galactic plane modulated by the cold shutter. (c) The signal of almost the same region shown in (b). This signal was taken while the IRTS was outside of the SAA. The sky signal itself is essencially the same between (b) and (c).

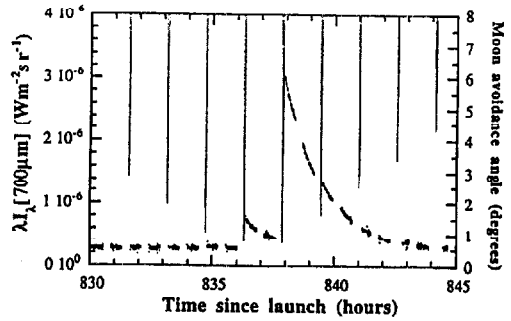

Figure 7: The signal of the 700 μm channel (small dots) and the Moon avoidance angle (solid line) versus time since launch. Only $|b| > 50°$ data are selected for the 700 μm signal. Significant signal increases are found at 834.7, 836.2, and 838 hours since launch when the Moon avoidance angle gets less than one degree.

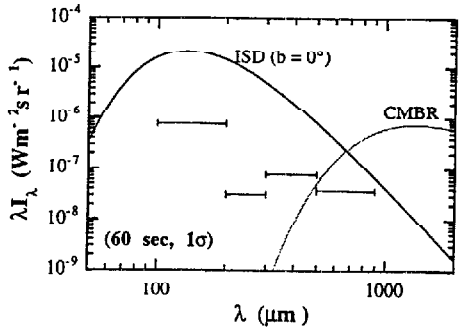

Figure 8: The preliminary sensitivity of the FIRP. All values correspond to $1\sigma/60$ seconds integration. The spectra of the 2.74 K cosmic microwave background radiation (CMBR) and the thermal emission from interstellar dust (ISD) on the galactic plane ($b = 0°$) are shown for comparison.

On-Orbit Thermal Behavior of the IRTS Cryogenic System

G. Fujii, S. Tomoya, M. Kyoya*, M. Hirabayashi*, M. Murakami+, T. Matsumoto++, T. Hirao++, H. Murakami++, H. Okuda+++ and T. Kanari+

Space Systems Development Div., NEC Corp., Yokohama, 226 Japan
*Sumitomo Heavy Industries Ltd., Toyo, Ehime 799-13 Japan
+Institute of Engineering Mechanics, Univ. of Tsukuba, Tsukuba 305 Japan
++Dept. of Physics, Nagoya University, Nagoya 464-01 Japan
+++Institute of Space and Astronautical Science, Sagamihara, Kanagawa 229 Japan

Accepted for Cryogenics

Abstract

The IRTS (Infrared Telescope in Space) was launched at 08:01 on March 18th UT by the H-II rocket as a part of the Space Flyer Unit (SFU), which is a re-usable free flyer designed as a multi-purpose common facility for scientific and engineering experiments. The He II tank was estimated to be approximately 85%-full at 1.84 K at the moment of launch, 11 hours after pumping was disconnected and the tank was sealed. The vapor evacuation through a porous plug was resumed 28 min. after the launch. The thermal state reached the anticipated steady state at 1.91 K on the 3rd day without any anomalous thermal behavior of the porous plug in the initial zero-g state. Over the course of 10 days the SFU transferred to an LEO at 486 km from the initial phase orbit at 340 km with the telescope aperture lid ejecting on day 11 after launch. A ^{3}He refrigerator was then activated to decrease the temperature of some bolometer detectors down to 302 mK for observations in the far IR region. Every detector worked quite satisfactorily. The stable thermal state of He II at 1.91 K was maintained until the depletion of He II at 09:30 on April 24 UT. The cold life is found to be fairly close to the prediction on the basis of the ground test data. On April 27 the sun shield was jettisoned for the safe retrieval by a US shuttle in January 1996, and the IRTS mission was completed because of the regular shift of the SFU mission time-line to another experiment. In this report the flight data of the thermal performance of the cryogenic system is discussed.

The IRTS[1] was launched by the H-II rocket on March 18th, and successfully completed its IR observation mission for 34 days. The IRTS consists of a superfluid helium cooled telescope with a primary mirror of 15 cm. The major observational objectives extend in wavelengths from the near infra-red to the far intra-red regions. The IRTS was launched on board the Space Flyer Unit (SFU)[2], which is a re-usable free flyer designed as a multi-purpose common facility for scientific and engineering experiments, and will be retrieved by the NASA Space Transportation System(STS) in January 1996. The telescope of the IRTS is cooled down to 1.9 K by stored superfluid helium. The observational plan demanded that the cooled life time was longer than 30 days, the detectors should be colder than 2 K and the highest temperature be lower than 10 K at the forebaffle tip. On the other hand, by a strong constraint on the volume allocated to the IRTS to be well accommodated to the SFU, the He II tank volume is limited to 100 dm^3. A porous plug (PP) is employed as a phase separator between He II and helium vapor.

In the present report, on-orbit thermal behavior of the IRTS cryogenic system is discussed. The flight data include several environmental house keeping data, several cryogenic temperatures at the He II tank, the PP, the forebaffle, the focal plane instrument, the still and the charcoal pump of the ^{3}He refrigerator, and the sun and the earth avoidance angles. The IRTS cryogenic system is not equipped with a vapor flow rate meter.

Description of SFU-1 and IRTS

SFU-1

The SFU was developed by three Japanese organizations; the Institute of Space and Astronautical Science (ISAS), the National Space Development Agency (NASDA), and the Institute for Unmanned Space Experiment Free Flyer (USEF). The general view of the SFU is schematically illustrated in Fig. 1. The system specification is summarized in Table 1. It is an octagonal truss in structure with an diameter of 4.5 m and a height of 2.8 m; the total weight is 4.0 ton. Eight thermally controlled payload boxes are attached to the truss, six of which are for the user experiments. The user instruments can also be accommodated on the exposed upper deck and in the center hole. The IRTS is directly attached to the SFU truss, replacing one of the payload boxes. Several co-onboard missions are prepared for this first flight in addition to the IRTS, such as a large deployable high voltage solar array, an electric propulsion experiment, electric furnaces for material experiments and life science experiment.

IRTS

The IRTS system schematic is given in Fig. 2. The interior structure, composed of the tank, the telescope and the focal plane instruments (FPI), is suspended by low thermal conductivity support straps from the outer shell to cut conduction heat leak. The telescope[3] is of a Richey-Chretien type with a 15 cm primary mirror and a focal length of 600 mm, F/4, having a field of view of 0.1 to 0.5 deg appropriate for high detectivities as well as moderate spatial resolution suitable for the observation of diffuse IR sources. The mirrors are made of aluminum alloy. The surface of the mirrors are coated with 0.2 μm Au and 0.1 μm SiO_2. The mirror cell and the secondary mirror support are also made of aluminum alloy to minimize the degradation of image quality due to differential thermal contraction. Four scientific instruments, the Near Infrared Spectrometer (NIRS), the Mid Infrared Spectrometer (MIRS), the Far Infrared Line Mapper (FILM), and the Far Infrared Photometer (FIRP), together with a near-IR star sensor, are installed in the FPI box to observe the sky brightness over the 1-1000 μm wavelength region. All of the FPIs are surrounded by a shield cooled to a temperature of approximately 2 K to reject the far-infrared emission from the vapor cooled shields. The bolometers for the FIRP are cooled down to 300 mK by a closed cycle ^{3}He refrigerator[4,5]. The detailed description of the IRTS design is given in Table 2. The size of the cryostat is 93 cm in diameter and 110 cm long. A circular aperture shade used for rejection of IR radiation from the earth is attached to the outer shell of the cryostat. The sun shield was deployed and the aperture lid was ejected on orbit by a spring mechanism prior to the IRTS observation. The IRTS astronomical observation lasted for 25 days.

SFU orbit and attitude control

After spending the first several days on initial orbit, the SFU-1 system completed a transfer to the experimental operation orbit, a circular orbit of 486 km altitude and 28.8-deg inclination by the end of the 11th day. Meanwhile the quantity of outgas and degas from the whole SFU system, being a potential contamination source, decreased below the tolerable level for the cooled IR observation. Accordingly, on the 11th day the sun shield was deployed and the aperture lid was ejected to start the IR observation (see Fig. 3).

The SFU-1 was operated in the solar-oriented attitude where the -X axis of the SFU-1 is pointed toward the Sun for the maximum solar cell performance as seen in Fig. 4. The IRTS itself has no pointing capability, instead it is rigidly fixed to the SFU structure. Thus, the SFU was rotated around the -X axis once per orbital revolution at a constant rate for the sake of wider IRTS observation sky coverage in the scanning mode along great circles in the sky at right angle to the Sun and of avoiding both solar and earth radiation. The direction and phase of the IRTS rotation was determined so as to maximize the angular distance from the IRTS optical axis to the earth limb to minimize the thermal radiation heat input. Basically two scanning modes are considered. At the center of the day side on the orbit, the IRTS is directed to the north when it passes through the northern side of the subsolar point (mode 1), or directed to the south when the SFU passes through the southern side (mode 2). As shown in Fig. 4, the -X axis

is, in fact, slightly off of the Sun line (angle g in the figure), southward or northward depending on the scanning mode because the earth limb is only 22 deg. below the horizontal direction on the spacecraft. The mode change from the mode 1 to 2 was operated on the 18th day after launch. The accuracy of the SFU attitude-control system is about 1 deg. The actual scan path is reconstructed to an accuracy of 1 arcmin. after the mission, using the data from the gyroscopes of the SFU core system and the IRTS star sensor.

After the completion of the IRTS observation on the 37th day the sun shield was jettisoned, and the shut-off valve of the helium tank was opened for the complete discharge of helium on the 39th day for the safety retrieval by NASA's STS system. The SFU will descend to the retrieval orbit of 315 km altitude at the end of its 5 month mission and then will be retrieved in January 1996.

IRTS cryostat and baffle system

A cross-sectional view of the IRTS cryostat is shown in Fig. 2. A full description of it is given elsewhere[6]. The capacity of the torus-shaped superfluid helium tank is 100 dm^3. The primary and secondary mirror assembly and the FPI box are fixed on the cold plate which keeps firm thermal contact with the bottom part of the tank, both of which are designed to operate at a temperature of 1.9 K. The telescope aftbaffle is also directly connected to the bottom part of the tank. A porous plug made of alumina ceramics is employed as a vapor-liquid helium phase separator. Helium vapor evaporated through the PP first cools the forebaffle and then circulates through the VCSs. This particular vapor cooling scheme is demanded to make the thermal radiation negligible even in the submillimeter region, which requires ultimate low temperature of the baffle system. The thermal performance of the cryostat system can be evaluated by using the thermal analysis program fully confirmed by the ground tests conducted for various thermal situations. The predicted temperature distribution is compiled in Table 3. The total heat load to the tank is estimated to be about 83 mW during the typical observation phase (Case 2 in Table 3), which figure will be compared with flight data. The half of it is due to heat conduction through the support straps, and the sum of the FPI heat dissipation and the conduction heat input from the forebaffle is 12 mW.

Because the IRTS is intended to make absolute measurements, good sidelobe rejection (good optical performance to reject any non-parallel components of IR signal disturbed by imperfection of optical system) is required for the baffle system. The design concept for it is schematically shown in Fig. 3[7]. The sun shield is a CFRP sheet, 2 m long, covered with an aluminized Teflon film on the surface. It, stowed rolled up, is deployed on orbit to block the direct incidence of solar radiation into the aperture shade. The aperture shade has a specular inner surface that reflects thermal radiation from the sun shield and the earth. It has a double structure, the radiation shield and the radiator at the patch portion. The forebaffle is a Winston-type reflector[8] made of aluminum alloy coated with Au to reflect the thermal radiation of the aperture shade back to the sky. This reflecting forebaffle is essential for the IRTS cryostat design, since it reduces the aperture heat load considerably. This design contributes to make the cryogenic system more compact. The heat switch[4], of gaseous conduction type, is equipped to enhance the thermal connection between the forebaffle and the helium tank to cool the forebaffle down to sufficiently low temperature in order to minimize the thermal emission even in the submilimeter region. However, it was, in fact, never activated during the IRTS mission, because the thermal noise from the forebaffle was kept low enough for the IR observation in every wave length region even at the temperature as high as 13 K due to better performance of the forebaffle than the design value. The aftbaffle consisted of a set of annular vanes coated with specially compounded paint for its mechanical strength against peel off and nearly perfect black properties in the near-IR to submillimeter wavelength regions[9].

On-Orbit Thermal Behavior of Cryogenic System

Overall thermal performance

The temperature in the cryogenic system area was measured only at three locations with germanium resistance thermometers, on the outer surface of the tank wall at the bottom T_{Tank}, on the downstream side of the porous plug phase separator element T_{PP}, and the forebaffle close to its base, T_{FB}. The data are shown in Fig. 5. T_{Tank} may be considered as the He II temperature in the tank as far as the system is in a thermal equilibrium state. The overall thermal performance of the system may be considered to be quite satisfactory through the whole mission. The steady state He II temperature was very stable at 1.91 K, which quite well agrees with the prediction on the basis of the ground test data, except at several periods of scheduled thermal events as stated below. And so does T_{PP}, that is T_{Tank} minus 40~50 mK, which is one of the evidences that the porous plug phase separator functioned properly. The stable thermal state of He II may be considered to last till the final stage, judging from the result that T_{PP} kept a constant temperature at 1.85 K till the depletion, though the temperature of the tank T_{Tank} showed a slow rise with a small fluctuation toward the final stage. It is also seen that T_{FB} was low enough for the absolute IR measurement in every wavelength regions. It is the reason why the heat switch did not need to be activated on orbit. It should be noted that the data in this particular graph are sampled every 2 or 3 hours and thus this is not adequate for detailed discussion. The data sampled at higher data rate, that is 3 sec sampling, are presented in the followings.

The cryogenic system nearly reached an equilibrium state by launch plus 70 hours. The aperture lid was ejected for the astronomical observation at 280 hours, which caused T_{FB} began to drop by about 2 K. The rather straightforward thermal conduction link between the outer shell and the forebaffle through the aperture lid structure was lost upon the ejection. After the opening of the aperture, the forebaffle underwent a quasi-periodic temperature variation according to the orbital revolution though it is not clearly shown in this figure. At 890 hours He II was depleted, and the temperatures rose rapidly. However, the temperature rise in the cryogenic system later on was found to be rather slow and to be still below 50 K at one day after the depletion. The 44 mW heater of the ^{3}He refrigerator was activated three times each for 12 hours and 30 min., starting at 291 hours, 551 hours and 760 hours after launch. During heating ^{3}He was desorbed from charcoal in the condenser, and condensed in the still for the subsequent cooling for more than 8 days. Accordingly the temperature of He II, T_{Tank}, and thus also T_{PP} rose by the magnitude corresponding to the residual mass of He II in the tank, and these heatings increased the evaporating vapor flow rate to cause temperature drop of the forebaffle due to augmentation in cooling power. The apparently irregular fluctuation of T_{FB} around 400 hours was caused by the solar and earth radiation as discussed later.

Initial phase thermal behavior

During the topping-off procedure liquid helium at 3.1 K was charged at the pressure of 40 kPa (300 torr). This was completed at 26 hours before launch when overflow of liquid helium from the tank was detected for more than 10 min. The final fill charge can be estimated to be 97 dm^3 from the ground test data. Then vapor evacuation through the bypass vent line (not through the PP) was continued until 12 hours before launch. The vapor flow meter on the ground indicated that 13.5 dm^3 of liquid helium was lost during this vapor evacuation process. The temperatures of He II and the forebaffle were 1.645 K and 4.0 K respectively, and the He II quantity was 83.5 dm^3 at the moment of valve-off. After this period all the electronic equipment was switched off until 3.5 hours after launch. During the short period for about 5 min. between the valve-off and the switched-off T_{FB} rose to 9 K while T_{Tank} indicated no significant change. The porous plug evacuation was started at 28 min. after launch. The thermal behavior during the period between the valve-off and the first data acquisition is considered to proceed almost as expected shown by the broken and dotted lines in Fig. 6. The estimated values of T_{Tank} and T_{FB} are 1.85 K and above 10 K, respectively, based on the first telemetry data and the ground test data, at the moment of the start of PP evacuation. The temperature rise of He II due to the internal heat generation in ductile material of the tank and baffle systems caused by structural vibration during rocket ascending period seemed to be smaller than the test result of 0.1 K during vibration test. It must be as small as 50 mK, judging from the first telemetry data of T_{Tank} and T_{PP}.. Immediately after the valve open for the PP evacuation, small amount of liquid helium flooded through the PP during the PP inactive phase first evaporated and flowed out to result in a rapid cooling down of the forebaffle. The general porous plug

flow performance indicates that limited amount of He II leak through the PP is inevitable during a PP inactive phase. But the amount of flooded liquid helium is estimated to be considerably less than 1 dm^3 on the basis of the following facts:

1) The location and the orientation of the entrance of the PP is carefully designed so that it is above the He II free surface and major He II leakage may not occur during a PP inactive phase in one-g state. Leakage may take place only for about 20 min before the PP open in zero-g. 2) Total volume of the vapor flow passage from the PP to the warm valve is about 1.3 litter including 300 K portion. 3) The thermal contact of the PP assembly with the He II tank and even with He II itself is very good in the IRTS design, and consequently the adverse temperature gradient across the PP element which may play the role as the very initial trigger towards the possible Castles's catastrophe is rather small during a PP inactive phase. 4) The permeability of the IRTS PP, $3*10^{-14}$ m^2, is too high for the element to act as a perfect fountain pump, that is as a super leak. It is experimentally found that reverse flow of the normal component occurs for high pressure difference across a PP element with a higher permeability than $1*10^{-14}$ m^2. High back pressure caused by the high rate of evaporation when He II contacts with high temperature thermal mass gives rise to a return flow of the normal component through a PP element to the tank rather than results in the catastrophe.

Thus, it is fair to suppose that no catastrophic leakage of He II occurred through the PP. The PP is considered to turn into a normal operation soon. In fact, the first data at about 3.5 hours after launch evidently indicated that the PP was already in a normal operation state characterized by T_{PP} lower than T_{Tank} by 40~50 mK, though the PP evacuation rate was still smaller than the anticipated steady value because of the lower temperature than the normal steady state temperature at 1.91 K. After this very initial stage, the PP evacuation rate increased to reach the steady operation value.

Such facts as the normal operation of the PP even at a few hours after launch and the cold life which agrees quite well with the prediction, as discussed later, suggest that no anomalous thermal behavior happened with the PP in the initial zero-g state. Moreover, the gradual temperature rise of the forebaffle in the very initial stage indicates the normal PP operation because the vapor flow rate is not so large as in a catastrophic state.

Thermal behavior in final He II depletion stage

The data in the final stage when He II was depleted are shown in Fig. 7. The small scale fluctuation of T_{Tank} seems to indicate that He II existed in localized areas in the tank and migrated slowly in it in this stage. Dry-out must have occurred on the inner surface of the tank leading to a temperature rise over the lambda temperature when He II was depleted. This caused drop in the vapor flow rate and thus rapid rise in T_{FB}. However, He II still remained in porous material of the PP keeping the same temperature for about 8 min. It is interesting to note that T_{PP} slightly dropped just prior to the dry-out of the PP. This is because the thermal link to the tank through He II was lost and consequently heat flow toward the PP was shut out upon the dry-out of the inner surface of the tank.

Cold life

The estimation of the heat leak to the tank by the thermal analysis on the basis of the ground test data is 96.7 mW for the period of closed aperture, and 83.0 mW for the normal observation phase with the aperture open. The latter figure is the total sum of the parasitic heat leak from the outer shell, 70.9 mW, the FPI heat dissipation, 8.8 mW, the thermal radiation through the aperture via thermal conduction through the forebaffle, 3.3 mW. The resulting cold life is estimated to be 35.5 days. Unfortunately, the temporal value of the heat leak could not be calculated for the IRTS was not equipped with a vapor flow rate meter. Actually, it was 37.5 days, being longer than the prediction by 5 %. The agreement between the prediction and the flight data is satisfactory. This fact seems also to support the conclusion that no anomalous flow phenomena through the PP happened during the initial zero-g coast state.

Temperature variation of the forebaffle

The temperature variation of the forebaffle was sufficiently small, as small as 0.3 K, through the major part of the mission due to adequate design of the sun shield and sun shade. Furthermore the base line temperature was quite stable at 5.0 K. However, quite a large temperature variation was observed between 350 and 500 hours as seen in Fig. 5. The temperature variation in this period is shown in Fig. 8. It is seen that the peak temperature rose as high as 13 K, one high and one low peak appeared per orbital revolution, and the base line temperature was still kept at a constant value 5 K. Shown in Fig. 9 is a typical example of T_{FB}, the earth and the sun avoidance angles plotted as a function of time during an orbital revolution. It is evident that the higher temperature peak occurred corresponding to the earth avoidance angle minimum on the day side but the lower peak also to the earth avoidance angle minimum on the night side. The latter nearly corresponds to the sun avoidance angle maximum at which angle the solar radiation hardly enters through the aperture. In order to examine the correlation among T_{FB}, the earth and the sun avoidance angles, the envelopes of the higher peak of T_{FB}, the local minima of the earth and the sun avoidance angles are plotted against time in Fig.10. A clearer one-to-one correspondence is recognized between T_{FB} and the earth avoidance angle rather than between T_{FB} and the sun avoidance angle. This is evidently demonstrated in Fig. 11, where the correlation between the temperature rise at the higher peak of T_{FB} and the corresponding minimum value of the earth avoidance angle is shown. It can be concluded that the two peaks of T_{FB} are caused by radiation heat input from the earth. The major distinction in thermal radiation from the earth between the day and night sides is that it is composed of the earth radiation and the albedo on the day side while it is of the earth radiation only on the night side. This result means that the reflectivity of the surface of the forebaffle is far better in the thermal radiation region than in the visible region where the spectral peak of the albedo exists.

Heat generation from ^{3}He condenser

The temperature rises during the second and the third heating of the condenser of the ^{3}He refrigerator are plotted against time in Fig. 12. The magnitudes of the temperature rises seem to correspond to the residual mass of He II in the tank, that is the temperature rise is approximately inversely proportional to the residual mass of He II. It is, however, found that this holds only qualitatively. The net heat to warm up He II is found to be considerably smaller than the total heating of 44 mW. Some amount of the heat does not make the He II temperature rise but just increases the evaporation rate as seen from the temperature drop of the forebaffle in Fig. 5. And the amount of heat to warm up He II seems to vary for three heatings according to the quantity of He II in the tank. Moreover, total thermal energy during the three heatings is rather small, equivalent to the evaporation of He II of only 1.3 dm^3 as compared with the total heat input to He II for the whole mission. The thermal performance of the ^{3}He refrigerator was quite satisfactory and demonstrated a capability to keep the bolometer at 302 mK for longer than 8 days for each condensation. The detail of the flight performance will be published elsewhere[3].

Environmental Thermal State of Outer Shell

The overall temperature variations of the outer environment of the IRTS is shown in Fig. 13. The thermometers of T_{DEP} and T_{DPU} are installed on the outer surface of the outer shell under the electronic packages, that is T_{DPU} on the solar side (-X direction) and T_{DEP} on the shadowy side (X direction), respectively. The effect of the orbital transfer to the IRTS attitude completed at 280 hours is clearly seen. The detail of the T_{DPU} variation due to the orbital revolution is shown in Fig. 14. It is seen from these results that the temperature of the outer shell on the solar side was higher than the design value and that on the shadowy side was lower than the design value.

Conclusion

The following conclusions are drawn from the flight data of the cryogenic performance of the IRTS.

i) A very stable cryogenic environment for the IR astrophysical observation was successfully achieved in the IRTS cryogenic system at 1.91 K for 37.5 days.
ii) No anomalous thermo-fluid dynamic behavior happened with the PP in the initial zero-g state.
iii) Cold life of the IRTS system on orbit was found to agree well with the prediction on the basis of the ground test data.
iv) The onboard ^{3}He refrigerator successfully cooled the bolometer down to 302 mK.

References

1 Murakami, H. , et al. The Infrared Telescope in Space (IRTS). Astrophys. J. 428 (1994) 354.
2 Natori, M. and Kuriki, K. SFU Mission-1 Experiments. Space Technolo., 11 (1991) 159.
3 Onaka, T., Yagi, T. Shibai, H. and Murakami, H. Optical System of the Infrared Telescope in Space. Appl. Opt.., 33 (1994) 1880-1888.
4 Duband, L., Hui, L. and Lange, A. E. Space-born ^{3}He Refrigerator. Cryogenics 30 (1990) 263.
5 Freund, M. M., Duband,L., Lange, A. E., Hirao, T., Matsumoto, T. and Sato, S. Design and Flight Performance of a Space Borne ^{3}He Refrigerator for the Infrared Telescope in Space. to be published in Cryogenics.
6 Murakami, M., Okuda, H., Matsumoto, T., Fujii, G. and Kyoya, M. Design of Cryogenic System for IRTS. Cryogenics 29-5 (1989) 553.
7 Bock, J. J., Lange A. E., Matsubara, H., Matsumoto, T., Onaka, T. and Sato, S. Cooled Baffle System for Spaceborne IR Telescopes. Applied Optics 34 (1995) 2268.
8 Winston, R. J. Light Collection within the Framework of Geometrical Optics. Opt. Soc. Am., 60 (1970) 245.
9 Bock, J. Ph. D thesis, Univ. of California at Berkeley (1994).

Figure Captions

Fig. 1 Side view and top view of the SFU-1, and the definition of the X-axis. The IRTS is shaded.

Fig. 2 Cross sectional view of the IRTS cryogenic system. Dimensions are given in millimeters.

Fig. 3 The IRTS sun shield, aperture shade and baffle system, and the definitions of the sun and the earth avoidance angles.

Fig. 4 Attitude control of the IRTS in the mode 1.

Fig. 5 Overall thermal performance and major thermal events during the IRTS mission.

Fig. 6 Initial phase thermal behavior of the IRTS cryogenic system. The estimated values of T_{TANK} and T_{FB} prior to the acquisition of telemetry data are shown by the broken and the dotted lines. respectively.

Fig. 7 Thermal behavior in He II depletion stage from 04/28 08:55:00 UT.

Fig. 8 Variation of T_{FB} according to orbital revolution in the phase of earth avoidance angle minimum.

Fig. 9 Typical transient variations of T_{FB}, the earth and the sun avoidance angles.

Fig. 10 Envelopes of the higher peak of T_{FB}, the local minimums of the earth and the sun avoidance angles plotted against time

Fig. 11 Correlation between the temperature rise of T_{FB} at the higher peak and the corresponding minimum value of the earth avoidance angle.

Fig. 12 Temperature rise records of T_{TANK} during the second and third heatings of the condenser of ^{3}He refrigerator.

Fig. 13 Overall temperature variations of the outer environment of the IRTS system. T_{DEP} and T_{DPU}.

Fig. 14 Typical T_{DPU} variation due to the orbital revolution

Fig. 1

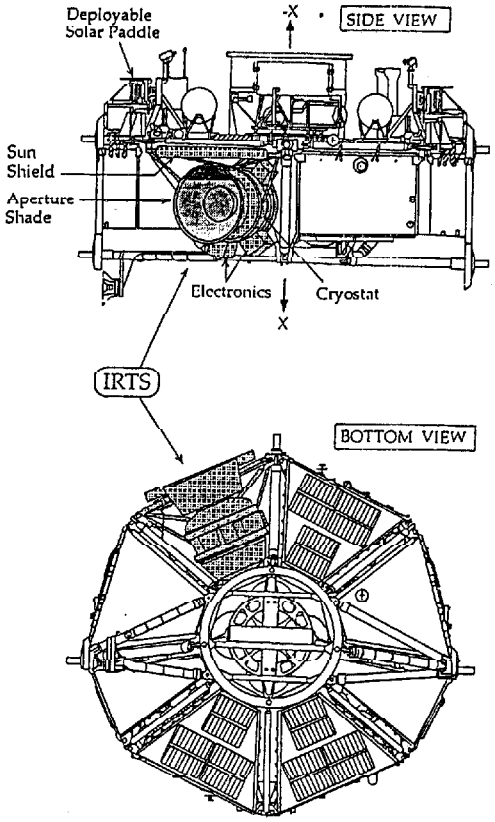
Deployable
Solar Paddle
-X
SIDE VIEW
Sun
Shield
Aperture
Shade
Electronics
Cryostat
X
IRTS
BOTTOM VIEW

Fig. 2

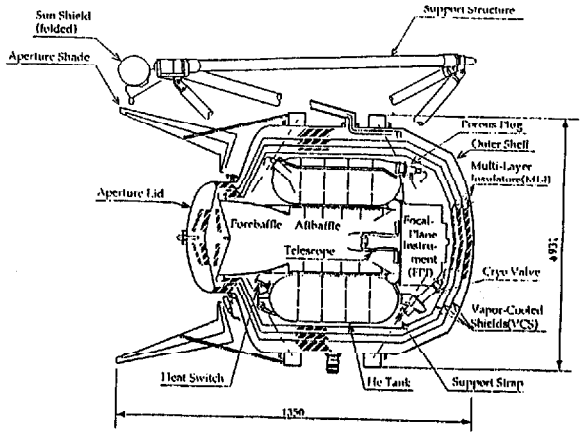
Sun Shield
(folded)
Aperture Shade
Support Structure
Outer Shell
Aperture Lid
Foreбaffle
Afibaffle
Telescope
Cryo Valve
Vapor-Cooled
Heat Switch
He Tank
Support Strap
1350

Fig. 3

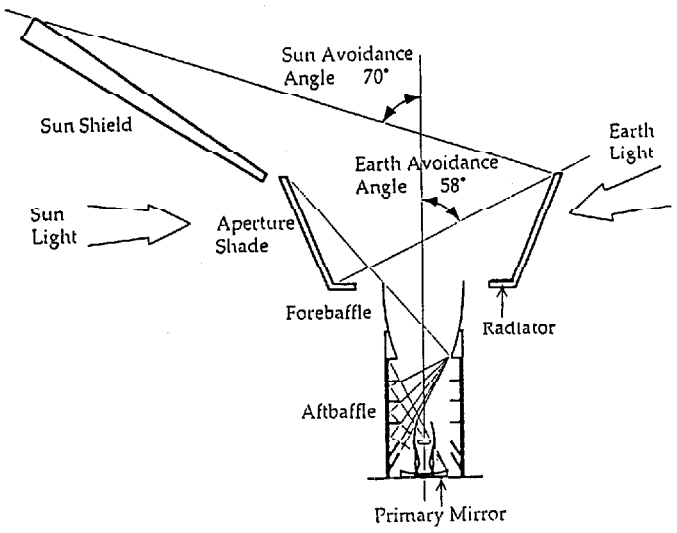
Sun Avoidance
Angle 70°
Sun Shield
Earth
Light
Earth Avoidance
Angle 58°
Sun
Light
Aperture
Shade
Forebaffle
Radiator
Aftbaffle
Primary Mirror

Fig. 4

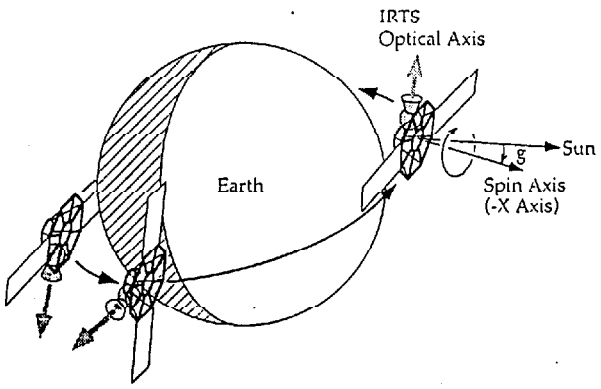
IRTS
Optical Axis
Sun
Earth
Spin Axis
(-X Axis)

Fig. 5

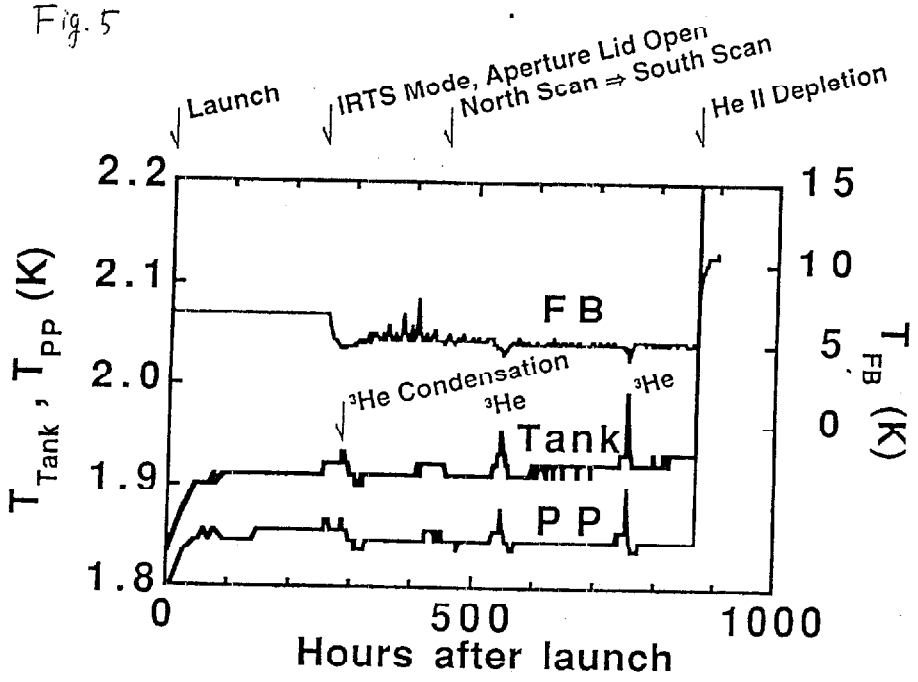
Launch
IRTS Mode, Aperture Lid Open
North Scan ⇒ South Scan
He II Depletion
2.2
2.1
2.0
1.9
1.8
15
10
5
0
FB
Tank
PP
³He Condensation
³He
³He
T Tank , T PP (K)
T FB (K)
0
500
1000
Hours after launch

Fig. 6

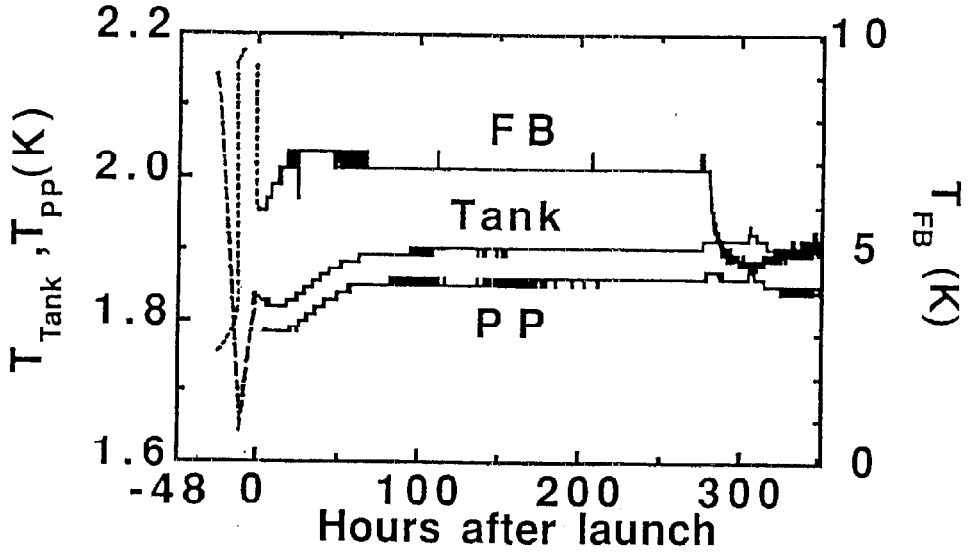
2.2
2.0
1.8
1.6
10
5
0
FB
Tank
PP
-48
0
100
200
300
T Tank , T PP (K)
T FB (K)
Hours after launch

Fig. 7

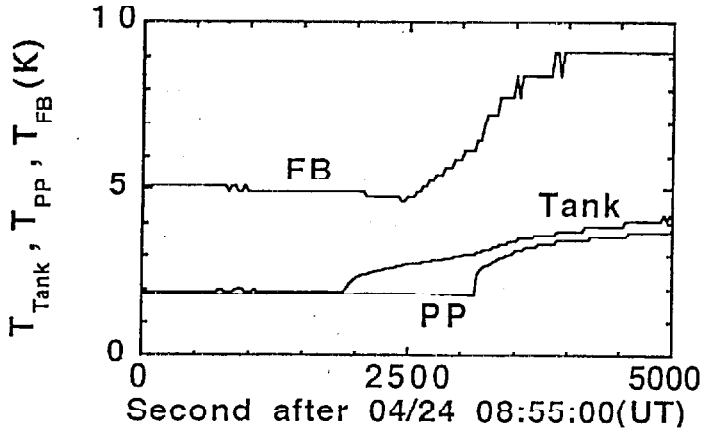
10
5
0
T_{Tank}, T_{PP}, T_{FB} (K)
FB
Tank
PP
0
2500
5000
Second after 04/24 08:55:00(UT)

Fig. 8

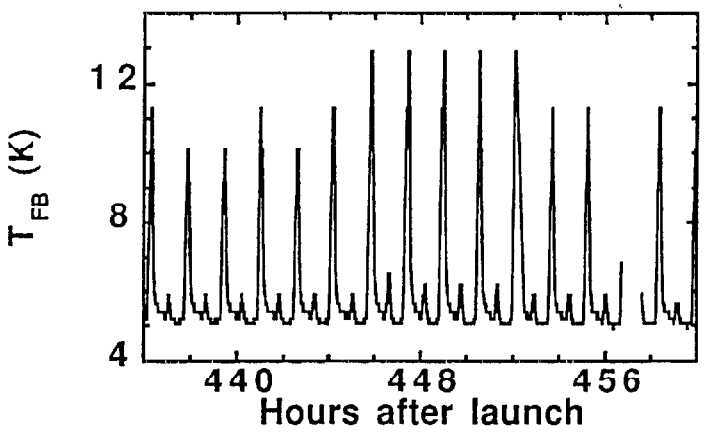
12
8
4
T_{FB} (K)
440
448
456
Hours after launch

Fig. 9

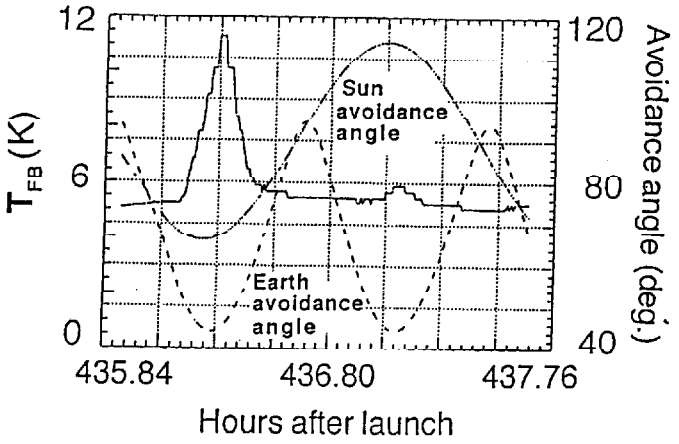
12
6
0
120
80
40
T_{FB} (K)
Avoidance angle (deg.)
Sun avoidance angle
Earth avoidance angle
435.84
436.80
437.76
Hours after launch

Fig. 10

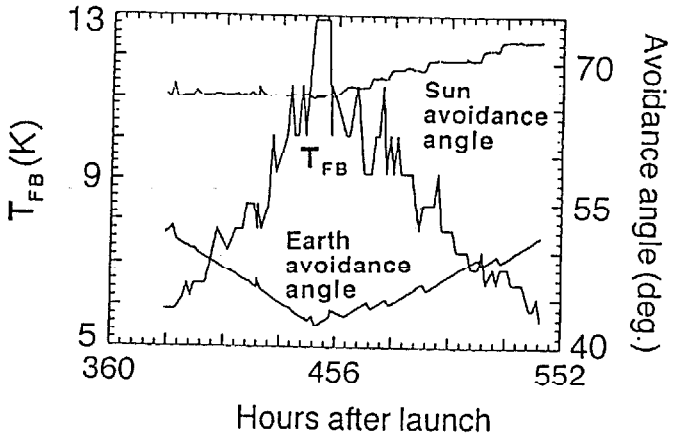
13
9
5
70
55
40
T_{FB} (K)
Avoidance angle (deg.)
Sun avoidance angle
T_{FB}
Earth avoidance angle
360
456
552
Hours after launch

Fig. 11

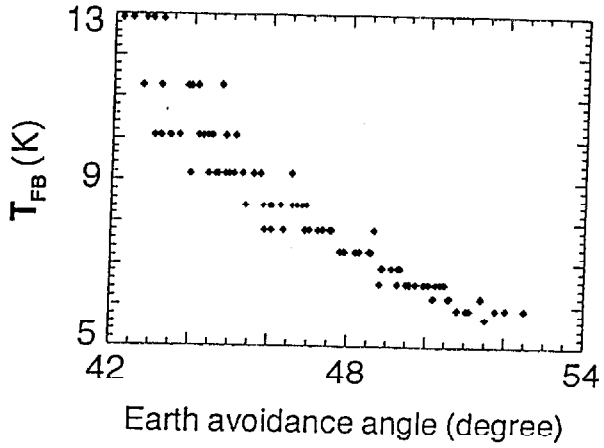
13
9
5
T_{FB} (K)
42
48
54
Earth avoidance angle (degree)

Fig. 12

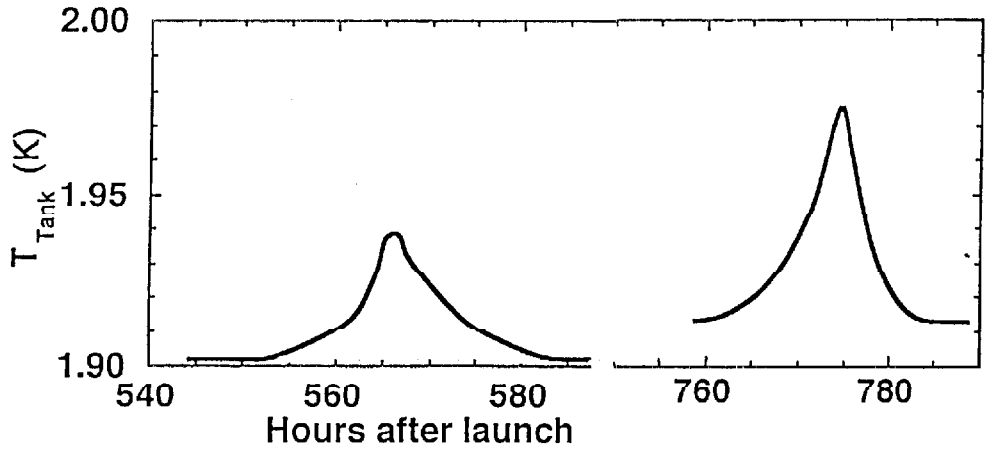
2.00
1.95
1.90
T_{Tank} (K)
540
560
580
760
780
Hours after launch

Fig. 13

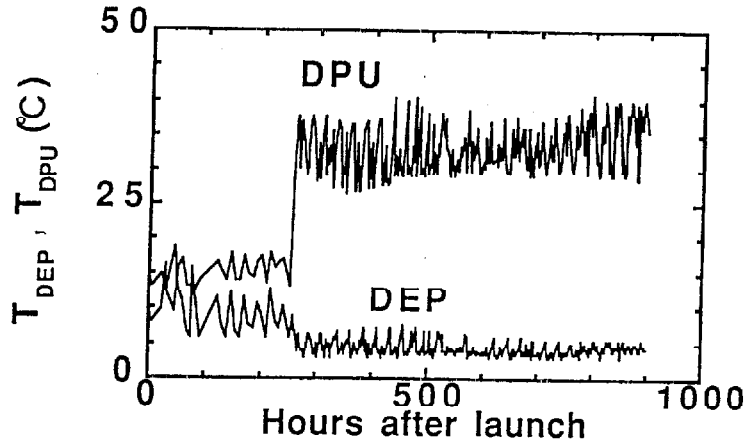
50
25
0
DPU
DEP
T_{DEP}, T_{DPU} (°C)
0
500
1000
Hours after launch

Fig. 14

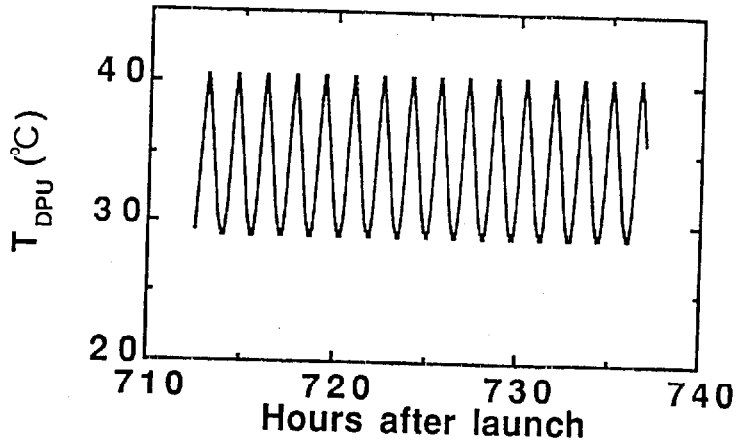
40
30
20
T_{DPU} (°C)
710
720
730
740
Hours after launch

TABLE 3

Predicted Temperature distribution of the cryostat in orbit

Position	Case 1[a]	Case2[b]
	Conditions	
Outer Shell[c]	300 K	300 K
Aperture heat load[d]	10 mW	200 mW
Heat Switch[e]	ON	OFF
	Temperatures	
Outer Vapor-Cooled Shield	201.3 K	191.6 K
Middle Vapor-Cooled Shield	107.5 K	96.5 K
Inner Vapor-Cooled Shield	24.3 K	26.1 K
Forebaffle	2.6 K	18.7 K
He Tank	1.9 K	1.9 K

a) The expected best case. The requirements of sun and earth avoidance are both satisfied.

b) The worst case. Radiation from the earth directly illuminates the upper part of the forebaffle. The heat switch is turned off to reduce the heat load to the helium tank.

c) The acurate calculation of the outer shell temperature is very difficult, because of the complex structure of the SFU. A temperature of 300 K is assumed here for both cases.

d) Heat absorbed by the forebaffle.

e) Heat switch for the forebaffle (see text).

TABLE 1 .

Item	Performance
Weight	approximately 4.0 metric tons at launch
Dimensions	4.46 m dia. x 2.8 m
Electric Power	1.4 kW (3 kW paddle generated power)
Command and Data Management System	S-band link Telemetry : 128 kbps Command : 1 kbps Data recorder : 80 Mbits Data rate : 16 kbps max.
Navigation & Guidance Control	Navigation : GPS and IMU Guidance : Onboard S/W Control : 3 axis stabilized, 1 accuracy
Reaction Control System	Hydrazine monopropellant system
Experiment resources	6 Payload Unit (PLU), 150kg/Unit Upper deck and center hole μG level : $< 10^{-4}$ G Available power for experiments : 1 kW

TABLE 2
Specifications of the IRTS

Item	Characteristics
Weight	Total weight : 183 kg Cryostat : 128 kg FPI +telescope : 9 kg Electronics : 16 kg Support structure : 18 kg Others : 12 kg
Dimensions	93 cm dia. (cryostat) x 135 cm (including aperture shade)
Power Consumption	80 W max.
Cryostat	Superfluid helium 90 liters FPI temperature : 1.9 K Cold lifetime : > 35 days after launch
Telescope	15 cm dia., F/4 Ritchey-Chretien type Effective collecting area : 113 cm^2
Focal plane instruments	Near-Infrared Spectrometer (NIRS) Mid-Infrared Spectrometer (MIRS) Far-Infrared Line Mapper (FILM) Far-Infrared Photometer (FIRP)
Telemetry	Data rate : 6 kbps (visible orbit) / 3 kbps (invisible orbit)
Observation	20 days, uniform sky survey
Sky coverage	approximately 10 % of the entire sky

Design and Flight Performance of a Space Borne ^{3}He Refrigerator for the Infrared Telescope in Space

M.M. Freund*, L. Duband**.

Dept. of Physics, UC Berkeley, Berkeley, CA 94720, U.S.A.

A.E. Lange

Mail Code 320-47, Caltech, 1201 E. California Blvd., Pasadena, CA 91125, USA

T. Matsumoto, H. Murakami

LIRA, ISAS, 3-1-1 Yoshinodai, Sagamihara-shi, Kanagawa-ken, Japan

T. Hirao and S. Sato

Dept. of Physics, Nagoya Univ., Furocho, Chikusa-ku, Japan

* Present address: MS 239-4, NASA Ames Research Center, Moffet Field, CA 94035-1000

** Present address: CEA/DRFMC/ Service des Basses Temperatures, 17 rue des Martyres, 38054 Grenoble Cedex 9, France

Accepted for Cryogenics

Abstract

We report the design, space-qualification and flight performance of a ^{3}He refrigerator that has achieved the first sub-Kelvin temperatures in orbit. The refrigerator has been used to cool the bolometric detectors of the Far Infrared Photometer (FIRP) on the Infrared Telescope in Space (IRTS). The refrigerator has no moving parts, and can be re-cycled indefinitely in zero-g with > 95% duty cycle using simple control electronics. It provides 10 μW of cooling power at T < 310 mK with ≤ 2 mW average power dissipation to a 2.0 K heat sink for about 10 days.

Keywords: ^{3}He refrigerator, Flight Performance, Space-Borne

Abbreviated Title: Design and Flight Performance of a Space Borne 3He Refrigerator...

Introduction

Although many techniques are available to cool below 1K, none has previously been realized in space. The design of space-borne cryogenic systems is complicated by many requirements that are not present in the laboratory. A space-borne system must be self-contained, compact, lightweight and very reliable. It must survive accelerations and vibrations during launch, and operate in zero-g for months or years without service or replenishment of cryogens. Strict limitations on power consumption and dissipation require high thermodynamic efficiency.

For these reasons, the lowest temperature available in orbit has been limited to ≈ 1.4 K first achieved by IRAS in 1983 by evaporation to space of superfluid ^{4}He through a porous plug phase separator. Several conventional laboratory techniques that provide sub-Kelvin temperatures, including adiabatic demagnetization [1-4] and ^{3}He/^{4}He dilution[5], are currently being adapted for use in space. Here, we report on the design, space-qualification and flight performance of a simple ^{3}He evaporation refrigerator that has achieved sub-Kelvin temperatures in orbit for the first time.

^{3}He evaporation refrigerators have been used for many years in laboratories, on balloon-borne payloads, and on board sounding rockets, typically to cool infrared bolometric detectors from the ≈ 1.4 K provided by a superfluid He bath to temperatures of 250 to 350 mK. The refrigerator described here, the concept of which has been previously described by Duband, Hui and Lange[6], is the first ^{3}He refrigerator suitable for use in orbit. The refrigerator was used to cool the bolometric detectors of the Far Infrared Photometer (FIRP) [7] on the Infrared Telescope in Space (IRTS) [8], a liquid He- cooled telescope that was launched into orbit in March, 1995 on board the Japanese Space Flyer Unit (SFU).

Principle of operation

A given pumping speed will produce lower temperatures in liquid ^{3}He than in liquid ^{4}He, because ^{3}He does not exhibit superfluid flow along the pump tube, and because of the difference in the vapor pressure curves of the two isotopes. Gravity is essential to the operation of conventional ^{3}He evaporative refrigerators in two respects. First, the ^{3}He liquid is typically condensed at a liquid ^{4}He heat sink positioned above the still, into which it drips. Second, gravity is used to separate the liquid and the gas phases when the pressure in the still is lowered.

The refrigerator described here is designed to condense ^{3}He into the still and to pump on the liquid ^{3}He in zero-g and in a wide range of orientations during ground-testing. The liquid is condensed directly into the still by a system of heat switches that establish the necessary temperature gradients during the condensation phase of the cycle, and is contained in the still via surface tension to a porous silica sponge [9] during the evaporation phase of the cycle.

The refrigerator is shown in the FIRP instrument in **Fig. 1**. (For a summary of the mechanical specification see **Table 1**). The thermal circuit of the refrigerator is illustrated in **Fig. 2**. The refrigerator has five major components. A still, holds the liquid ^{3}He inside a silica sponge during operation. A helical pump tube connects the still to a charcoal-filled sorption pump, which physisorbes the ^{3}He gas from the still. Two heat switches, one each for the pump and the still are used to make and break thermal contact with the ^{4}He cryostat. The still and the pump are each held in a Kevlar support system. The refrigerator is charged with 16.8 S.T.P. liters of ^{3}He gas, and permanently sealed by a crimped tube. The room temperature pressure is ≈68 MPa. A cold shunt on the pump tube limits the heat flow from the pump to the still during cycling.

Both heat switches are initially closed in order to cool all of the components to the temperature of the heat sink (~1.8 K). The refrigeration cycle is started by turning off the heat switch to the pump, thus thermally isolating the pump, and turning on a resistive heater on the pump. The heat switch on the still is kept on, making the still the coldest point in the system. The gas is desorbed from the charcoal in the pump, and cooled to about 3-4 K at the cold shunt on the helix before reaching the still. The cold shunt reduces the heat load on the still by about a factor of ten, since the enthalpy of ≈ 33 K ^{3}He gas is more than ten times the latent heat of condensation. The combination of the still heat switch and the cold shunt maintains the still temperature below ≈ 2.1 K, providing a high condensation efficiency of the refrigerator. As the pump reaches ≈ 10 K, the vapor pressure of ^{3}He in the pump exceeds the saturation vapor pressure at 2 K, and ^{3}He condenses in the still. The liquid is held in the still by surface tension to the silica sponge. A full condensation cycle, which condenses > 95 % of the gas, requires heating the pump to > 33 K. The speed of condensation is limited by the thermal resistance to the 1.8 K heat sink, which is dominated by the thermal resistance of the Al shell of the ^{4}He cryostat. Complete condensation requires ≈ 12 hours. During condensation 44 mW of power are applied to the pump, of which ≈ 13 mW flow to the 1.8 K heat sink, and the remainder is stored in the heat of adsorption of the ^{3}He driven off of the charcoal and in the heat capacity of the pump.

After all the ^{3}He gas is condensed inside the still, the still heat switch is turned off, thermally isolating the still. Next the pump heat switch is turned on, thermally grounding the pump. During this cool-down phase the cold shunt on the pump tube intersects the heat from the pump and thus reduces the heat load on the still, significantly enhancing the hold time of the refrigerator. As the pump cools, so does the still, reaching ≈295 mK after several hours.

During the cold phase the liquid ^{3}He is retained inside the still by a silica sponge. The ^{3}He desorbed gas from the still is adsorbed inside the pump. For every 1 μW of heat on the still, 48 μW are released as the heat of adsorption inside the pump. The heat of adsorption of the ^{3}He passes to the cold plate via the pump heat switch, keeping the pump at ≤ 2.5 K.

pressure vessel, including the pump tube and associated fittings, were designed to have a burst pressure of ≥ 240 MPa, 3.5 x the pressure at ambient temperature. The various parts of the pressure vessel were either hard soldered or welded together. Each joint was leak tested as the refrigerator was assembled. After completion of the assembly, but before attaching the burst disk, the entire refrigerator was thermally cycled several times to 77 K and pressure tested several times to 172 MPa. Some plastic deformation was observed during the first pressure cycle, but none during subsequent cycles.

After pressure testing, the burst disk was hard-soldered to the refrigerator via a stainless steel capillary. The refrigerator was leak tested and an upper limit of the leak rate of 0.3×10^{-9} S.T.P. cm^3/s was established. The refrigerator was electro polished to minimize the emissivity of the outer surface and then baked out at T > 115 °C for 15 hours while being evacuated to a pressure of $< 10^{-6}$ torr, in order to remove all of the water adsorbed on the charcoal. Finally, the refrigerator was cooled to 4 K and filled with 16.8 S.T.P. liters of ^3He via a capillary, which was crimped and sealed after warming to room temperature.

Support System and Vibration Tests

The support system must firmly restrict the possible movements of the refrigerator during launch and at the same time minimize the parasitic heat load on the system. We have developed a support system that satisfies both conditions, using braided 100 lb. Kevlar cords. Kevlar has a low thermal conductivity, high tensile strength and high Young modulus[14].

The pump and the still are supported in the same manner, illustrated in Fig. 5. Four pulleys are affixed to each of the two ends of the pump and the still, and three pulleys and two small capstans are attached to titanium brackets. The Kevlar cord runs between these pulleys and is fastened at the capstans, which are used to tension the Kevlar. The Kevlar cords are oriented in such a way as to equalize the resonance frequencies of the translational modes in all three axes. The geometry of, and the materials composing the suspension system have been carefully chosen as to minimize the change in tension due to thermal expansion of Kevlar at low temperatures.

The support system was designed to withstand a 400 g static acceleration. The minimum three resonance frequencies along the three principal axes were measured at room temperature, and at 77 K, and found to be between 250 and 400 Hz. The maximum test levels for the qualification tests of the flight model were 30 g between 2Hz and 200 Hz in a sinusoidal sweep, and 6 g_{rms} in a random test with frequencies between 20 and 2000 Hz.

Thermal Connections

The ^3He refrigerator will fail to condense unless excellent thermal contact to the ^4He bath is maintained during condensation. The maximum temperature gradient allowed between the liquid ^4He and the refrigerator during condensation is 0.5 K. The thermal contact between the FIRP housing and the liquid ^4He is especially

important because it will determine both the condensation temperature of the still during the recycling phase, and the housing temperature during the low temperature phase. The hold time of the refrigerator is strongly dependent on both of these temperatures. The important thermal resistances include metal-metal interface resistances, Kapitza resistance and bulk resistances. We minimized the metal-metal interfaces by plating most interfaces by a thin gold layer. The bulk resistances were also minimized by using annealed ultra high purity copper heat straps. Measurements show that the dominant thermal resistance is due to the aluminum IRTS cryostat itself.

During condensation the heat from the still flows through the still heat switch and a copper heat strap directly to the IRTS ^{4}He cryostat wall. This strap ($A \approx 0.40$ cm^2, $l \approx 15$ cm) is attached to the IRTS cryostat with 13 M3 screws in a flat flange, with a surface interface area of ≈ 13 cm^2. In order to provide electrical isolation of the FIRP from the rest of the IRTS an isolating copper-stycast-copper interface was inserted between the Cu strap and the IRTS cryostat wall. The isolating interface has a thermal conductivity of 250 mW/K at 2 K. To reduce the thermal resistance, all copper pieces were made using ultra high purity (99.9999%) copper, which is annealed after machining. When designing the dimensions of the copper joints on the wall of the pressure vessel, the reduced tensile strength of the copper due to annealing has been taken into account.

The thermal circuit (see **Fig. 2**) is designed to keep the liquid ^{3}He inside the still as close as possible to the temperature of the IRTS cryostat during condensation. During this phase 12.5 mW of power flows to the aluminum cryostat. Most of this power (11.7 mW) is due to the enthalpy of the desorbed hot gas, which is intercepted at the cold shunt. This reduces to 0.8 mW the power flowing through the still heat switch. In order to minimize the power dissipation of the pump, it must be thermally well isolated during condensation. Contributions to the thermal contact between the pump and the 2 K stage include conduction through the mechanical support, the helical pump tube, the heat switch, Taconis oscillations and convection. Taconis oscillations have been eliminated by inserting stainless steel wool inside the pump tube near the pump. Convection is not present in zero-g, and is not effective inside the helical pump tube in most orientations in the laboratory. Convection is only present when the angle between the refrigerator axis and the gravitational acceleration vector is smaller than 5 °. The sum of these parasitic heat contributions is small compared to the total power dissipation.

During the cold phase ($T_{still} \approx 295$ mK) there are five important contributions to the heat load to the still: the still heat switch, the pump tube, the still Kevlar support system, the manganin wires for the still thermometer, and the photometer, with its support system and its wiring. Using the known thermal conductivities and geometric ratios of the different components, we calculate that the still heat switch contributes 7.7 μW, the pump tube 3.2 μW, the still Kevlar support 0.7 μW, the manganin wires 0.3 μW, and the photometer 4.1 μW for a total of 16 μW, assuming a housing temperature of 2 K.

Thermodynamic Performance

To optimize the efficiency and duty cycle of the refrigerator requires an understanding of the energy budget for the various phases of the refrigerator cycle. The fundamental limit to the thermodynamic efficiency of a charcoal pumped ^{3}He refrigerator is the heat of adsorption of ^{3}He on charcoal, which is much larger than the latent heat of condensation. Therefore, the Carnot efficiency of the refrigerator is relatively poor. During condensation, most of the power supplied to the pump is stored in the latent heat of adsorption of the ^{3}He gas. It is transmitted to the 2 K cold stage during the evaporation phase, when the gas is adsorbed.

As shown by Duband et al.[6] the adsorption isotherms of ^{3}He are the same as for ^{4}He[15]. The ratio of charcoal to ^{3}He (2.9 g/liter S.T.P.) is chosen to ensure that the pumping speed is always determined by the pump tube and not by the charcoal. This provides a stable operating temperature. Duband et al. measure that 43 Joules per liter S.T.P. are required to desorb 90 % of the gas from the charcoal.

Assuming a cold plate temperature of 2.0 K, and a charge of 16.8 liter S.T.P. of ^{3}He inside the FIRP ^{3}He refrigerator, one can calculate the different contributions to the total energy required to cycle the refrigerator: (i) the latent heat of adsorption of the ^{3}He gas is 651 J. (ii) the integrated heat capacity of the ^{3}He gas ($c_V(^3He)$) between 2 K to ≈ 33 K is 207 J, (iii) the heat capacity of the pump (c_V(pump)) between 2 K to ≈ 33 K is 188 J, and (iv) the integrated power dissipation through the thermal connections between the hot pump and the 2 K cold stage is 123 J, (v) the energy required to keep the still heat switch on at a cost of 50 μW is 2.2 J, for a grand total of 1171 J. The measured value is 1166 J.

During the heating phase of the condensation cycle (i) 186 J are dissipated on the cold plate to cool the desorbed ^{3}He gas (90 %) from 33 K to 2 K. (ii) The power to the still heat switch contributes 2.2 J, (iii) and 133 J are dissipated through the thermal connections for a total of 321 J over 13 hours (12 hours of heating + 1 hour before cool down), for an average power dissipation on the cold plate of 7.1 mW during heating.

During the cool down phase (5 hours) from 33 K to ≈ 3 K: (i) the c_V(pump) contributes 188 J, (ii) and the $c_V(^3He)$ of the remaining 10 % of ^{3}He still adsorbed adds another 21 J. (iii) To cool the still from ≈ 2 K to 300 mK about 19 % of the ^{3}He gas is desorbed at a cost of 15 J. (iv) This adsorbing ^{3}He gas dissipates another 137 J, for a total energy dissipation during the cool down phase of 361 J, or an average power dissipation of 20 mW.

During the cold phase (operational phase) the heat load on the still is 15 μW, which results in a power dissipation of 0.72 mW on the cold plate. Additionally, 50 μW is required to keep the pump heat switch closed. The average heat load on the cold plate is then the time averaged sum of the heat dissipated during heating (321 J, 13 hours), the heat dissipation during the cool down (361 J, 5 hours) and the heat dissipated during operation (698 J, 10.5 days) for a total energy input of 1380 J, or an average of 1.42 mW. The efficiency of the refrigerator is the ratio of the operating time over the total time, or 93.5 %. The load on the refrigerator over the hold time at 295 mK is 13.6 J, corresponding to a thermal efficiency 0.0098. The efficiency of a Carnot machine operating between 0.3 K and ≈ 2 K is 0.18. Thus, the ^{3}He refrigerator has 5.5 % of Carnot efficiency.

The performance of the refrigerator is strongly dependent on the temperature of the heat sink. For the same condensation efficiency and a colder heat sink, the pump temperature will be reduced, less liquid will be used during the initial cool down process, and the parasitic heat load on the still will be smaller. Therefore, the hold time, the operating temperature and the thermodynamic efficiency are all sensitive to the heat sink temperature. We have written a computer simulation program to calculate the lifetime, hold time and thermal efficiency of the refrigerator. **Fig. 6** depicts the dependence of the lifetime of the still as function of both the housing temperature ($T_{housing}$) and the condensation temperature ($T_{condensation}$).

Performance in Ground Tests

The refrigerator originally designed and built for the FIRP was different from that described above in the detailed design of the still. The original still design is shown in **Fig. 4(b)**. The FIRP and this refrigerator were first integrated with the rest of focal plane of the IRTS in July 1991. The entire focal plane assembly was mounted in a test cryostat such that the orientation of the FIRP was as illustrated in **Fig. 1**, with the still above the pump and the still-pump axis at 45 degrees to the vertical. During the course of the focal planes tests, the refrigerator was cycled several times. The temperature of the cryostat at the position of the FIRP heat strap was approximately 2.0 K. The performance of the refrigerator was identical from one condensation to the next, with the still always stabilizing at slightly below 300 mK. After the initial testing was complete, the entire focal plane was removed from the test cryostat and was subjected to a vibration test. After confirming that there was no mechanical or electrical damage to the focal plane instruments, the instruments were separated from the focal plane for refurbishment.

During refurbishment of the FIRP, an electrical isolation interface was added to the heat strap that increased the thermal impedance between the refrigerator and the LHe cryostat. The FIRP was installed in a small test cryostat and the post-vibration test performance of the refrigerator was confirmed. During these tests, the refrigerator was operated with the still-pump axis horizontal, and with a heat sink temperature of 1.7 K. The performance of the refrigerator was excellent, and the still cooled reproducibly to below 300 mK, despite the increase in thermal impedance of the heat strap.

The FIRP was re-integrated with the IRTS focal plane in October 1991, in the same orientation as the July 1991 tests. The performance of the refrigerator in all subsequent testing was significantly degraded. After an apparently normal condensation cycle, the still would begin to cool normally but would stabilize at a temperature of between 390 and 450 mK. We found two ways to cool the refrigerator to 300 mK: (i) when we tilted the IRTS test cryostat, so that the FIRP was in an almost horizontal position, we reached 300 mK. (ii) Briefly closing the heat switch on the still, and thus putting a heat pulse on it, the still cooled to 300 mK. The inability to reach 300 mK persisted after integration into the flight cryostat. Furthermore, after a second vibration test of the focal plane (inside the IRTS flight cryostat at 2 K) we were unable to condense any liquid ^{3}He in the refrigerator at all (Aug. 1992). Because of the incremental deterioration in the performance of the ^{3}He refrigerator after each vibration test, we first suspected internal damage to the refrigerator.

Careful study of the detailed thermal performance of refrigerator in the July and October tests, however, led to the hypothesis that the elevated temperature of the refrigerator in October was due not to damage sustained during the vibration test but to the presence of a small amount of liquid ^{3}He present in the pump tube immediately outside the still. The added thermal resistance caused by the electrical insulation at the cold strap on the cryostat increased the still temperature during condensation by ~ 0.3 K. As a result the ^{3}He vapor pressure during condensation rose from 90 Torr to 250 Torr. This in turn decreased the surface tension of the liquid inside the ceramic sponge[16, 17]. The combination of (i) an increase of vapor pressure inside the still, (ii) a decrease in the surface tension of the liquid ^{3}He, and (iii) the action of gravity downwards resulted in an accumulation of a liquid ^{3}He plug in the "elbow" formed by the still-to-helix joint. The column height of the liquid ^{3}He inside this trap resulted in an increased vapor pressure inside the still and a thus in a still temperature of ≈ 450 mK.

Based on this hypothesis, we concluded that the refrigerator was likely to operate satisfactorily in zero-g. Because of the difficulty of operation in ground testing, however, we decided to replace the refrigerator with one in which the design of the still was modified to that shown in Fig. 4(a). The improved design reduces the likelihood that liquid ^{3}He will migrate outside of the still during the ground test condensation, and also strengthens the internal structure of the still to reduce the risk of damage during vibration tests. The new refrigerator was fabricated and installed into the FIRP during a final refurbishment of the instrument in January, 1994. The new refrigerator successfully and reproducibly cooled to 300 mK when the FIRP was re-installed in the focal plane.

In order to verify the hypothesis regarding the failure of the original refrigerator, we conducted tests with it after it was removed from the IRTS focal plane. The refrigerator was installed in a test cryostat that reproduced the orientation of the FIRP and the heat sink temperature in the IRTS test cryostat. In addition to the usual thermometry, a thermometer was added to the elbow just above the position of the hypothesized liquid in the pump tube. We found that the temperature of the still stabilized at 390 mK, consistent with the performance in the IRTS test cryostat, and that the thermometer located on the elbow in the pump tube cooled to simultaneously recorded temperature of 290 mK, indicating that there was, in fact, liquid in the elbow that was creating an increased vapor pressure inside the still.

Flight Performance

The IRTS was launched into orbit on March 18, 1995. A complete description of the performance of the superfluid He cryostat is given by Murakami et al. [8]. The FIRP ^{3}He refrigerator was activated on March 30th, one day after the aperture lid of the IRTS cryostat was ejected and observations had begun.

The refrigerator was cycled three times on orbit at approximately weekly intervals. Fig. 7 shows a comparison of the still and pump temperatures during ground testing and in flight. The performance of the refrigerator during all three cycles was excellently reproducible (Table 3). The pump was heated to 33.5 K over a 12.5 hour interval by a 44 mW heater. The still reached a temperature of 303 mK, 6 hours after turning

off the still heat switch and turning on the pump heat switch, and stabilized at 302 ± 1 mK within 24 hours. The slightly higher temperature (302 mK in orbit vs. 295 mK during ground testing in the flight cryostat) is consistent with the higher temperature of the ^{4}He cryostat (1.91K in orbit vs. 1.75K during ground testing). At these elevated temperatures, the predicted lifetime of the ^{3}He refrigerator was decreased from 10.5 to 8.0 days. The refrigerator was re-cycled after a maximum of 7.5 days to prevent lost observation time.

The detailed temperature stability of the still is shown in **Fig. 8**. During the first 4 days of operation, the temperature is extremely stable, with small variations around 302 mK that are correlated with fluctuations in the temperature of the ^{4}He heat sink. After four days, the temperature rises monotonically from 302 to 305 mK over the course of about 6 hours, and then remains stable at 305 mK until the next condensation is begun. This phenomena was never observed in the laboratory tests, which never lasted more than 36 hours. Qualitatively similar phenomena have been observed in laboratory refrigerators. These phenomena might be due to a change in pumping speed of the charcoal sorption pump as it fills with ^{3}He, or to liquid ^{3}He being confined more deeply in the sponge material, but they are not entirely understood. The transient observed in the FIRP refrigerator was reproduced in all three cycles. It has only a minor effect on the performance of the bolometric detectors, reducing the responsivity by <5 %.

Conclusions

We have obtained the first sub-Kelvin temperatures in zero-g using a simple ^{3}He refrigerator operating from a 1.9K heat sink. The refrigerator was successfully cycled three times on orbit at weekly intervals, and reproducibly provided cooling to below 310 mK between condensations. The temperature stability was generally excellent, though a significant transient was present approximately four days after each condensation. The duty cycle of operation was 93.5 %.

The thermodynamic efficiency of the ^{3}He refrigerator is poor relative to adiabatic demagnetization, due to the large heat of adsorption on the activated charcoal pump. In comparison with this and other techniques for sub-Kelvin cooling, however, the ^{3}He refrigerator is simple, compact and easy to implement.

Acknowledgments

We wish to thank all the members and especially G. Weber of the U.C. Berkeley Physics Dept. machine shop, and H. Suzuki of the Nagoya Univ. Physics Dept. machine shop for their expert mechanical work in building the refrigerator and heat switches. Undergraduate students S. Lumetta and G. Brubaker have done most of the CAD drawings. We also acknowledge the help and hospitality of H. Okuda at ISAS. This work was supported in part by NASA grant #NAGW1597.

References

1. Hagmann, C. & Richards, P.L. *Cryogenics*, 35, 303-309 (1995).
2. Serlemitsos, A.T., Warner, B.A., SanSebastian, M. & Kunes, E. *Proc. of SPIE*, 1340, 303-310 (1990).
3. Serlemitsos, A.T., SanSebastian, M. & Kunes, E.S. *Adv. Cryo. Eng.*, 37, 899 (1991).
4. Lesnya, L., Roellig, T., Werner, M. & Kittel, P. *Adv. Cryo. Eng.*, 33, 955-961 (1988).
5. Benoit, A. & Pujol, S. *Cryogenics*, 34, 421-423 (1994).
6. Duband, L., Hui, L. & Lange, A. *Cryogenics*, 30, 263 (1990).
7. Lange, A.E., *et al. ApJ*, 428, 384 (1994).
8. Murakami, H. *ApJ*, 428, 354 (1994).
9. Silica Sponge, Lockheed Martin Missles & Space Devision, composed of SiO_2, ZrO
10. Fike Metal Products, B.S. Missouri.
11. Conte, R.R. *Eléments de cryogénie* , (Masson & Cie., Paris, 1970).
12. Frank, D.J. & Nast, T.C. *Adv. Cryo. Eng.*, 31, 933-940 (1986).
13. Torre, J.P. & Chanin, G. *Rev. Sci. Instrum.*, 55, 213-215 (1984).
14. Duband, L., Hui, L. & Lange, A.E. *Cryogenics*, 33, 643-647 (1993).
15. Roubeau, P., Nigohossian, G.D. & Avenel, O. in *Colloque international vide et froide* (Grenoble SFITV, 1969).
16. Dalfovo, F. & Stringari, S. *Journal of Low Temperature Physics*, 77, 307–317 (1989).
17. Suzuki, M., Okuda, Y., Ikushima, A.J. & Iino, M. *Europhysics Letters*, 5, 333-7 (1988).

Table 1. ^{3}He Refrigerator Mechanical Specifications

Mass	
Pump	≈ 370 g
Weight of charcoal	≈ 59 g
Still	≈ 137 g
Stainless steel helix and joints	≈ 47 g
Brackets and support system	180 g
Heat switches	46 g
Burst Disk	75 g
Electrical components	≈ 15 g
Total weight	870 g
Mechanical dimensions	
Volume of the pump	197 cm^3
Volume of the still	35 cm^3
Dimension of the tube	
Outside diameter	0.952 cm
Wall thickness	254 μm
Total length	63 cm
Dimensions of the helix	
Outside diameter	7.4 cm
Inside diameter	5.5 cm
Number of turns	≈ 3.4

Table 2. Heat Switch characteristics

Length	72 mm
Outer tube O.D.	7.07 mm
Outer tube wall thickness	70 μm
Gap between Cu pieces	127 μm
Active area A/L ratio	330 cm
^{4}He pressure at 300 K	1 MPa
On position (2 K)	18 mW/K
Off position (2K/ 300mK)	7.5 μW/K
On/Off ratio	2400

Table 3. Refrigerator performance

The thermal efficiency is defined as the ratio of cooling power to power needed to cycle the refrigerator.

Operating parameters	
Nominal operating temperature	295–305 mK
Estimated total heat load	15 μW
Estimated cooling capacity	13.5 J
Estimated lifetime	≈ 10 days
Heat load on the ^{4}He bath	< 1 mW
Condensation Parameters	
Still temperature	2-2.1 K
Maximum Pump temperature	33 K
Heater power on the pump	27 mW
Total cycle time	17 hours
Condensation efficiency	> 95 %
Thermal efficiency	8 mW/W

Figure Legends

Fig. 1) The FIRP, viewed from top along the optical axis of the telescope. The photometer and the refrigerator are optically isolated from each other. Two gas-gap heat switches are used to cycle the ^{3}He refrigerator in zero-g. Kevlar suspension systems thermally isolate the pump, still, and photometer from the 2 K housing. The Cu cold strap minimizes thermal gradients between the FIRP and the ^{4}He cryostat. A burst disk attached to the refrigerator prevents overpressure. In ground testing and in the flight cryostat, the FIRP is oriented as shown, with the heat strap of the FIRP on top, and the refrigerator axis oriented on a 45° axis from the horizontal, with the still on top.

Fig. 2) Schematic view of the thermal circuit of the FIRP refrigerator. During condensation most of the heat (11.7 mW) is carried through the shunt resistance via the FIRP housing through the Cu heat strap to the IRTS cryostat. During the cold phase most of the heat load to the still is carried through the helix. the still heat switch and the photometer (see text). The location of the various thermometers (T) and the pump heater (H) is indicated.

Fig. 3) Cross-sectional view of the pump. The Al charcoal cup (dark gray) holds ≈ 60 g of activated charcoal (small circles) and is held in place by a fine Cu-mesh at the top of the cup. The Cu plug (light gray) connects to the pump heat switch. A Si diode thermometer and a carbon heater are attached to this plug (See Fig. 1 H,T).

Fig. 4 a) A side view of the flight still. Here we see several improvements over the old still (shown in 4b): (i) There is an internal pump tube, which prevents the flow of liquid ^{3}He from the still into the still-helix-joint. Its diameter has been adjusted, so that the pressure drop across it will raise the temperature of the bath by not more than 5-7 mK. (ii) All internal parts are gold plated, to reduce thermal resistances between metal to metal interfaces. (iii) The photometer and heat switch sides of the still are always at the same temperature, due to a continuous Cu rod through the center of the still. (iv) The inside between the spacers is filled with a low density silica sponge.

Fig. 4 b) A cut away view of the still of the first ^{3}He refrigerator (see text for description). The light shaded regions indicate copper and the dark shaded parts are aluminum spacers, whose function is to increase the thermal contact to the liquid ^{3}He inside the still. Note the gap between the Cu-rod from the photometer side and the heat switch.

Fig. 5) Schematic view of the Kevlar suspension system for both the pump and the still.

Fig. 6) The calculated lifetime of the ^{3}He refrigerator as a function of housing temperature during operation and condensation temperature (2.0, 2.2, and 2.4 K). The FIRP housing temperature during flight was 1.91 K and the condensation temperature was approximately 2.0 K. Therefore, the estimated lifetime of the ^{3}He refrigerator is consistent with the lower limit of the lifetime of > 7.5 days as measured in flight.

Fig. 7) A comparison of the still and pump temperatures during ground testing (continuous and dashed lines, respectively), and during the first condensation in flight (rectangles and circles, respectively). Note that the temperature characteristics in the laboratory and in space are very similar.

Fig. 8) The Still temperature after the first condensation cycle as function of time after we close the heat switch on the pump. Notice the unexpected rise on day four, as the still temperature rose from 302 mK to 306 mK over a period of less than 12 hours. This was also observed in subsequent runs. The preliminary error bar on the thermometry is indicated for one data point on the second day.

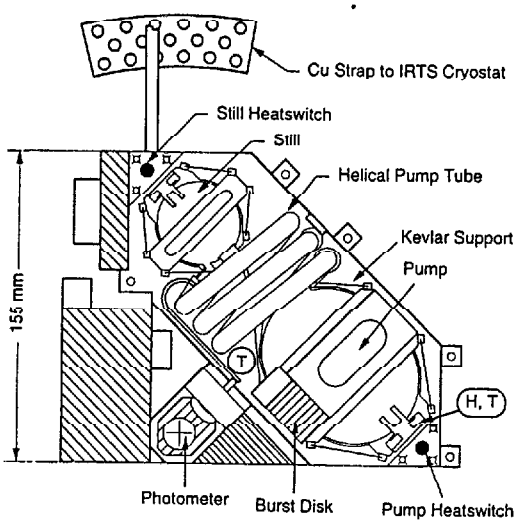
Cu Strap to IRTS Cryostat
Still Heatswitch
Stlll
Helical Pump Tube
Kevlar Support
Pump
155 mm
T
H, T
Photometer
Burst Disk
Pump Heatswitch

Fig. 1

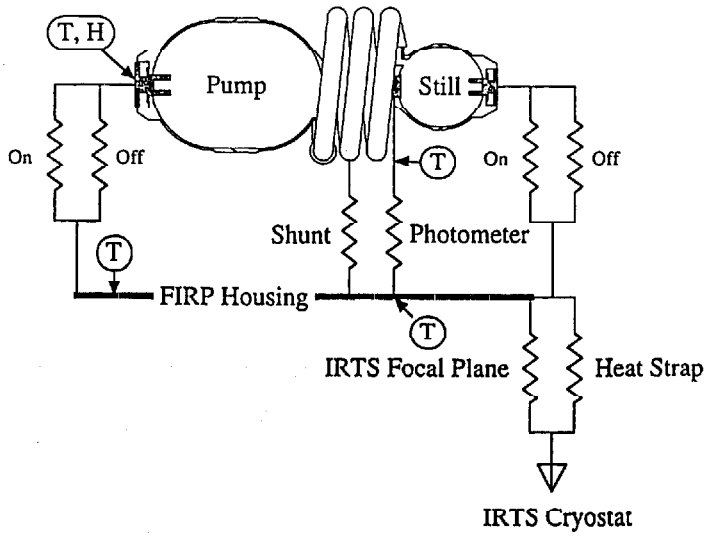
T, H
Pump
Still
On
Off
T
On
Off
Shunt
Photometer
T
FIRP Housing
T
IRTS Focal Plane
Heat Strap
IRTS Cryostat

Fig. 2

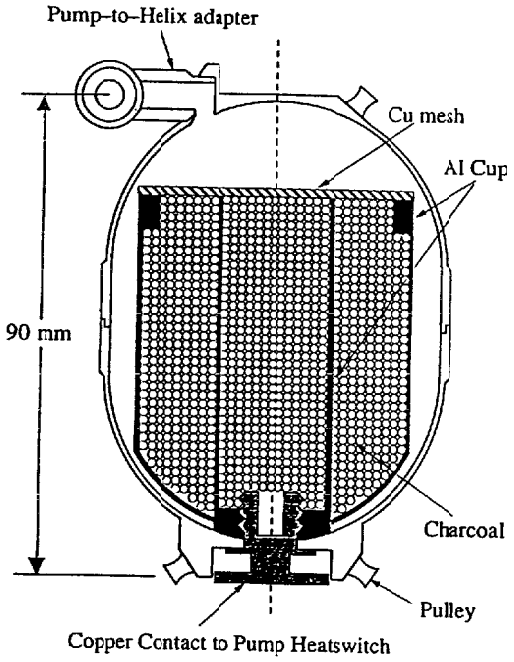
Pump–to–Helix adapter
Cu mesh
Al Cup
90 mm
Charcoal
Pulley
Copper Contact to Pump Heatswitch

Fig. 3

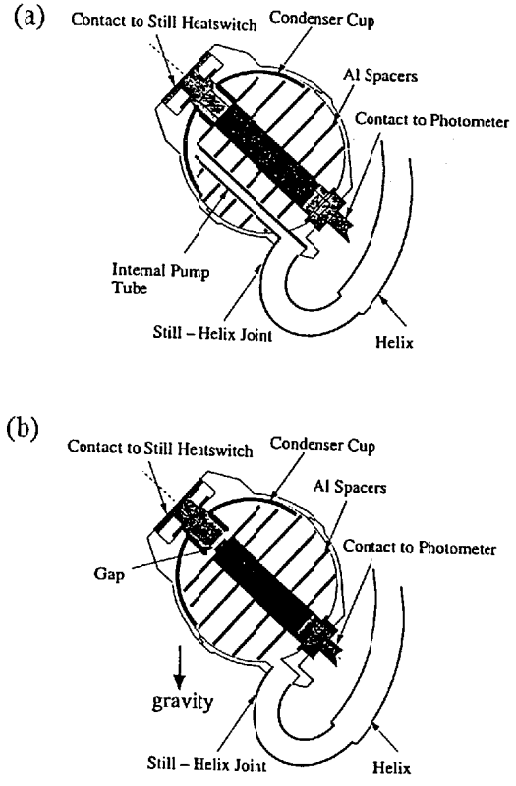
(a)
Contact to Still Heatswitch
Condenser Cup
Al Spacers
Contact to Photometer
Internal Pump Tube
Still – Helix Joint
Helix
(b)
Contact to Still Heatswitch
Condenser Cup
Al Spacers
Contact to Photometer
Gap
gravity
Still – Helix Joint
Helix

Fig 4

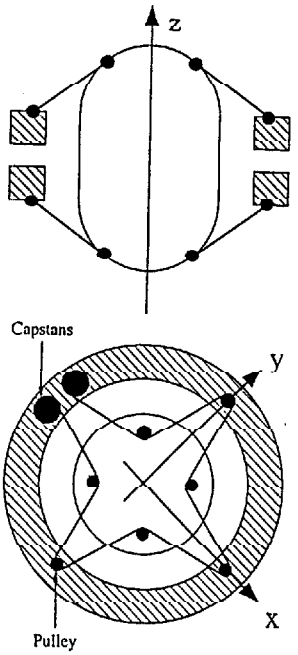
z
Capstans
y
x
Pulley

Fig. 5

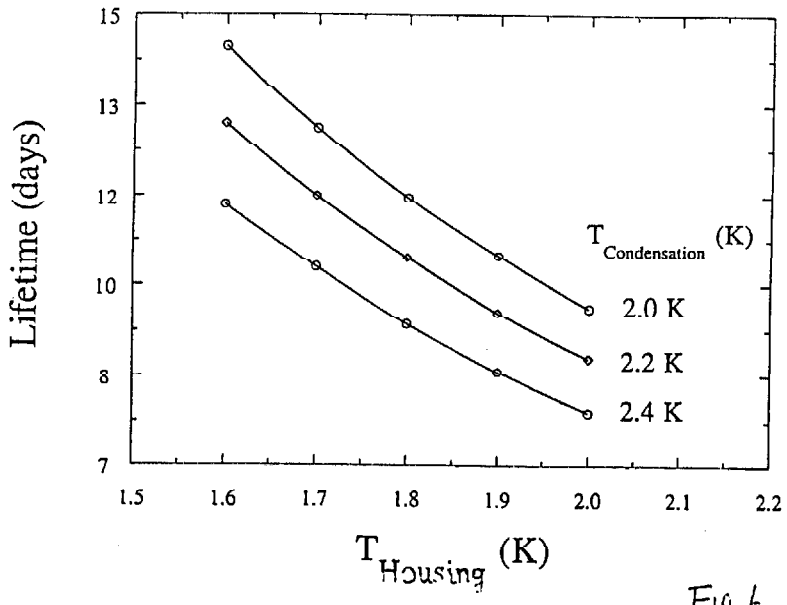
Lifetime (days)
15
13
12
10
8
7
1.5
1.6
1.7
1.8
1.9
2.0
2.1
2.2
T Housing (K)
T Condensation (K)
2.0 K
2.2 K
2.4 K

Fig. 6

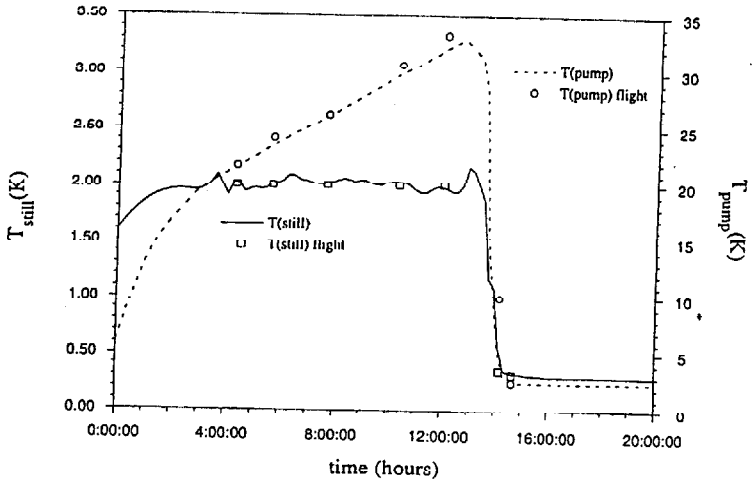
T(pump)
T(pump) flight
T(still)
T(still) flight
T_{still}(K)
T_{pump}(K)
time (hours)
0:00:00
4:00:00
8:00:00
12:00:00
16:00:00
20:00:00

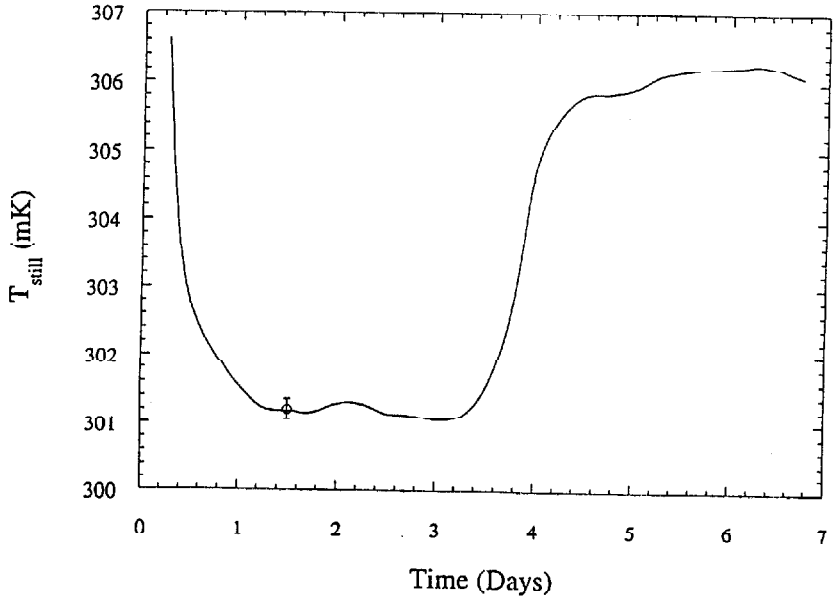
T_{still} (mK)
Time (Days)